2023

EXPLORING SPATIAL ASSOCIATIONS AND COMPLEX INTERACTIONS BETWEEN GEOTECHNICAL PROPERTIES AND ELECTRICAL RESISTIVITY VALUES IN CLAYEY SOILS

Mina Zamanian

EXPLORING SPATIAL ASSOCIATIONS AND COMPLEX INTERACTIONS BETWEEN GEOTECHNICAL PROPERTIES AND ELECTRICAL RESISTIVITY VALUES IN CLAYEY SOILS

by

Mina Zamanian

DISSERTATION

Submitted to the Academic Faculty of

The University of Texas at Arlington

In Partial Fulfillment of the Requirements

for the Degree of

DOCTOR OF PHILOSOPHY

The University of Texas at Arlington

August 2023

EXPLORING SPATIAL ASSOCIATION AND COMPLEX INTERACTIONS BETWEEN GEOTECHNICAL PROPERTIES AND ELECTRICAL RESISTIVITY VALUES IN CLAYEY SOILS

Committee Members:

Dr. Mohsen Shahandashti, P.E., Advisor
Department of Civil Engineering
The University of Texas at Arlington

Dr. Kyeong Rok Ryu
Department of Civil Engineering
The University of Texas at Arlington

Dr. Nilo Tsung, P.E.
Department of Civil Engineering
The University of Texas at Arlington

Dr. Atefe Makhmalbaf
College of Architecture, Planning, and Public Affairs (CAPPA)
The University of Texas at Arlington

Dedicated to

My Mother Masoumeh, and My Father Abbas

ACKNOWLEDGEMENTS

I would like to express my sincere gratitude to my academic advisor and mentor, Dr. Mohsen Shahandashti, for his endless support, invaluable guidance, and constant encouragement throughout my Ph.D. program. Indeed, his vision and profound insight have been instrumental in accomplishing this milestone. Working with him and being part of his research team has been a privilege and an immensely valuable experience that has broadened my professional capabilities and self-growth. I will always be indebted to him for his mentorship and guidance which played a pivotal role in shaping my future career path.

I would also like to thank my supervising committee Dr. Kyeong Ryu, Dr. Nilo Tsung, and Dr. Atefe Makhmalbaf for being part of my Ph.D. program and for providing their insightful comments and advice that helped me enrich the content of my dissertation. I am also thankful to the Texas Department of Transportation (TxDOT), particularly Dr. Natnael Asfaw, for supporting my research and their encouragement throughout the program.

I am grateful to my colleagues and friends at UTA, especially Bahram Abediniangerabi, Ferika Farooghi, Anil Baral, Abhijit Roy, Sumaya Sharveen, Ahmad Bani Hani, Sooin Kim, Sushil Bhatta, and Santosh Acharya for making this journey easier and more enjoyable. I will always cherish my invaluable experience at UTA.

My family has my deepest appreciation, my parents, Masoumeh Massahi and Dr. Abbas Zamanian, my sister, Maryam, and my brother, Amirhossein, for their unwavering support, love, and encouragement throughout this journey.

Last but not least, I am thankful to my beloved husband, Pooya, for his belief in me and his steadfast support and presence during the entire journey that helped me cope with the challenges and difficulties that come with a Ph.D. program.

June 7th, 2023

ABSTRACT

Exploring Spatial Association and Complex Interactions between Geotechnical Properties and Electrical Resistivity Values in Clayey Soils

Mina Zamanian, PhD

The University of Texas at Arlington

Supervising Professor: Dr. Mohsen Shahandashti

A successful design and construction of infrastructure systems such as highways and bridges highly depend on accurate estimation of geotechnical properties and understanding their spatial distributions, especially in reliability-based designs such as the load and resistance factor design (LRFD) method. Insufficient and inaccurate subsurface information has a major contribution to cost overruns and delays in up to 50% of all infrastructure projects. Insufficient site investigation may also contribute to inadequate or conservative designs, leading to costly failures or increased project costs. Hence, geophysical methods, such as electrical resistivity imaging, that can potentially transform the existing subsurface investigations are used to develop tools for subsurface characterization based on data analytic approaches. The main objective of this study is to assess the validity of the developed linear regressions in the literature by empirically evaluating one of the critical assumptions of linear regressions – independence of regression residuals. This research argues that linear regression analysis must not be used for defining the relationships between electrical resistivity and geotechnical properties since it may lead to misleading information about the subsurface conditions. First, to achieve this objective, linear regression

analysis was performed on an experimental dataset to identify the impacts of geotechnical properties on electrical resistivity variations. Second, a problem was articulated with the aim of investigating whether any spatial correlation exists between geotechnical properties and electrical resistivity values. A spatial regression model was then developed that best explains the spatial variability of electrical resistivity values with the variations of geotechnical properties. The second objective of this study was to provide practical recommendations for extracting useful information from complex and non-linear interactions between geotechnical properties and electrical resistivity values using machine learning techniques with deep structures such as deep learning. The proposed approach for characterizing the soil conditions using deep learning outperformed the existing methods used in the literature.

This study identified a new research direction in the future for studying the relationships between geoelectrical and geotechnical properties through the investigation and quantification of the spatial relationships between these properties in clayey soils. The proposed approach helps create and use spatial regression models for a given site to determine the spatial distribution of geotechnical properties at each point (not necessarily those sampled using conventional site investigation methods) and conduct reliability analysis accordingly. The proposed analytical framework based on the deep learning technique also allows transportation agencies to have a better understanding of the effects of geotechnical properties on the variability of electrical resistivity values to obtain more reliable assessments of the subsurface characteristics.

TABLE OF CONTENTS

ACKNOWLEDGEMENTS ii

ABSTRACT iii

TABLE OF CONTENTS v

LIST OF FIGURES viii

LIST OF TABLES xi

CHAPTER 1 INTRODUCTION 1

CHAPTER 2 BACKGROUND 4

2.1. Electrical Resistivity Imaging Technology 4

2.2. Electrical Mixing Model 6

2.3. Existing Relationships between Geotechnical Properties and Electrical Resistivity Values 8

2.3.1. Regression Analysis 8

2.3.2. Artificial Intelligence Techniques 14

2.4. Gaps in Knowledge 15

2.5. Research Objectives 16

CHAPTER 3 EXPLORING SPATIAL ASSOCIATION BETWEEN ELECTRICAL RESISTIVITIES AND GEOTECHNICAL PROPERTIES USING SPATIAL REGRESSION ANALYSIS 17

3.1. Methodology 17

3.1.1. Design of Experiments 17

3.1.2. Data Collection 18

3.1.3. Spatial Autocorrelation 32

3.1.4. Spatial Regression Analysis 36

3.2. Results 39

3.2.1. Results of Standard Regression Analysis 39

3.2.2. Results of Spatial Regression Analysis 47

3.2.3. Robustness of Spatial Regression Models Based on Threshold Distance 53

CHAPTER 4 INVESTIGATING COMPLEX RELATIONSHIP BETWEEN ELECTRICAL RESISTIVITY VALUES AND GEOTECHNICAL PROPERTIES USING DEEP LEARNING 57

4.1. Methodology 57

4.1.1. Data Collection 58

4.1.2. Deep Learning Model 60

4.2. Results 65

4.2.1. Descriptive Statistics 65

4.2.2. Deep Learning Results 70

4.2.3. Model Comparison of Deep Learning Model with ANNs, SVMs, and MLR 73

CHAPTER 5 CONCLUSION and Future Work 79

APPENDIX BOREHOLE LOGS 84

REFERENCES 124

LIST OF FIGURES

Figure 2.1 A comparison of the number of applications of advanced geophysical methods 5

Figure 3.1 Number of boreholes and collected soil samples on clay map of Texas, US............ 19

Figure 3.2 General soil map of Texas 21

Figure 3.3 Annual average precipitation map of Texas 22

Figure 3.4 Annual average temperature map of Texas 23

Figure 3.5 Specific gravity testing of soil 25

Figure 3.6 Liquid limit testing: (a) the soil is flattened in the device cup, and (b) a groove was made at the center 26

Figure 3.7 Plastic limit testing (a) Rolling device and (b) cracked and broken threats of 3 mm. 27

Figure 3.8 Particle size distribution testing using the hydrometer procedure............................. 29

Figure 3.9 (a) and (b) preparation of soil specimens, (c) a schematic setup of laboratory electrical resistivity test, and (d) experimental setup of laboratory resistivity test 30

Figure 3.10 An example of the data points arrangement (i.e., borehole locations) and neighboring structure of the observations based on their distances. 34

Figure 3.11 Residuals versus fitted values for the OLS model with no transformation on the electrical resistivity values. 42

Figure 3.12 Normal probability plot for the OLS model with no transformation on the electrical resistivity values... 42

Figure 3.13 Residuals versus fitted values for the OLS model with transformed electrical resistivity values. 45

Figure 3.14 Normal probability plot for the OLS model with transformed electrical resistivity values. 45

Figure 4.1 Locations of the soil sample collection on the Texas map 58

Figure 4.2 Structure of a deep learning model with four input features and an output feature 61

Figure 4.3 Water content frequency distribution 65

Figure 4.4 Dry unit weight frequency distribution 66

Figure 4.5 Plasticity index frequency distribution 66

Figure 4.6 Clay fraction frequency distribution 67

Figure 4.7 Fine fraction frequency distribution 67

Figure 4.8 Specific gravity frequency distribution 68

Figure 4.9 Spearman's correlation coefficient heatmap of the electrical resistivity and geotechnical properties 69

Figure 4.10 MSE loss function for the training and testing datasets 71

Figure 4.11 MAE loss function for the training and testing datasets 71

Figure 4.12 Relative importance of geotechnical properties in predicting electrical resistivity 73

Figure 4.13 Training and testing accuracies for the developed deep learning to predict the electrical resistivities 75

Figure 4.14 Training and testing accuracies for the developed ANN to predict the electrical resistivities 76

Figure 4.15 Training and testing accuracies for the developed SVM to predict the electrical resistivities 76

Figure 4.16 Training and testing accuracies for the developed MLR to predict the electrical resistivities 77

Figure 4.17 Accuracy metrics of the deep neural network, artificial neural network, support vector machine, and multiple linear regression for the testing dataset 78

LIST OF TABLES

Table 2.1 Examples of empirical studies relating electrical resistivity to the geotechnical properties (before 2010)........ 11

Table 2.2 Examples of empirical studies relating electrical resistivity to the geotechnical properties (between 2012 and 2014)........ 12

Table 2.3 Examples of empirical studies relating electrical resistivity to the geotechnical properties (between 2016 and 2021)........ 13

Table 3.1 Factors and corresponding factor levels in experimental design 18

Table 3.2 Basic statistics for the dependent and independent variables 32

Table 3.3 Summary of results of OLS model before and after transforming the electrical resistivity values 40

Table 3.4 Diagnostic test results for multiple linear regression before transformation 43

Table 3.5 Diagnostic test results for multiple linear regression after transformation 46

Table 3.6 Summary of results of Moran's I tests for the OLS residuals........ 47

Table 3.7 Summary of results of Lagrange Multiplier tests for the OLS residuals 48

Table 3.8 Summary of results of spatial regression models with the transformed data........ 49

Table 3.9 Average effects of explanatory variables on the electrical resistivity values for the SAR model........ 52

Table 3.10 Variations of log-likelihood, pseudo-R-squared, residual standard error, and Moran's I of OLS residual considering different threshold distances for the SEM 55

Table 3.11 Variations of log-likelihood, pseudo-R-squared, residual standard error, and Moran's I of OLS residual considering different threshold distances for the SAR 56

Table 4.1 Basic statistics of the input and output parameters 59

Table 4.2 Model hyperparameters' ranges in grid search 64

CHAPTER 1 INTRODUCTION

A successful design and construction of infrastructure systems such as highways and bridges highly depend on accurate estimation of geotechnical properties and understanding their spatial distributions, especially in reliability-based designs such as the load and resistance factor design (LRFD) method (Shahandashti et al. 2022a; Baral and Shahandashti 2022b; Sudha et al. 2009; Cosenza et al. 2006). It is also vital in identifying critical slope segments to help maintain highway embankments and cut slopes to minimize slope failures and improve transportation system efficiency (Baral et al. 2023; Baral and Shahandashti 2022a). Insufficient and inaccurate subsurface information has a major contribution to cost overruns and delays in up to 50% of all infrastructure projects (Shahandashti et al. 2022b; Baynes 2010). According to a recent nationwide study of 55 transportation agencies in the United States, the annual cost incurred due to change orders resulting from the inadequate subsurface investigation is estimated to be in the millions of dollars (Boeckmann and Loehr 2016). Insufficient site investigation may also contribute to inadequate or conservative designs, leading to costly failures or increased project costs (Adhikari et al. 2021; Shahandashti et al. 2019; Sirles 2006). Lack of continuous subsurface information may also lead to infrastructure failures caused by unforeseen circumstances (Shahandashti et al. 2021), leading to road maintenance expenses that significantly impact the state transportation budgets (Darghiasi and Shahandashti 2023a). For example, the average repair cost of karst-related damages to the infrastructures was estimated to be at least $300 million per year in the U.S. (Weary 2015). This lack of sufficient information is due to the inherent limitation of the conventional geotechnical site investigation methods to provide continuous assessment of the subsurface. In other words, the conventional methods only sample and provide information about a small percentage of a total sample space (Shahandashti et al. 2021). Meanwhile, the Federal Highway Administration (FHWA) has identified several subsurface exploration technologies through the EDC-5 program that are proven effective in evaluating geological, hydrological, geotechnical, and environmental site assessments. Despite the evident advantages of these technologies that can potentially transform existing subsurface investigations, many of these technologies are underutilized by many state departments of transportation because of a lack of proven implementation details for different applications, geotechnical conditions, and operational environments (FHWA 2018; Rosenblad and Boeckmann 2020). These methods offer a unique opportunity to mitigate repairing costs and limitations of conventional geotechnical site investigation methods by providing a rapid and continuous assessment of subsurface conditions using a non-invasive, and cost-effective method (Zamanian et al. 2023b).

Among the geophysical methods, the Electrical Resistivity Imaging (ERI) technique is widely used in the literature to characterize the geotechnical properties in clayey soils based on the electrical resistivity values. Empirical and analytical studies have been conducted to establish statistical models using linear, power, and exponential regression functions to investigate the effects of different hydraulic and solid phase properties of clayey soils on electrical resistivity values. Although most of these studies presented models with a relatively high goodness-of-fit, none of them have investigated the spatial association between the electrical resistivity values and geotechnical properties. The presence of autocorrelated residuals in the standard regression model leads to wrong interpretations of the regression parameters and goodness-of-fit of the models. Spatial regression models consider the spatial dependence of the error terms to accurately determine the effects of a change in geotechnical properties on the variability of electrical resistivity values. Yet there is a lack of an analytical tool for exploring the complex and non-linear relationship between electrical resistivities and geotechnical properties.

The goals of this research are: (1) to explore and quantify the spatial association between geotechnical properties and electrical resistivity values by spatial regression analysis and propose the most appropriate spatial regression model that best explains the variability of electrical resistivity values with the variations in geotechnical properties, and (2) to propose an analytical approach for extracting meaningful information from complex and non-linear interactions between geotechnical properties and electrical resistivity values by deep learning model to overcome the limitations of the linear regression analysis.

Chapter 2 presents a comprehensive literature review on the influencing geotechnical properties affecting electrical resistivity values and the existing empirical correlations between them in the literature. Chapter 2 also describes the gaps in knowledge and research objectives. Chapter 3 elaborates on a methodology for assessing the spatial autocorrelation in the regression residuals and developing an appropriate spatial regression model that best explains the variability of electrical resistivity values with the variations in geotechnical properties. Chapter 4 describes a methodology for developing a deep learning model to explore the non-linear and complex relationship between electrical resistivity values and geotechnical properties. Chapter 5 presents the conclusion.

CHAPTER 2 BACKGROUND

2.1. Electrical Resistivity Imaging Technology

Electrical Resistivity Imaging (ERI) technology employs fundamental physics principles of Ohm's law to determine the resistance of soil, rock, and groundwater to the flow of electrical current (Kearey et al. 2013). The ERI technology is used to uncover the horizontal and vertical discontinuities in the earth's materials. The soil electrical resistivity is a function of soil and rock matrix, degree of saturation, pore fluid conductivity, soil fabric structure, and soil compressibility (Ekwue and Bartholomew 2010; Samouëlian et al. 2005; Lapenna et al. 2005; Friedman 2005; Giao et al. 2003; Rinaldi and Cuestas 2002; Yang 2002). The soil's electrical properties can be studied by inducing a direct or a very low-frequency current into the ground. The current is induced into the ground across two electrodes (current electrodes), and then the resulting voltage is received by the other two electrodes (potential electrodes) (ASTM Standard D6431-18 2018; ASTM Standard D6429-99 2011). In practice, a large number of electrodes (e.g., 28, 56, or more) and multi-electrode cables are used to speed up the data acquisition and improve the quality of large datasets (Akingboye and Ogunyele 2019). Simultaneous measurements can be recorded using a multi-electrode array; a switching box automatically selects and switches the relevant four electrodes based on the predefined sequence stored in the resistivity meter (Bernard et al. 2006).

The main benefit of electrical resistivity imaging over the other advanced geophysical methods is its wide range of applications in determining various subsurface anomalies and soil properties. Figure 2.1 shows a comparison of the number of applications of advanced geophysical tools in the subsurface investigation (ASTM Standard D7400-19 2019; ASTM Standard D5753-18 2018; ASTM Standard 6285-99 2016; Rivers 2016; Li et al. 2014; ASTM Standard D5778-12 2012; ASTM Standard D6429-99 2011; British Standards Institution 2010; Edet 2009; Rogers 2009; Anderson et al. 2008; Sirles 2006; Fenning and Donnelly 2004; Wightman et al. 2004; Williams and Johnson 2004).

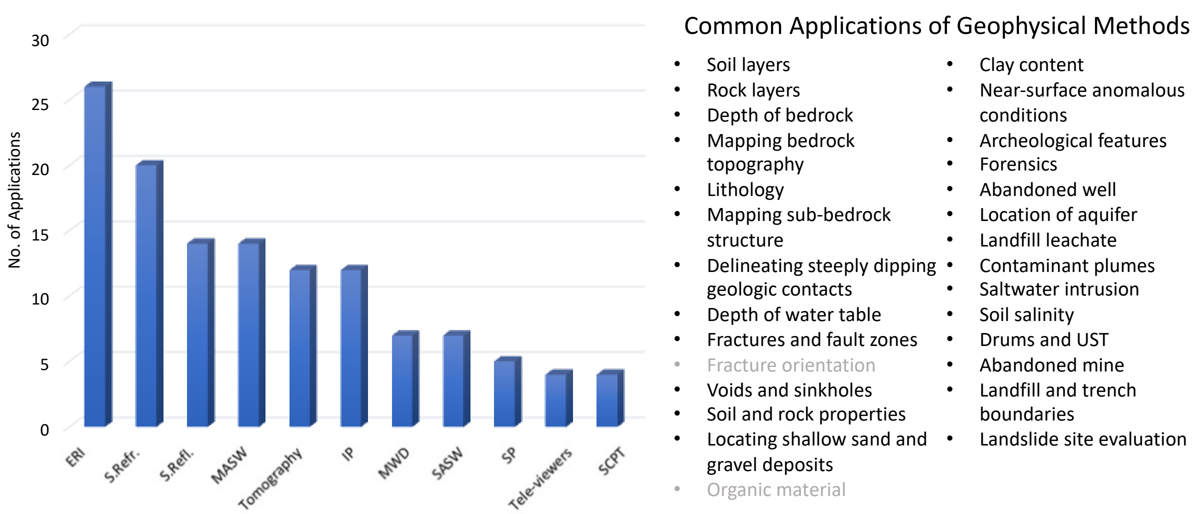

Notes: "ERI" denotes Electrical Resistivity Imaging, "S.Refr." denotes Seismic Refraction, "S.Refl." denotes Seismic Reflection, "MASW" denotes Multi-channel Analysis of Surface Wave, "IP" denotes Induced Polarization, "MWD" denotes Measurements While Drilling, "SASW" denotes Spectral Analysis of Surface Wave, "SP" denotes Self Potential, and "SCPT" denotes Seismic Cone Penetration Test.

Figure 2.1 A comparison of the number of applications of advanced geophysical methods

(Source: Adapted from Shahandashti et al. 2021)

The capital cost of ERI equipment is evaluated at around $60,000 (AGI, IRIS Instrument, GuideLineGeo) and a total annual salary of $210,000 is considered for a crew of three persons to perform the ERI surveys and data analysis. In addition to providing a continuous assessment of subsurface conditions, the ERI incurs no additional costs. On the other hand, aside from the equipment cost of conventional geotechnical site investigation such as CPT and SPT which starts from $150,000 (TMG Manufacturing), the soil test drilling incurs a cost of $156 and $77 per meter of advancement through the depth, respectively (Crisp et al. 2018).

2.2. Electrical Mixing Model

Electrical mixing models describe how the bulk electrical resistivity of a conducting medium is associated with the resistivity of components of porous media. According to Archie (1942), the bulk electrical resistivity of fully saturated coarse-grained soils is related to the geometry of pore spaces and pore fluid's electrical resistivity. Keller and Frischknecht (1966) later expanded Archie's model for partially saturated porous media as given by Equation 2.1.

$$\rho = a\rho_w n^{-m} S^{-p} \quad \text{Eq. 2.1}$$

where ρ is bulk electrical resistivity, ρ_w is pore water resistivity, *a* is compaction constant, *n* is porosity, *S* is degree of saturation, *p* is saturation parameter, and *m* is cementation parameter. The cementation parameter depends on the pore tortuosity and pore network interconnectivity, and the saturation parameter represents the pore water in the soil matrix. The values of a, p, and m are typically obtained by regression analyses (Bryson 2005).

A generalized form of Archie's model for fine-grained soil that includes the effect of surface conductivity in the cementation factor is as follows (Shah and Singh 2005):

$$\sigma_b = c\sigma_w\theta^m \quad \text{Eq. 2.2}$$

where σ_b is bulk electrical conductivity, c is a fitting parameter, σ_w is pore water conductivity, θ is volumetric water content, and m is cementation parameter. The values of c and m are calculated by Equations 2.3 and 2.4 for soils with a clay fraction above 5%.

$$c = 0.6\ CL^{0.55} \quad \text{Eq. 2.3}$$

$$m = 0.92\ CL^{0.2} \quad \text{Eq. 2.4}$$

where CL is the percentage of clay. For soils with less than 5% clay fractions, values of 1.45 and 1.25 are considered for c and m. In clayey soils, the electrical current flows through pore space by the movement of ions in pore water and surface charges at the soil and water interface (Rhoades et al. 1989). Therefore, the specific surface area and surface conductance of clayey soil particles, which also correlate with the residual friction angle (Tiwari and Marui 2005), affect the electrical resistivity (Klein and Santamarina 2003).

2.3. Existing Relationships between Geotechnical Properties and Electrical Resistivity Values

2.3.1. Regression Analysis

The regression analysis has a variety of applications in assessing construction and transportation infrastructure resiliency (Zamanian et al. 2024; Darghiasi et al. 2023b and 2023c; Zamanian and Shahandashti 2022). Likewise, in the field of geotechnical engineering, various empirical and analytical studies have been conducted to develop statistical models using linear, power, and exponential regression functions to investigate the effects of different hydraulic and solid phase properties of clayey soils on electrical resistivity. Among the hydraulic properties, soil water content has been identified as one of the significant factors affecting soil electrical resistivity (Zamanian and Shahandashti 2022; Robinson et al. 2008; Samouelian et al. 2005; Friedman 2005). Besson et al. (2010) also showed that 48% of the total variations of the electrical resistivity are attributed to the volumetric water content of the soil. The soil's electrical resistivity decreases as the water content increases since the electrical current is transmitted through the movement of ions in pore water (Siddiqui and Osman 2012). The indirect relationship between the water content and electrical resistivity of clayey soils was also identified by Shahandashti et al. (2021), Rezaei et al. (2018), Abidin et al. (2013), Siddiqui and Osman (2012), Kibria and Hossian (2012), and Michot et al. (2003). Abu-Hassanein et al. (1996) investigated the effect of degree of saturation on the soil's electrical resistivity. They concluded that an increase in the degree of saturation of clayey soil leads to a decrease in the electrical resistivity values. Rinaldi and Cuestas (2002) showed that the void ratio (one of the controlling factors of gravimetric water content) significantly affects electrical resistivity variations. The electrical resistivity of clayey soil decreases as the dry unit weight increases while keeping gravimetric water content constant (Lin et al. 2016). Nevertheless, the variability of electrical resistivity is less sensitive to the variations of dry unit weight than the gravimetric water content, and it is almost negligible at the gravimetric water contents above 30% (Kibria and Hossain 2012). Rashid et al. (2018) observed a 50% reduction in the electrical resistivity for a 20% increase in the dry density. An increase in dry density results in less pore space and more interparticle contacts, decreasing soil resistance to electrical current flow. The rate of reduction in the electrical resistivity with increasing dry density depends on soil type. In another study, Alsharari et al. (2020) assessed the combined effects of gravimetric water content, dry unit weight, salinity, and percentage of a clay mineral on the variability of electrical resistivity of clayey soils using multiple regression analysis. The effects of Atterberg limits on the variations of electrical resistivity were studied by Abu-Hassanein et al. (1996) and Long et al. (2012). They showed that the lower electrical resistivity values are associated with the higher plasticity index/liquid limit measures. Lin et al. (2016) also showed that the electrical resistivity of clayey soils is more correlated to the plasticity index than the liquid limit. Abu-Hassanein et al. (1996) also concluded that the percentage of fines (percent of soil finer than 75 microns) or percentage of clay (percent of soil finer than 2 microns) of soils impacts the electrical resistivity of fine-grained soils. Soils with more percentage of fines and clays yield lower electrical resistivity values because they have higher specific surface areas, which promotes the transmission of electrical current (Morin 2006).

Tables 2.1 to 2.3 show examples of empirical studies relating the electrical resistivity value to the geotechnical properties. The standard linear regression model has been widely used to explain the variability of electrical resistivity with the water content, plasticity index, void ratio, and porosity. The second-order regression models (quadratic regression models) are proposed by Lin et al. (2016) and Kibria and Hossain (2012) to study the effects of unit weight on the variations of electrical resistivity values. The power law and exponential regression functions have also been used to provide estimates for the unit weight, degree of saturation, and porosity using electrical resistivity values.

Table 2.1 Examples of empirical studies relating electrical resistivity to the geotechnical properties (before 2010)

Authors	Soil type	No. of data points	Correlation	Parameter values [a]	Coefficient of determination
Goyal et al. 1996			Linear, w-ρ	a = 500, b = -10	0.980
Michot et al. 2003	Loamy clay	30-250	Linear, w-ρ	a = 28.5 to 37.7, b = -0.05 to 0.36	0.212 – 0.941
Cosenza et al. 2006	Sand and clay	20	Power law, ρ-w	a = 1.187, b = -2.444	0.821
Fallahsafari et al. 2010	Clay	25	Exponential, w-ρ	a = 21.66, b = -0.19	0.619
			Exponential, γ_d-ρ	a = 11426, b = 0.181	0.568
			Linear, e-ln(ρ)	a = 0.702, b = -0.36	0.484
			Linear, n-ln(ρ)	a = 0.415, b = -0.18	0.480

Notes: "ρ" denotes electrical resistivity, "w" denotes water content, "γ" denotes bulk unit weight, "γ_d" denotes dry unit weight, "PI" denotes plasticity index, "e" denotes void ratio, "n" denotes porosity, and "S_r" denotes degree of saturation.

[a] *Coefficient of a, b, and c represent constant parameters in the linear ($\boldsymbol{y}=a+b.\boldsymbol{x}$), power law ($\boldsymbol{y}=a.\boldsymbol{x}^b$), exponential ($\boldsymbol{y}=a.exp(b.\boldsymbol{x})$), and quadratic ($\boldsymbol{y}=a.\boldsymbol{x}^2+b.\boldsymbol{x}+c$) regression functions.*

Table 2.2 Examples of empirical studies relating electrical resistivity to the geotechnical properties (between 2012 and 2014)

Authors	Soil type	No. of data points	Correlation	Parameter values [a]	Coefficient of determination
Kibria and Hossain 2012	Clay	59	Linear, ρ-w	a = 119.26 to 328.03,	0.810 – 0.880
				b = -1.094 to -1.351	
			Power law, ρ-S_r	a = 2.41 to 2.73,	0.550 – 0.960
				b = -1.64 to -0.58	
			Quadratic, ρ-γ	a = 0.095 to 0.7107,	0.98 – 1.0
				b = -24.541 to 3.461,	
				c = 34.099 to 217.98	
Siddiqui and Osman 2012			Linear, w-ln(ρ)	a = 0.644, b = -0.0451	0.659
			Power law, γ-ρ	a = 14.999, b = 0.0353	0.368
Abidin et al. 2013	Clayey silt	25	Power law, w-ρ	a = 121.88, b = -0.363	0.69 - 0.89
				a = 109.98, b = -0.268	
Osman et al. 2014	Clay	16	Power law, w-ρ	a = 81.12, b = -0.34	0.818
Akinlabi and Adeyemi 2014		7	Linear, PI-ρ	a = 29.04, b = - 0.002	0.920

Notes:

[a] *Coefficient of a, b, and c represent constant parameters in the linear ($\boldsymbol{y}=a+b.\boldsymbol{x}$), power law ($\boldsymbol{y}=a.\boldsymbol{x}^b$), exponential ($\boldsymbol{y}=a.exp(b.\boldsymbol{x})$), and quadratic ($\boldsymbol{y}=a.\boldsymbol{x}^2+b.\boldsymbol{x}+c$) regression functions.*

Table 2.3 Examples of empirical studies relating electrical resistivity to the geotechnical properties (between 2016 and 2021)

Authors	Soil type	No. of data points	Correlation	Parameter values [a]	Coefficient of determination
Lin et al. 2016	Marine clay		Power law, w-ρ	a = 427.8, b = -1.13	0.930
			Exponential, PI-ρ	a = 124.34, b = -0.239	0.850
			Linear, e-ln(ρ)	a = 4.1663, b = -1.458	0.880
			Quadratic, γ-ρ	a = 0.16, b = -0.0166, c = 20.6	0.720
Jusoh and Osman 2017	Clay		Power law, w-ρ	a = 123.93, b = −0.252	0.816
			Linear, PI-ln(ρ)	a = 29.793, b = -2.71	0.634
Hazreek, et al. 2018	Clayey silt	25	Power law, w-ρ	a = 110.68, b = -0.347	0.938
Rezaei et al. 2018		15	Power law, ρ-w	a = 2028.2, b = -1.496	0.68
Shahandashti et al. 2021	Clay	842	Linear, $\rho^{-0.5}$-ln(w)	a = -0.3267, b = 0.215	0.66

Notes:

[a] *Coefficient of a, b, and c represent constant parameters in the linear ($\boldsymbol{y}=a+b.\boldsymbol{x}$), power law ($\boldsymbol{y}=a.\boldsymbol{x}^b$), exponential ($\boldsymbol{y}=a.exp(b.\boldsymbol{x})$), and quadratic ($\boldsymbol{y}=a.\boldsymbol{x}^2+b.\boldsymbol{x}+c$) regression functions.*

2.3.2. Artificial Intelligence Techniques

Artificial Intelligence (AI) techniques have the potential to revolutionize designs, construction, and maintenance of the infrastructure systems by providing advanced analytics, automation, and predictive capabilities (Zamanian et al. 2023a; Darghiasi et al. 2023a; Baral et al. 2022). In the field of geotechnical engineering, researchers adopted AI techniques such as artificial neural networks and support vector machines to establish relationships between the geotechnical properties and electrical resistivity values. Alsharari et al. (2020) compared the performance of multivariate linear regressions with non-linear regressions and artificial neural networks (ANNs) in quantifying the soil electrical resistivity based on water content, dry unit weight, pore water salinity, and percentage of fine and coarse grains of soils. They found that non-linear regressions perform better than linear regressions in explaining the non-linear and complex interdependencies between the electrical resistivity values and geotechnical properties; however, both models show higher prediction errors than the ANNs. Other researchers also explored the applicability of the ANNs in predicting the soil electrical resistivity based on geotechnical properties. Bian et al. (2015) adopted the ANNs to estimate the electrical resistivity values based on water content, degree of saturation, and porosity. In a similar study, Rashid et al. (2018) performed an experimental study to investigate the variations in the electrical resistivity values of kaolinite-dominant clay liners due to variations in water content and dry unit weight. They developed ANNs to predict electrical resistivity values and concluded that ANNs could be used to assess the level of heterogeneity of compacted clay liners.

Samui (2013) examined the application of Support Vector Machines (SVMs) and Least Square Support Vector Machines (LSSVMs) in investigating the associations between electrical resistivity and soil thermal resistivity, coarse-grained fraction, and degree of saturation. He compared the accuracy of the developed SVMs and LSSVMs with ANNs and found that the SVMs and LSSVMs outperform the ANNs, with a slightly better performance of LSSVMs over SVMs. Likewise, Samui (2014) found that the ANNs do not perform as well as Gaussian Process Regression (GPR) in quantifying the soil electrical resistivity values based on the soil thermal resistivity, degree of saturation, and coarse-grained fraction. Although ANNs are more flexible at handling non-linear interactions between the variables, feature extraction and feature engineering are still necessary before training the networks to improve prediction accuracy. In other words, the ANNs cannot derive meaningful features from the unprocessed data due to their shallow structures (Abediniangerabi et al. 2021).

2.4. Gaps in Knowledge

While previous studies have shed light on the correlations between geotechnical properties and electrical resistivity values, there remain significant gaps in understanding the spatial effects of geotechnical properties on electrical resistivity values, as well as the non-linear and complex interactions between them. The following gaps were identified from the literature:

1) The presence of spatial autocorrelation between the geotechnical properties and electrical resistivity values in clayey soil has not been studied.
2) There is a lack of an analytical tool to extract meaningful information among non-linear and complex relationships between electrical resistivity values and geotechnical properties.

2.5. Research Objectives

The objectives of this research are to:

1) Assess the presence of spatial association between electrical resistivity and geotechnical properties. If so, determine the most appropriate spatial regression model to explain the variability of electrical resistivity values considering the spatial effects of geotechnical properties.

2) Explore non-linearity and complexity of interactions between the electrical resistivity values and geotechnical properties using artificial intelligence techniques with deep structures such as deep learning model.

The following chapters present the work performed to achieve the research objectives.

CHAPTER 3 EXPLORING SPATIAL ASSOCIATION BETWEEN ELECTRICAL RESISTIVITIES AND GEOTECHNICAL PROPERTIES USING SPATIAL REGRESSION ANALYSIS

Accurate estimation of geotechnical properties and characterization of spatial distributions of geotechnical properties at a site are critical for any successful construction or development activity, especially when considering reliability-based designs such as load and resistance factor design (LRFD) method (Shahandashti et al. 2023). This chapter aims to explore the spatial association between the electrical resistivity values and geotechnical properties (Zamanian and Shahandashti 2023).

3.1. Methodology

3.1.1. Design of Experiments

A full factorial design was established to investigate the effects of water content and dry unit weight on the electrical resistivity of various soil samples with different fine/clay fractions and plasticity indices. A full factorial design generates observations by all possible combinations of factor levels in each complete experiment; it is particularly useful in studying the factor effects when the number of factors is less than five (Zamanian and Yazdandoust 2021 and 2022; Antony et al. 2014; Davim 2012). The water content and dry unit weight were studied at four and three levels. The factors and corresponding factor levels are shown in Table 3.1. The design resulted in at least 12 experimental runs for each soil sample.

Table 3.1 Factors and corresponding factor levels in experimental design

Factor	Unit	Factor Levels			
		1	2	3	4
Water content	%	10	20	30	40
Dry unit weight	kN/m^3	11.8	13.4	14.9	-

3.1.2. Data Collection

Soil Sample Collection

A total of 44 soil samples were obtained from 13 locations (in four districts) across the state of Texas, US. Figure 3.1 shows the number of boreholes and obtained soil samples on the map of Texas.

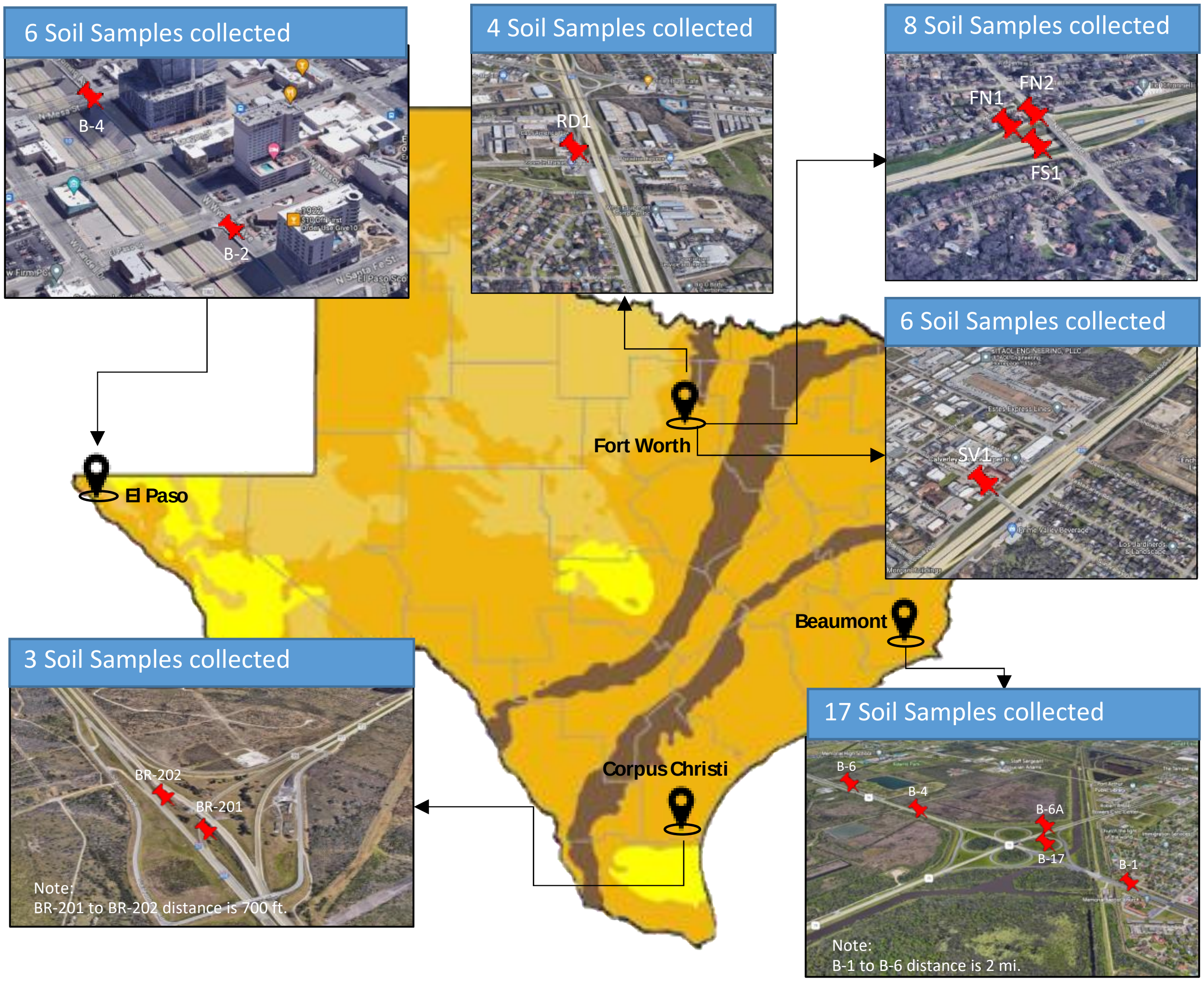

Over 50 percent of these areas are underlain by soils with abundant clays of high swelling potential

Less than 50 percent of these areas are underlain by soils with clays of high swelling potential

Less than 50 percent of these areas are underlain by soils with abundant clays of light to moderate swelling potential

These areas are underlain by soils with little to no clays with swelling potential

Figure 3.1 Number of boreholes and collected soil samples on clay map of Texas, US

(Source: Clay map adapted from Olive et al. 1989)

The selected locations are situated in four TxDOT districts in the East, West, South, and North of Texas (Beaumont, Corpus Christi, Fort Worth, and El Paso), representing various TxDOT operational environments and geotechnical conditions. The criteria for selection of these districts include but are not limited to:

- diverse geotechnical characteristics (e.g., soil type, topography, etc.)
- various levels of rainfalls or frequent wetting and drying cycles
- having the most recent projects, which included subsurface investigation (especially those that have problems with the subsurface investigation)

Figures 3.2 to 3.4 illustrates the general soil map, annual average precipitation map, and annual average temperature map of Texas, respectively.

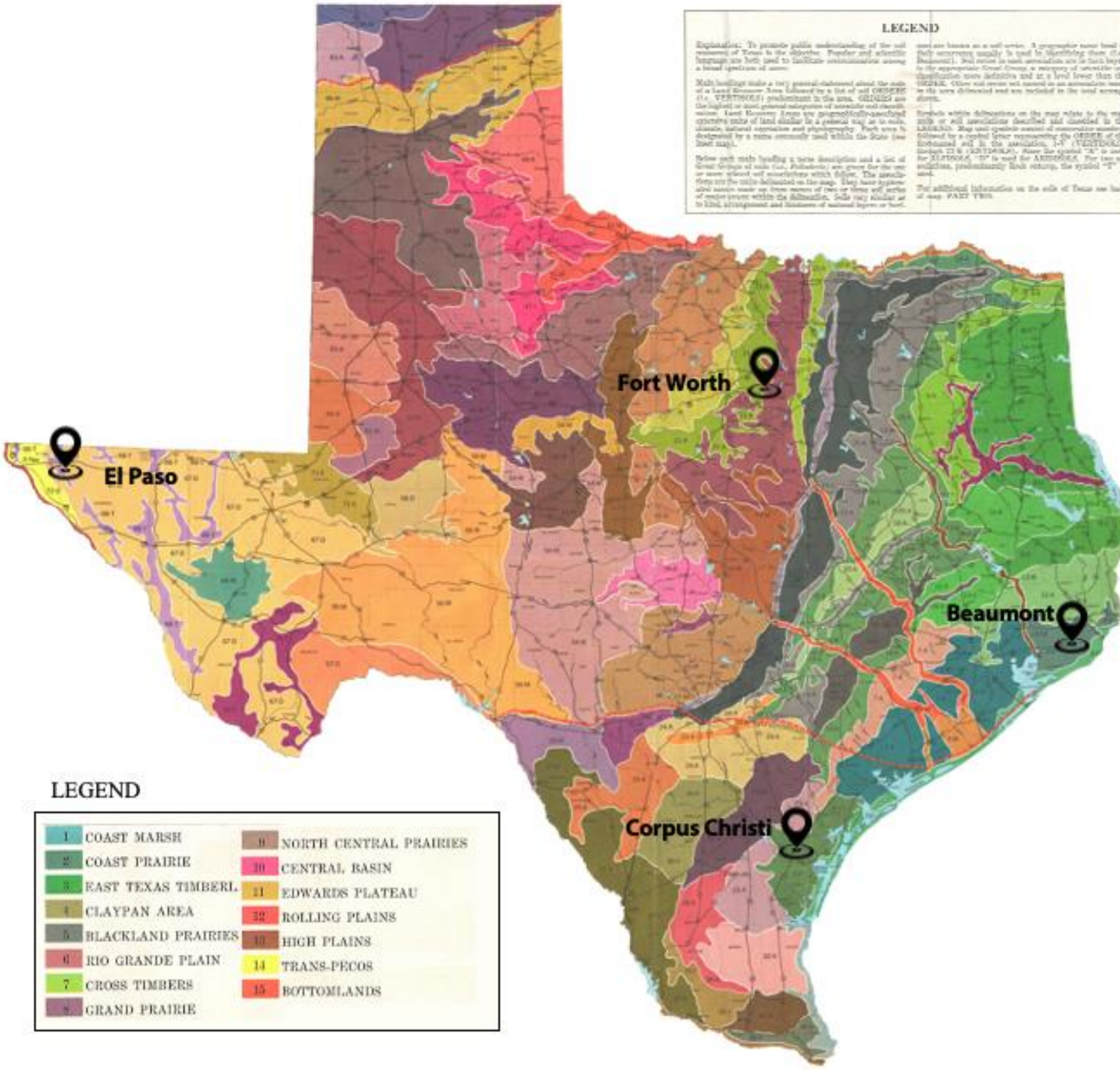

Figure 3.2 General soil map of Texas

(Source: Adapted from Godfrey et al. 1973)

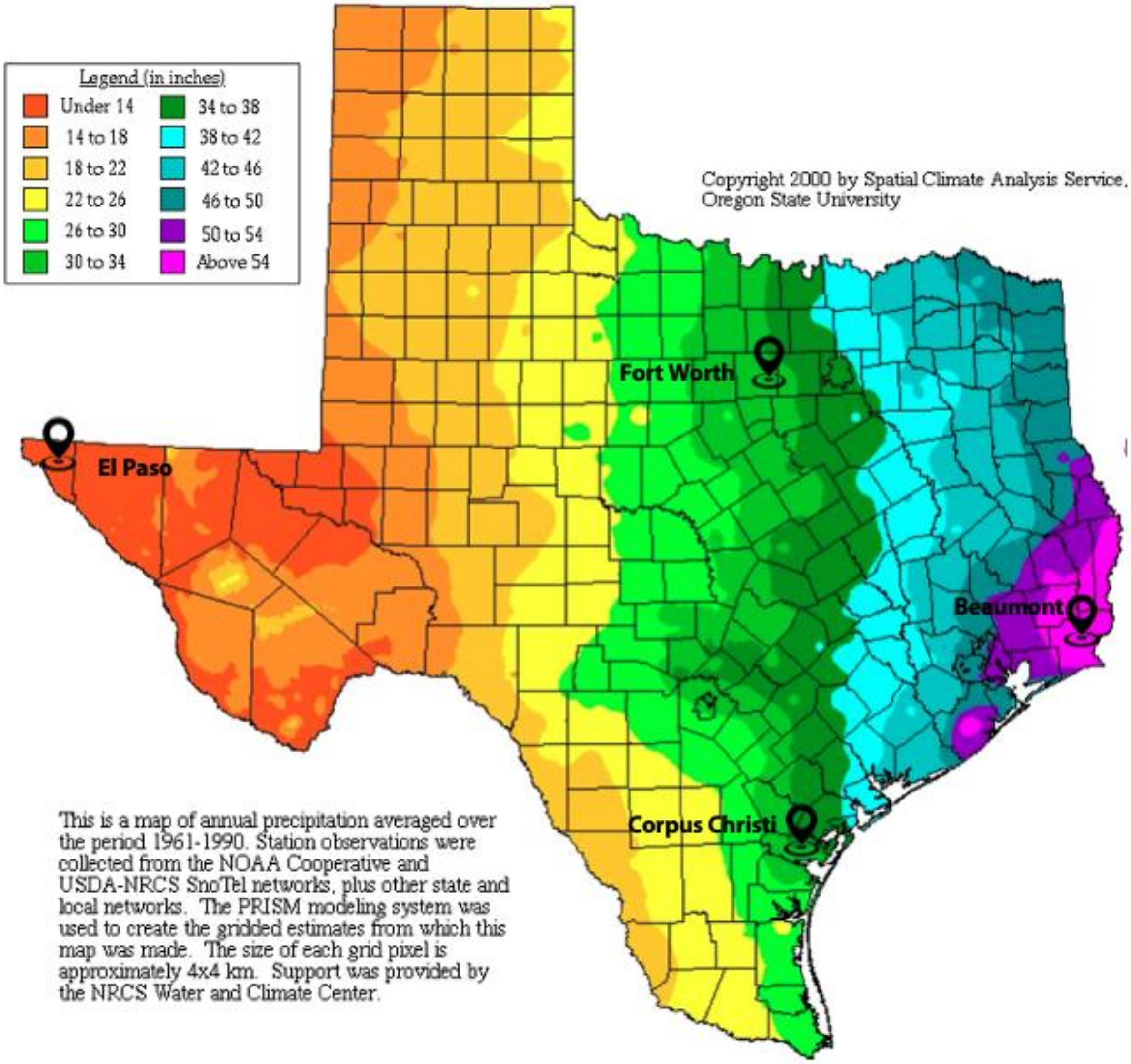

Figure 3.3 Annual average precipitation map of Texas

(Source: Adapted from Spatial Climate Analysis Service, 2000)

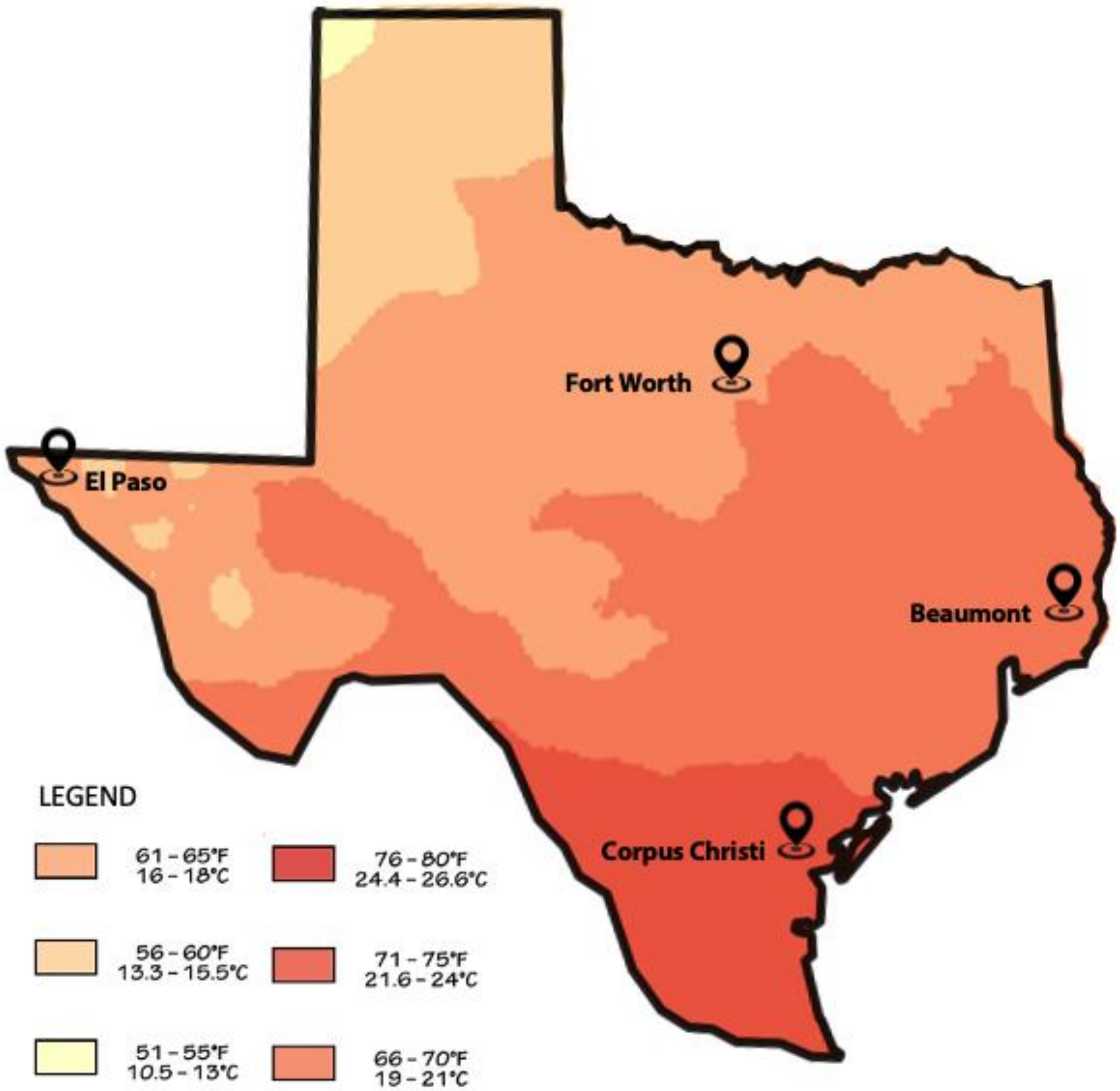

Figure 3.4 Annual average temperature map of Texas

(Source: Adapted from Paleontological Research Institution)

Laboratory Testing to Collect Data

Specific Gravity: Specific gravity of soil samples was measured using a water pycnometer according to ASTM D854-14 standard test method. About 50 grams of dried soil material passing the No. 10 (2.00 mm) sieve used in the test. The soil was added to the pycnometer, and the pycnometer was filled about one-half with distilled water. The weights of the empty pycnometer and pycnometer with specimens were measured separately. To remove the entrapped air between the soil particles, a partial vacuum was applied. It is started by applying a low vacuum and then the vacuum level was increased gradually until the water in the flash boils. Then, water was added up to the graduation mark of the pycnometer and weighted. The distilled water was poured in a clean pycnometer, and the combined weight was measured. Using the equations presented in ASTM D54-14, the specific gravity of soil was determined. Figure 3.5 shows the testing procedure on the clayey soil specimens.

Figure 3.5 Specific gravity testing of soil

(Source: Shahandashti et al. 2021)

<u>Atterberg Limits:</u> The performing agency determined the Atterberg limit (liquid limit and plastic limit) of the soil samples according to ASTM D4318-17 standard test method. These tests were conducted on materials passing the No. 40 (0.475-mm) sieve.

Liquid limit is defined as the water content, in percent, of a cohesive soil at the arbitrarily defined boundary between the semi-liquid and plastic states (ASTM D4318-17). First, to conduct the test, small increments of distilled water was added into the soil using a spray bottle to apply a uniform mist of water to the sample. Then, a sufficient amount of soil was placed in the liquid limit device cup, flattened, and finally divided using a grooving tool at the point of maximum thickness. The cup was lifted and dropped at a rate of 2 drops per second until the groove closure was about 13 mm (appropriate water contents should yield to 15 to 35 number of blows). The test was repeated three times with different water contents. Then to determine the water content, samples were dried in the oven at 100-110 degrees of Centigrade for 24 hours. The water content corresponding to 25 blows was considered as the liquid limit of the soil specimen. Figure 3.6 illustrates the testing procedure using the liquid limit device.

Figure 3.6 Liquid limit testing: (a) the soil is flattened in the device cup, and (b) a groove was made at the center

(Source: Shahandashti et al. 2021)

Plastic limit is defined as the lowest water content, in percent, of a cohesive soil at the boundary between the plastic and semi-solid states (ASTM D4318-17). First, to determine the plastic limit, distilled water was added into the soil and kneaded repeatedly. Then a sufficient amount of soil was placed on a glass plate and rolled back and forth until threads of about one-eighth inch in diameter (3 mm) were formed and broken into pieces. Then to determine the water content, samples were placed and dried in the oven at 100-110 degrees of Centigrade for 24 hours. The water content corresponding to this stage was considered as the plastic limit of the soil specimen. Figure 3.7 illustrates the rolling device and the state of cracked threats resulted from the experiment.

(a) (b)

Figure 3.7 Plastic limit testing (a) Rolling device and (b) cracked and broken threats of 3 mm

(Source: Shahandashti et al. 2021)

<u>Particle Size Distribution:</u> The performing agency determined the particle size distribution of fine-grained soil using the hydrometer method according to ASTM D7928-17 standard test method. The test was performed on material passing the No. 10 (2.0-mm) or finer sieve.

First, approximately 5.0 grams of sodium hexametaphosphate was dissolved in water and added to the sedimentation specimen. The contents were completely mixed with a spatula until all of the soil aggregations are broken-up. The slurry should be soaked overnight (at least 12 hours). Then the slurry was dispersed using a stirring device and transferred into the hydrometer cylinder. A sufficient amount of distilled water was added to bring the level of the water to 1000 ml. Then the cylinder was placed in a constant temperature water bath.

When the soil suspension reaches the temperature of the bath, its contents were completely agitated for about one minute. Then the hydrometer cylinder was placed on the table, and immediately the hydrometer was lowered into the suspension, and the time was recorded. The peak of the meniscus formed on the stem of hydrometer was read to the nearest 0.5 g per liter at the end of two minutes from the time the graduate was set on the table. The cylinder was removed and again placed into the constant temperature bath. The hydrometer readings were obtained at time intervals of 1, 2, 4, 15, 30, 60, 240, and 1440 minutes after the beginning of sedimentation. Figure 3.8 shows the hydrometer test on the clayey soil specimens. Using the equations presented in ASTM D7928-17, particle diameters and the percent finer than a specific diameter were determined.

Figure 3.8 Particle size distribution testing using the hydrometer procedure

(Source: Shahandashti et al. 2021)

Laboratory Electrical Resistivity Test: A four-electrode soil box, current source, resistance measuring equipment, and electrical connections were used to conduct the laboratory testing. First, a specific amount of water was added to the soil and mixed. Then, the soil was placed in the resistivity box and compacted to reach the desired compaction. The soil water contents and dry unit weights were altered from 6 to 45% and 10.2 to 15.7 kN/m3 (60 to 100 pcf), respectively. After the installation of equipment, direct current was applied using two electrodes located at the end of the resistivity box, and the potential drop was measured between two points at the specimen by the AGI SuperSting R8 instrument (ASTM G57-20 2020). The preparation of soil specimens and experimental setup of laboratory resistivity testing are illustrated in Figure 3.9.

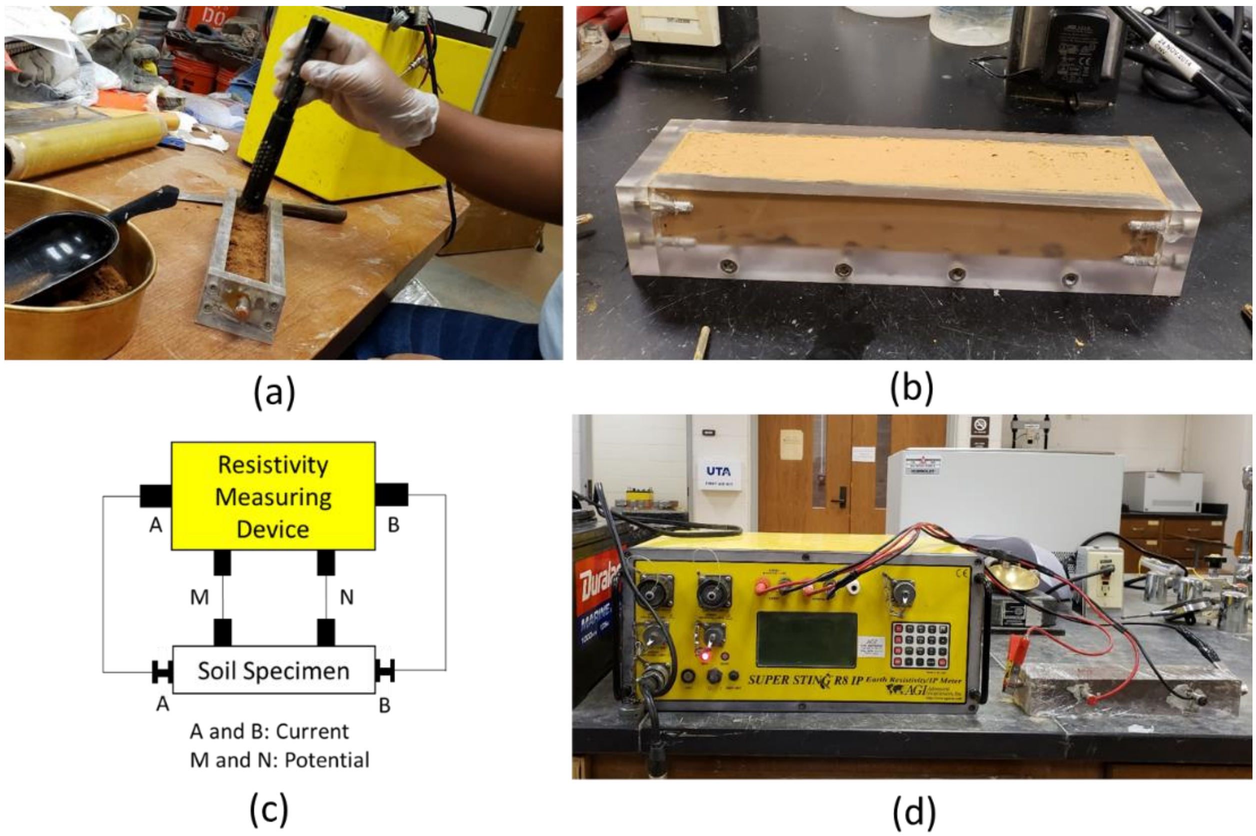

Figure 3.9 (a) and (b) preparation of soil specimens, (c) a schematic setup of laboratory electrical resistivity test, and (d) experimental setup of laboratory resistivity test

(Source: Shahandashti et al. 2021)

The measured electrical resistivity of soil is a function of the cross-sectional area of the soil box and electrode spacings (ASTM G57-20 2020) and can be expressed by $\rho = AR/d$, where ρ is electrical resistivity (Ω.m), A is the cross-sectional area of the soil box perpendicular to the current flow (m^2), d is the inner distance between the potential electrodes (m), and R is the electrical resistance according to Ohm's law. To eliminate the variability of electrical resistivity measurements because of temperature variations, the measured electrical resistivity values were corrected at a reference temperature of 15.5°C (60°F) using the following equation (ASTM G57-20):

$$\rho_{15.5} = \rho_T \ \frac{(24.5+T)}{40} \qquad \text{Eq. 3.1}$$

where $\rho_{15.5}$ is the corrected electrical resistivity at 15.5°C, ρ_T is the electrical resistivity measured at the temperature of T°C.

A total of 627 data points were collected from the laboratory physical property tests (e.g., gravimetric water content, Atterberg limits, and specific gravity) and laboratory electrical resistivity tests. Table 3.2 shows the basic statistics for the independent and dependent variables.

Table 3.2 Basic statistics for the dependent and independent variables

Parameters	Abbreviation	Minimum Value	Maximum Value	Mean	VAR	n
Water content	ω (%)	6.6	44.4	23.4	104.2	627
Dry unit weight	γ_d (kN/m^3)	10.2	15.7	12.5	1.3	627
Plasticity index	PI (%)	10.6	46.5	28.2	60.7	627
Specific Gravity	G_s	2.6	2.7	2.6	0.0003	627
Electrical resistivity	ρ ($\Omega.m$)	2.3	810.8	24.1	3513.2	627

3.1.3. Spatial Autocorrelation

Spatial autocorrelation (i.e., spatial dependence) is the degree of dependency among similar/dissimilar neighboring observations and mainly emerges when the observations are collected from different locations in space. Linearity, homoscedasticity, independence, and normality are some critical assumptions associated with the linear regression model (Neter et al. 1996). The model assumptions need to be checked before making inferences regarding the model estimates by evaluating the residual plots and performing diagnostic tests such as the Breusch-Pagan test for homoscedasticity, Shapiro-Wilk test for normality, and Moran's I test for spatial autocorrelation. If any of the assumptions are violated, the OLS model is inappropriate and statistical inferences from the model are unreliable (Voss et al. 2006). This study collected data from different locations and investigated the spatial association between the electrical resistivity values and geotechnical properties. Moran's I test was used to examine the existence of an overall clustering in the OLS regression residuals. The Moran's I test is represented as follows:

$$I = \frac{n}{\sum_i \sum_j w_{ij}} \frac{\sum_i \sum_j w_{ij}(x_i - \bar{x})(x_j - \bar{x})}{\sum (x_i - \bar{x})^2} \qquad \text{Eq. 3.2}$$

where *n* is the number of spatial units, *x* is the variable of interest, $\bar{x}$ is the mean of *x*, and w_{ij} is an element of a spatial weight matrix. The spatial weight matrix (**W**) identifies the spatial structure of the observations. Each element of this matrix defines the dependency between two observations (Getis 2009). The spatial weight matrix has different experimental forms based on the geometry of the spatial units, either by their boundaries or distances from each other (Anselin 2005). The selection of a proper weight function is essential to achieve convincing results from spatial modeling, especially when the spatial autocorrelation is strong (Yan-guang 2009; Elhorst 2010). General distance between the locations of the collected soil samples was utilized in this study to identify the neighboring structure of the observations and construct the spatial weights. Figure 3.10 shows an example of the data points arrangement (i.e., borehole locations) and neighboring structure of the observations based on their distances.

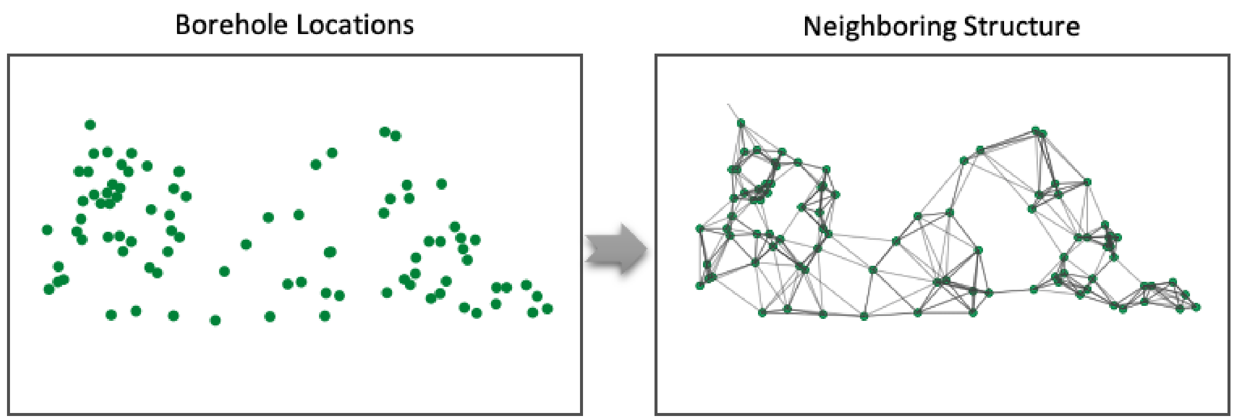

Figure 3.10 An example of the data points arrangement (i.e., borehole locations) and neighboring structure of the observations based on their distances.

The distance-based weight matrices are the most appropriate form for a data set with point locations (Anselin and Sergio 2014). If "d_{ij}" denotes the distance between the location of i and j, and "d" indicates a distance threshold where direct spatial influence between the observations no longer exists, the spatial weights of the corresponding weight matrix are constructed as follows (Chen 2012):

$$w_{ij} = \begin{cases} 1 \quad , & 0 \leq d_{ij} \leq d \\ 0 \quad , & d_{ij} > d \end{cases} \qquad \text{Eq. 3.3}$$

which gives a binary matrix of 0 and 1. Typically, there is no unique approach to determine the threshold distance for identifying the neighboring locations (Walker et al. 2000; Anselin 2005). The most widely used approaches are to assess the robustness of estimated spatial regression models and the magnitude of Moran's I for a series of threshold distances. The distance at which the model shows the maximum log-likelihood value, highest Moran's I value, highest pseudo-R-squared, and lowest residual standard error is determined as the appropriate threshold distance (Wang et al. 2007; Chi and Zhu 2008; Stakhovych and Bijmolt 2009; Elhorst 2010). The other approach is to identify the threshold distance by creating a semi-variogram of the variables (Hession and Moore 2011). The off-diagonal elements of the weight matrix with non-zero values denote the dependency of the neighboring observations. However, the diagonal elements of the weight matrix represent the self-influence of the observations that were excluded from the spatially lagged variables (i.e., diagonal elements of the weight matrix were set to zero). Then the weight matrix was standardized using a row-normalization approach in which all the weights in each row sum to unity ($\sum_{j=1}^{n} w_{ij} = 1$).

The null hypothesis of the Moran's I test is that the regression residuals are randomly distributed in space. By rejecting the null hypothesis, it is concluded that there is evidence of spatially autocorrelated residuals (alternative hypothesis). Ignoring the presence of spatial dependence in the OLS model leads to underestimation or overestimation of actual variance in the case of positive and negative dependence, respectively, which consequently affects the significance of the model (Schabenberger and Gotway 2005; Cressie 2015). Moran's I value ranges from -1 and +1, and its significance is evaluated using a P-value and z-score. The negative values represent the clustering between dissimilar values, while positive values represent the clustering between similar values. The zero value for Moran's I implies that there is no spatial autocorrelation in the regression residuals, and the residuals are randomly distributed.

3.1.4. Spatial Regression Analysis

The spatial dependence between the observations is accounted into a regression model using the spatial weight matrix by three methods; (1) inclusion of the effect of a change in the dependent variable of one location on the dependent variable of a neighboring location (endogenous interaction effects), (2) inclusion of the effect of a change in the independent variables of one location on the dependent variable of a neighboring location (exogenous interaction effect), and (3) inclusion of the effect of dependency in the residuals in one location on a neighboring location (Calderon 2009). In this study, three spatial regression models were examined: Spatial Durbin Model (SDM), Spatial Lag or Autoregressive Model (SAR), and Spatial Error Model (SEM). The SDM is a general model that includes both exogenous and endogenous interaction effects and has the form of:

$$\boldsymbol{\rho}_{\mathbf{15.5}} = \eta \boldsymbol{W} \boldsymbol{\rho}_{\mathbf{15.5}} + \boldsymbol{X\beta} + \boldsymbol{WX\theta} + \boldsymbol{\varepsilon} \qquad \text{Eq. 3.4}$$

where $\boldsymbol{\rho}_{\mathbf{15.5}}$ is an (n×1) vector of observations on the corrected electrical resistivity at 15.5°C (dependent variable), $\boldsymbol{X}$ is an (n×k) matrix of observations on the geotechnical engineering parameters (independent variables), $\boldsymbol{W}$ is an (n×n) matrix of spatial weight, $\boldsymbol{\beta}$ is a (k×1) vector of regression parameters, η is a coefficient on the spatially lagged dependent variable, $\boldsymbol{\theta}$ is a (k×1) vector of the spatially lagged independent variable, and $\boldsymbol{\varepsilon}$ is an (n×1) vector of independently and identically normally distributed errors. In this research, to avoid multicollinearity in the analyses, the geotechnical parameters (degree of saturation, liquid limit, and void ratio) with the lowest significant test statistics that have a high correlation with the other variables were removed from the model. The simple linear regression used gravimetric water content, and the multiple linear regression used gravimetric water content, dry unit weight, and plasticity index as independent variables to explain the variability of electrical resistivity in the analyses. The SAR model only includes the endogenous interaction effects ($\boldsymbol{\theta}$=0 in equation 4) and is expressed as:

$$\boldsymbol{\rho_{15.5}} = \eta \boldsymbol{W} \boldsymbol{\rho_{15.5}} + \boldsymbol{X\beta} + \boldsymbol{\varepsilon} \qquad \text{Eq. 3.5}$$

where the variables are defined as the same for the SDM model. In the SDM model, the beta coefficients of the SAR model are not represented by partial derivatives along the diagonal (Golgher and Voss 2016). Therefore, the changes in the dependent variable in one location due to a one unit increase in the independent variables in the same location (direct effect) and another location (indirect effect) are calculated for SAR models. The direct, indirect, and total effects (i.e., direct and indirect effects) can be presented by the following equations:

$$Direct\ Effect = \frac{1}{n}\ tr\big(S_k(W)\big) \qquad \text{Eq. 3.6}$$

$$Indirect\ Effect = Total\ Effect - Direct\ Effect \qquad \text{Eq. 3.7}$$

$$Total\ Effect = \frac{1}{n}\ i_n'\big(S_k(W)\big)i_n \qquad \text{Eq. 3.8}$$

where $tr(S_k(W))$ is the trace of the partial derivative matrix for variable k, n is the number of spatial units, and i_n is the identity matrix. In contrast, the spatial dependence in the SEM is modeled only by the spatially lagged error terms and considers neither the exogenous nor endogenous interaction effects ($\boldsymbol{\theta}$=0 and η=0 in equation 4), which has the form of:

$$\boldsymbol{\rho}_{\mathbf{15.5}} = \boldsymbol{X\beta} + \boldsymbol{u}\,, \qquad \boldsymbol{u} = \lambda \boldsymbol{W}\boldsymbol{u} + \boldsymbol{\varepsilon} \qquad \text{Eq. 3.9}$$

where $\boldsymbol{u}$ is an (n×1) vector of error terms and λ is a spatial error lag coefficient. The Lagrange Multiplier (LM) tests were performed on the OLS residuals to decide whether the spatial lag (SAR) or spatial error model (SEM) is the most appropriate model for the analysis of the data (Anselin 2005). There are four LM test statistics: standard LM-Error, standard LM-Lag, Robust LM-Error, and Robust LM-Lag. First, the standard LM tests are performed, and then the model with the significance test statistic is selected. If neither of the tests is significant, it indicates that the OLS model is more appropriate. However, if both standard LM tests are significant, which commonly happens in practice, the Robust forms of LM test are used, and the model with the (most) significance test statistic is selected as the most appropriate model (Anselin 2005). Another approach is to start with the widely used model (i.e., SDM) if there is a global effect (Lesage 2014). Then to further evaluate the goodness-of-fit of the nested models (when a complex model can be reduced to a simpler model by restricting certain parameters), the Likelihood Ratio (LR) test was utilized (Anselin 2005). The null hypothesis of the test is that a complex model should be reduced to a simpler model by restricting some of the model parameters. By rejecting the null hypothesis, it is concluded that the complex model is more appropriate and should not be restricted to the simpler model (alternative hypothesis). Log-Likelihood (LIK), Bayesian Information Criterion (BIC) (Schwarz Information Criterion), and Akaike's Information Criterion (AIC) were also used to compare the performance of the non-nested models (Yang and Fik 2014; LeSage 2014). The model with the highest LIK and lowest AIC or BIC was considered the best model that fits the data.

3.2. Results

3.2.1. Results of Standard Regression Analysis

The simple and multiple linear regression models were fitted to the electrical resistivity data to test the performance of OLS models in defining a relationship between the geotechnical parameters and electrical resistivity values and checking the model assumptions. The simple and multiple linear regression models developed using the original data are as follows:

$$\rho = 77.80 - 2.293\ \omega \qquad \text{Eq. 3.10}$$

$$\rho = 283.79 - 2.742\ \omega - 16.840\ \gamma_d + 0.533\ PI \qquad \text{Eq. 3.11}$$

where ρ is electrical resistivity, ω is water content, γ_d is dry unit weight, and PI is plasticity index. Table 3.3 presents the results of the fitted standard regression models (OLS) before and after transforming the electrical resistivity values.

Table 3.3 Summary of results of OLS model before and after transforming the electrical resistivity values

	Multiple Linear Regression		**Simple Linear Regression**	
	OLS with no transformation	OLS using Box-Cox transformation	OLS with no transformation	OLS using Box-Cox transformation
Intercept	283.79**	-0.524**	77.80**	0.093**
Water Content	-2.742**	0.011**	-2.293**	0.010**
Dry Unit Weight	-16.840**	0.038**		
Plasticity Index	0.533*	0.004**		
Adjusted R-squared	0.26	0.76	0.15	0.62
Standard Error of Residual	51.05	0.067	54.5	0.084
LIK	-3353.54	807.23	-3395.57	661.37
AIC	6717.08	-1604.47	6797.14	-1316.73
BIC	6739.29	-1582.27	6810.46	-1303.41
No. of Observations	627	627	627	627

Notes: '' indicates the significance at the 5% level and '**' indicates the significance at the 1% level. "OLS" denotes Ordinary Least Squares, "LIK" denotes Log-Likelihood, "AIC" denotes Akaike's Information Criterion, and "BIC" denotes Bayesian Information Criterion.*

According to Table 3.3, from the initial analysis using multiple linear regression with no transformation, the regression coefficients show statistically significant negative values for gravimetric water content and dry unit weight (at the 5% significance level) and a positive value for plasticity index (at the 1% significance level). The negative regression coefficients imply that the gravimetric water content and dry unit weight have inverse relationships with the electrical resistivity values. For example, a unit increase in the gravimetric water content results in a 2.742 decrease in the electrical resistivity, keeping other independent variables constant. However, the positive regression coefficient for the plasticity index shows a direct relationship with the electrical resistivity value, which is inconsistent with the literature. Figures 3.11 and 3.12 illustrate the residual plots of the OLS regression model with no transformation of the electrical resistivity values. The presence of a funnel in the plot of residuals versus fitted values and skewness in the normal probability plot are indications of heteroskedasticity and non-normality of the error terms, respectively. Besides, as shown in Table 3.4, the Breusch-Pagan test and Shapiro-Wilk test show that the assumptions of homoskedasticity and normality of the linear regression model are not satisfied (rejection of null hypotheses at the 10% level of significance). The results of simple linear regression agree with those of multiple linear regression. Therefore, the electrical resistivity values were transformed using the Box-Cox transformation to stabilize the error variance and mitigate the problem of non-normality of the error terms.

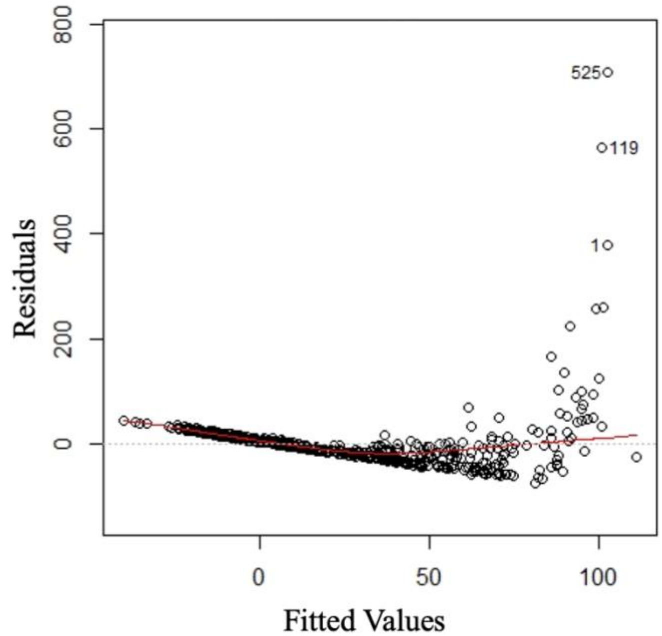

Figure 3.11 Residuals versus fitted values for the OLS model with no transformation on the electrical resistivity values.

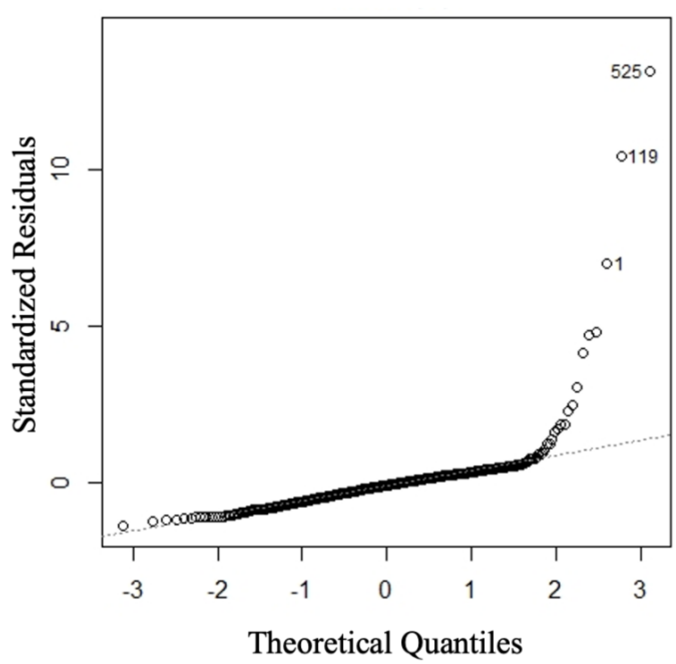

Figure 3.12 Normal probability plot for the OLS model with no transformation on the electrical resistivity values.

Table 3.4 Diagnostic test results for multiple linear regression before transformation

Test	Value	Prob
Shapiro-Wilk	0.4710	0.0000
Breusch-Pagan	29.311	0.0000

The regression analysis using a Box-Cox transformation yielded the following equations:

$$\rho^{-0.5} = 0.093 + 0.010\ \omega \qquad \text{Eq. 3.12}$$

$$\rho^{-0.5} = -0.524 + 0.011\ \omega + 0.038\ \gamma_d + 0.004\ PI \qquad \text{Eq. 3.13}$$

The results of the OLS analysis with the transformed dependent variable (λ=-0.5) are presented in Table 3.3. The regression coefficients for gravimetric water content, dry unit weight, and plasticity index show statistically significant positive values (at the 5% level of significance). Note that the positive signs mean that the independent variables directly correlate with the inversed electrical resistivity values. In other words, the results imply that the gravimetric water content, dry unit weight, and plasticity index have significant inverse relationships with the electrical resistivity value, which is consistent with the literature. Figures 3.13 and 3.14 illustrate the residual plots of the OLS regression model using Box-Cox transformation on the electrical resistivity values. No clear pattern can be observed in the plot of residuals versus fitted values shown in Figure 3.13. Table 3.5 presents the diagnostic test results for multiple linear regression after transformation. The Breusch-Pagan test also shows that the assumption of the constant variance of error terms is satisfied after transformation at the 1% level of significance. The skewness of data in the normal probability plot is removed after transforming the electrical resistivity values; however, it can be observed that the residuals are less spread than the normal distribution (lighter-tailed). The Shapiro-Wilk test also confirms that the normality assumption is violated (rejection of null hypothesis at the 10% level of significance). Although the non-normality of error terms has remained even after transformation, no more transformations were used since the OLS model is relatively robust to non-normality in the absence of skewness (Neter et al. 1996). The diagnostic tests showed similar results for the simple linear regressions.

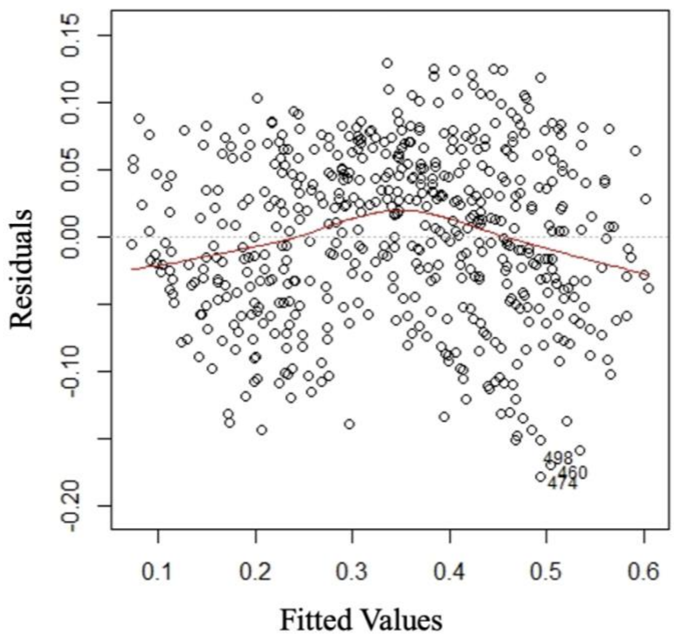

Figure 3.13 Residuals versus fitted values for the OLS model with transformed electrical resistivity values.

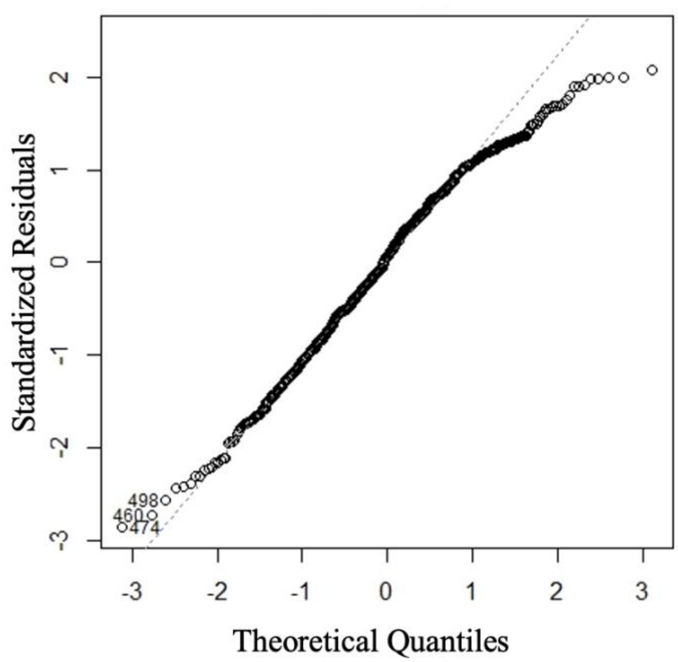

Figure 3.14 Normal probability plot for the OLS model with transformed electrical resistivity values.

Table 3.5 Diagnostic test results for multiple linear regression after transformation

Test	Value	Prob
Shapiro-Wilk	0.9857	0.0000
Breusch-Pagan	27.185	0.0101*

Note: '' indicates the significance at the 1% level.*

The Moran's I test provides strong evidence of positive spatial autocorrelation (Table 3.6) in the regression residuals, implying that the residuals are not independently distributed. According to Table 3.6, although the Moran's I value for multiple linear regression is greater than its value for simple linear regression, the higher z-score for simple linear regression indicates a stronger spatial autocorrelation between the regression residuals for simple than multiple linear regression (i.e., the greater the z-score, the stronger the spatial autocorrelation). Since the assumption of independence of the linear regression is violated, the OLS model might be an inappropriate approach to quantify the relationship between electrical resistivity and geotechnical properties. Besides, any statistical inferences regarding the coefficient estimates might be unreliable. Therefore, the spatial regression models were examined to account for the spatially autocorrelated residuals.

Table 3.6 Summary of results of Moran's I tests for the OLS residuals

	Multiple Linear Regression	Simple Linear Regression
Moran's I	0.281	0.152
P-value	0.000*	0.000*
z-score	32.872	44.714

Notes: '' indicates the significance at the 1% level.*

3.2.2. Results of Spatial Regression Analysis

The simple and robust forms of Lagrange Multiplier tests (LM) were used on the OLS results to determine the most appropriate spatial model for the analysis. Table 3.7 presents a summary of the results of LM tests for the simple and multiple linear regression models. Since both simple tests (LM error and LM lag) are highly significant and suggest using the spatial regression models, the robust form of LM error and LM lag tests were tested. The robust tests also show highly significant values for both SAR and SEM; however, it appears that the test statistic for the spatial error model (SEM) is more significant.

Table 3.7 Summary of results of Lagrange Multiplier tests for the OLS residuals

Test	Result	
	Multiple Linear Regression	Simple Linear Regression
LM error	935.47*	1363.10*
LM lag	306.75*	814.26*
Robust LM error	629.29*	557.77*
Robust LM lag	30.567*	8.90*

Notes: '' indicates the significance at the 1% level.*

Although it is concluded from the LM tests that the SEM is the most appropriate model, the SAR and SDM were also examined to compare the performance of different spatial regression models. The results of these spatial analyses with the transformed electrical resistivity values are summarized in Table 3.8.

Table 3.8 Summary of results of spatial regression models with the transformed data

	Multiple Linear Regression			Simple Linear Regression		
	SDM	SAR	SEM	SDM	SAR	SEM
Intercept	-0.020	-0.731*	-0.534*	-0.021	-0.159*	0.094*
Water Content	0.011*	0.011*	0.011*	0.010*	0.010*	0.010*
Dry Unit Weight	0.042*	0.041*	0.042*			
Plasticity Index	0.003*	0.004*	0.003*			
Lag. Water Content	-0.009*			-0.007		
Lag. Dry Unit Weight	-0.045*					
Lag. Plasticity Index	-0.002*					
$\boldsymbol{\eta}$ / λ Coefficient	0.765	0.576	0.817	0.800	0.749	0.808
Pseudo-R-squared	0.83	0.82	0.83	0.67	0.67	0.67
Standard Error of Residual	0.055	0.040	0.044	0.082	0.070	0.078
LIK	906.91	888.87	904.45	704.97	703.79	704.88
AIC	-1795.8	-1765.7	-1796.9	-1399.95	-1399.58	-1401.76
BIC	-1755.8	-1739.1	-1770.3	-1377.74	-1381.81	-1384.00
LM Test for Residual Autocorrelation	5.25*	20.85	1.54**	114.68	3.30*	6.96*
No. of Observations	627	627	627	627	627	627

Notes: '' indicates the significance at the 1% level, '**' indicates the significance at the 10% level. "SDM" denotes Spatial Durbin Model, "SAR" denotes Spatial Lag Model, "SEM" denotes Spatial Error Model, "$\boldsymbol{\eta}$" denotes coefficient of spatially lagged dependent variable, "λ" denotes coefficient of spatial error lag, "LIK" denotes Log-Likelihood, "AIC" denotes Akaike's Information Criterion, and "BIC" denotes Bayesian Information Criterion.*

The SDM which includes both exogenous and endogenous interaction effects is presented by the following equations:

$$\rho_i = -0.020 + 0.765\,\boldsymbol{W}\rho + (0.011 - 0.009)\,\omega + (0.042 - 0.045\,\boldsymbol{W})\,\gamma_d + (0.003 - 0.002\,\boldsymbol{W})\,PI \qquad \text{Eq. 3.14}$$

where $\boldsymbol{W}$ is the average value in neighboring locations. According to Table 3.8, for multiple linear regression, the spatial lag coefficient of the SDM is positive, meaning that a change in the electrical resistivity of one location has positive effects on the electrical resistivity values of neighboring locations. These effects decay as moving toward higher-order neighbors. In other words, the variations of electrical resistivity values in one location influence the electrical resistivity of nearby locations more than further locations. The likelihood ratio test and Wald statistics show that the spatial lag coefficient of the SDM (η=0.765) is significant at the 1% level.

Similarly, the SAR models were developed and can be estimated as follows:

$$\rho_i = -0.731 + 0.576\,\boldsymbol{W}\rho + 0.011\,\omega + 0.041\,\gamma_d + 0.004\,PI \qquad \text{Eq. 3.15}$$

For multiple linear regression, the spatial lag coefficient of the SAR model is positive and significantly different from zero at the 1% level (η=0.576). The SAR model presents positive but lower spillover effects in the neighboring locations rather than the SDM.

The SEMs are presented by the following equations:

$$\rho_i = -0.534 + 0.011\,\omega + 0.042\,\gamma_d + 0.003\,PI + 0.817\,\boldsymbol{Wu} \qquad \text{Eq. 3.16}$$

where $\boldsymbol{Wu}$ is the average error of prediction in neighboring locations. The spatial error lag coefficient of the SEM is positive and significantly different from zero at the 1% level (λ=0.809). The spatial error lag coefficient of the SEM shows the strength of spatial autocorrelation among the error terms meaning that the unexplained variabilities of the electrical resistivity values follow a systematic distribution in space. The results of the simple linear regression show similar patterns to multiple linear regression results.

The signs and magnitudes of the SEM model parameters are similar to the standard regression models. The SEM model parameters are also highly significant for the three geotechnical parameters (gravimetric water content, dry unit weight, and plasticity index). Since the coefficients of the SAR model do not accurately explain the effects of geotechnical properties on electrical resistivity, a direct comparison of the regression parameters of the SAR model and standard regression model is inappropriate (LeSage and Dominguez 2012). Therefore, the average direct, indirect, and total effects of a change in each of the three geotechnical parameters on the electrical resistivity were calculated for the SAR model and summarized in Table 3.9.

Table 3.9 Average effects of explanatory variables on the electrical resistivity values for the SAR model

Variable	**Direct effect**	**Indirect effect**	**Total effect**	**P-value**
Water Content	0.011	0.015	0.026	0.000*
Dry Unit Weight	0.041	0.055	0.096	0.000*
Plasticity Index	0.004	0.005	0.009	0.000*

Note: '' indicates the significance at the 1% level.*

According to Table 3.9, the corresponding direct effects of gravimetric water content, dry unit weight, and plasticity index are smaller than the indirect effects, holding the same signs, which are associated with the transformation used on the electrical resistivity values. Similar to the standard regression model, the total effects of geotechnical properties on the electrical resistivity value are positive and highly significant at the 1% level. It again implies that an increase in the geotechnical properties has a decreasing effect on the electrical resistivity values. A noticeable difference is that the coefficients of the geotechnical parameters in the SAR model are shifted toward positive values compared to the standard regression model due to considering both direct and indirect effects. The coefficient variations imply that the variability of electrical resistivity is less influenced by the variation of geotechnical properties while considering the spatial effects.

The results of Lagrange Multiplier diagnostic tests for the spatial dependence of multiple linear regression show that the SEM and SDM models removed the problem of spatially autocorrelated residuals at the 10% and 1% level of significance. However, the spatial autocorrelation has remained in the SAR residuals (the null hypothesis is rejected at the 1% level of significance). Moreover, the likelihood ratio (LR) test was utilized to evaluate the goodness-of-fit of the nested models (i.e., SAR and OLS, or SEM and OLS). The test results show that the SAR and SEM models outperform the standard regression models at the 1% level of significance, and they should not be restricted to a simpler model (i.e., the OLS model). Comparing the LIK, AIC, and BIC statistics, it appears that the SEM is a better fit for the electrical resistivity data compared to the SDM. Therefore, according to the diagnostic tests and statistics, it is concluded that the spatial error model (SEM) is the best spatial model compared to the SDM and SAR models. Besides, the SEM provides more accurate estimates of the regression parameters in comparison to the standard regression model due to considering the spatial effects in the analysis.

3.2.3. Robustness of Spatial Regression Models Based on Threshold Distance

In this paper, threshold distances of 0.4 km (0.25 mi), 0.8 km (0.5 mi), 1.2 km (1 mi), 1.6 km (2 mi), 6.4 km (4 mi), 9.6 km (6 mi), 12.8 km (8 mi), 16.1 km (10 mi), 32.2 km (25 mi), 48.3 km (30 mi), 80.5 km (50 mi), and 160.9 km (100 mi) were examined to construct spatial weight matrices to assess the robustness of spatial regression models and investigate the spatial autocorrelation in the regression residuals of electrical resistivity data (at shorter threshold distances than 0.4 km (0.25 mi), no neighbor was found for some locations). Table 3.10 and 3.11 represent the values of log-likelihood, pseudo-R-squared, residual standard error, and Moran’s I of OLS residual considering different threshold distances for the SEM and SAR, respectively. Although the log-likelihood of the SEM shows more variation than the SAR model, its value decreases as the threshold distance increases in both models. The log-likelihood has the highest value at 0.4 km (0.25 mi) threshold distance in both models. Similarly, the value of Moran's I decreases as the threshold distance increases and has the highest value at 0.4 km (0.25 mi) threshold distance. The pseudo-R-squared and residual standard error have approximately constant values at different lag distances. Therefore, a threshold distance of 0.4 km (0.25 mi) was determined to construct the spatial weights and perform the spatial regression analyses on the electrical resistivity data based on the highest log-likelihood, highest Moran's I, highest pseudo-R-squared, and lowest residual standard error.

Table 3.10 Variations of log-likelihood, pseudo-R-squared, residual standard error, and Moran's I of OLS residual considering different threshold distances for the SEM

Spatial Model	Threshold Distance in km (mi)[a]	Log-Likelihood	Pseudo-R-Squared	Residual Standard Error	Moran's I OLS Residual
SEM	0.4 (0.25)	904.45	0.83	0.0437	0.280*
	0.8 (0.5)	882.38	0.81	0.0586	0.241*
	1.2 (1)	889.73	0.82	0.0512	0.236*
	1.6 (2)	884.19	0.81	0.0526	0.212*
	6.4 (4)	884.19	0.81	0.0526	0.218*
	9.6 (6)	884.12	0.81	0.0526	0.212*
	12.8 (8)	884.89	0.81	0.0529	0.211*
	16.1 (10)	884.89	0.81	0.0529	0.211*
	32.2 (25)	884.89	0.81	0.0529	0.211*
	48.3 (30)	884.89	0.81	0.0529	0.210*
	80.5 (50)	884.89	0.81	0.0529	0.210*
	160.9 (100)	873.37	0.80	0.0612	0.194*

Notes: '' indicates the significance at the 1% level. "OLS" denotes Ordinary Least Squares, "SAR" denotes Spatial Lag Model, and "SEM" denotes Spatial Error Model.*

[a] *numbers in parentheses represent threshold distances in miles.*

Table 3.11 Variations of log-likelihood, pseudo-R-squared, residual standard error, and Moran's I of OLS residual considering different threshold distances for the SAR

Spatial Model	Threshold Distance in km (mi)[a]	Log-Likelihood	Pseudo-R-Squared	Residual Standard Error	Moran's I OLS Residual
SAR	0.4 (0.25)	888.87	0.82	0.0401	0.280*
	0.8 (0.5)	879.00	0.81	0.0457	0.241*
	1.2 (1)	886.29	0.81	0.0437	0.236*
	1.6 (2)	881.65	0.81	0.0451	0.212*
	6.4 (4)	881.65	0.81	0.0451	0.218*
	9.6 (6)	881.65	0.81	0.0451	0.212*
	12.8 (8)	883.67	0.81	0.0493	0.211*
	16.1 (10)	883.67	0.81	0.0493	0.211*
	32.2 (25)	883.67	0.81	0.0493	0.211*
	48.3 (30)	883.67	0.81	0.0493	0.210*
	80.5 (50)	883.67	0.81	0.0493	0.210*
	160.9 (100)	875.66	0.80	0.0679	0.194*

Notes: '' indicates the significance at the 1% level. "OLS" denotes Ordinary Least Squares, "SAR" denotes Spatial Lag Model, and "SEM" denotes Spatial Error Model.*

[a] *numbers in parentheses represent threshold distances in miles.*

CHAPTER 4 INVESTIGATING COMPLEX RELATIONSHIP BETWEEN ELECTRICAL RESISTIVITY VALUES AND GEOTECHNICAL PROPERTIES USING DEEP LEARNING

Linear regression analysis and artificial intelligence techniques with shallow structures cannot discover non-linear and complex relationships between electrical resistivity values and geotechnical properties. Deep learning models can capture highly non-linear relationships in large datasets because of their algorithm's flexibility (Jalal et al. 2021). However, the deep learning models' generalization capabilities are in doubt due to overparameterization in which a trained deep learning model can overfit and assign overconfident predictions (Maronas et al. 2021). This chapter proposes an approach to extracting meaningful information from the non-linear and complex relationship between electrical resistivity and geotechnical properties (Zamanian et al. 2023c).

4.1. Methodology

The proposed approach includes two main steps: (1) collecting data from laboratory soil physical property and electrical resistivity tests and (2) training a deep learning model using the obtained laboratory data.

4.1.1. Data Collection

To introduce more variability in the previous dataset used in the spatial regression analysis, an additional 19 soil samples were collected and tested to identify the influencing geotechnical properties on the electrical resistivity values in clayey soil. Figure 4.1 shows the locations of soil sample collection on the Texas map. These sites are located within a distance of up to 420 miles.

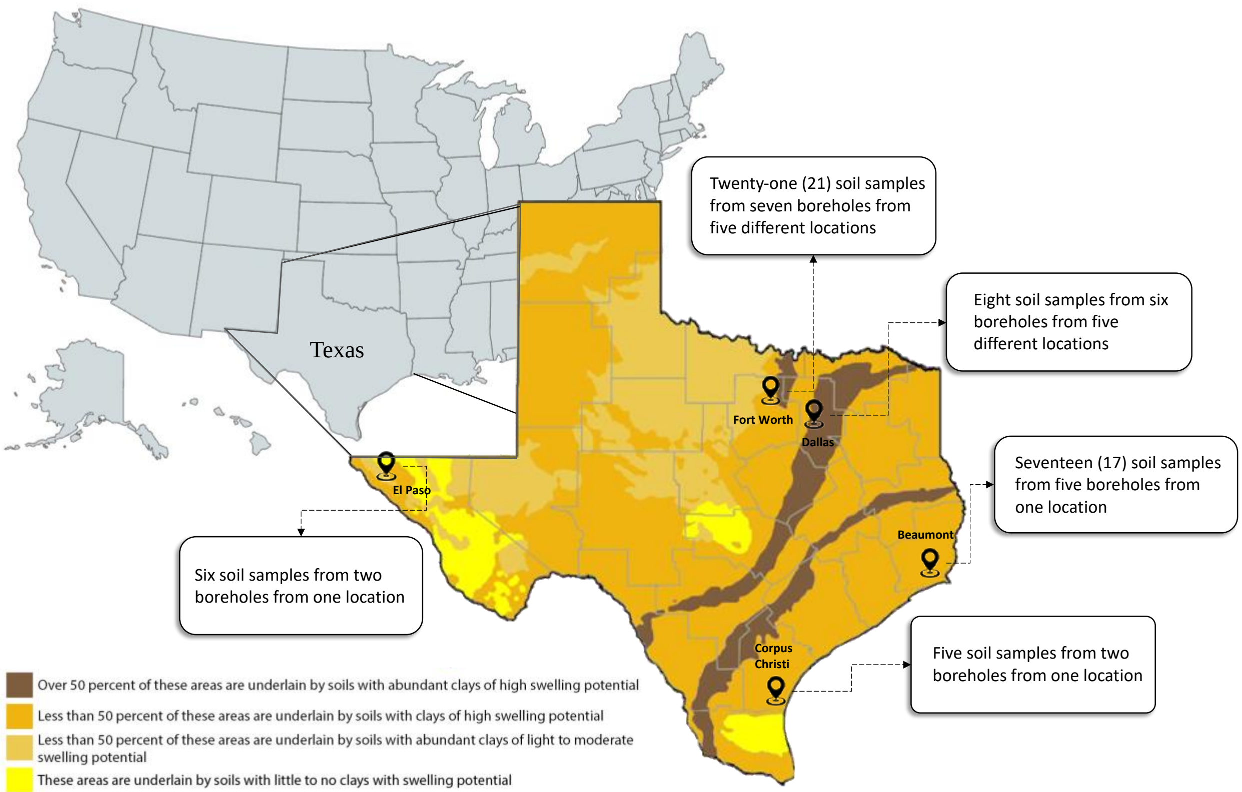

Figure 4.1 Locations of the soil sample collection on the Texas map

(Source: Adapted from Olive et al. 1989)

Based on the experimental design, each soil sample was mixed with different amounts of water and compacted in a soil box with three compaction efforts to conduct the electrical resistivity tests. A total of 842 laboratory measurements were conducted using the AGI SuperSting R8 instrument following the standard test method for measuring electrical resistivity using the Wenner four-electrode method (ASTM G57-20 2020). In addition to the laboratory electrical resistivity measurements, soil physical property tests were conducted to quantify the plasticity index, fine fraction, clay fraction, and specific gravity of the soil samples. Table 4.1 summarizes the basic statistics (e.g., range of values, mean, variance) of the measured parameters. According to Table 4.1, the soil samples are classified as low (CL) to high (CH) plasticity clayey soils based on the unified soil classification system (USCS).

Table 4.1 Basic statistics of the input and output parameters

Parameters	Abbreviation	Minimum Value	Maximum Value	Mean	VAR	n
Water content	ω (%)	6.6	66.0	24.1	125.7	842
Dry unit weight	γ_d (kN/m^3)	7.8	15.8	12.7	1.3	842
Plasticity index	PI (%)	6.5	46.5	28.4	65.6	842
Fine fraction	F (%)	54.2	98.0	85.7	94.5	842
Clay fraction	C (%)	9.4	68.8	43.3	188.2	842
Specific Gravity	G_s	2.6	2.72	2.65	0.001	842
Electrical resistivity	ρ ($\Omega.m$)	2.3	995.0	27.3	5394.1	842

4.1.2. Deep Learning Model

Artificial neural networks (ANNs) mimic the biological learning mechanism of the human brain, enabling the exploration of intricate and non-linear associations between input and output features (Abediniangerabi et al. 2021). The neural networks are composed of one input and output layer, and one or multiple hidden layers. Each layer comprises one or more neurons, and each layer's neurons are interconnected to neurons at the next layer by weighted connections. The neurons process elements of a neural network and resemble human brain cells (Darghiasi et al. 2024). The networks that possess multiple hidden layers are referred to as "Deep Learning" or "Deep Neural Networks" (DNNs). Figure 4.2 shows the structure of a deep learning model with four input features (geotechnical properties) and one output feature (electrical resistivity). The deep learning models use simple but non-linear algorithms to extract multiple higher levels of representation from the raw data and reveal complex patterns (LeCun et al. 2015). While shallow and deep neural networks possess the universal approximation property, research shows that deep network architectures (i.e., networks with two or more hidden layers) perform better than shallow network architectures (i.e., networks with one hidden layer) with an exponentially lower number of training parameters (Bengio and LeCun, 2007).

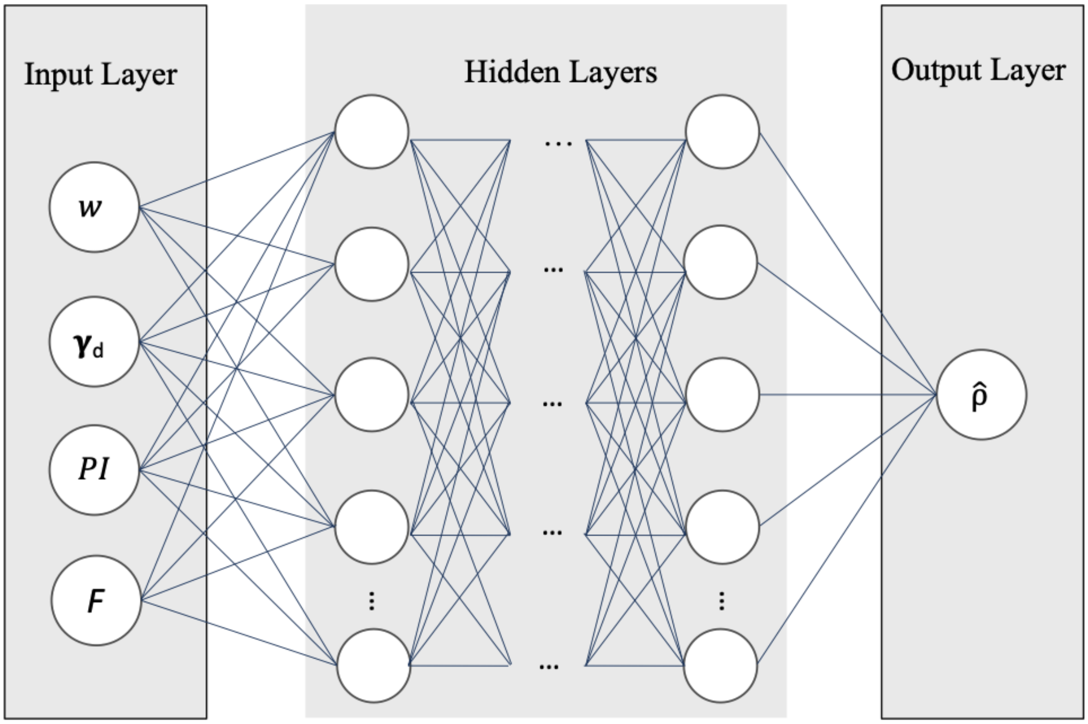

Notes: Input layer: "ω" denotes water content, "γ_d" denotes dry unit weight, "PI" denotes plasticity index, and "F" denotes fine fraction. Output layer: "ρ" denotes electrical resistivity

Figure 4.2 Structure of a deep learning model with four input features and an output feature

The neural networks represent and compute the non-linear associations between the input and output features in the hidden layers (Erzin et al. 2010). Each hidden layers' neuron uses a non-linear activation function to establish a relationship between the input and output features. Mathematically, a combination of the non-linear weighted sum is approximated by Equation 4.1.

$$f(\mathrm{X}) = \phi(W^T\mathrm{X} + b) \qquad \text{Eq. 4.1}$$

where X is the matrix of input features, ϕ is the activation function, W is the vector of neuron's weights, and b is the bias term at a hidden layer. The commonly used activation functions in hidden layer's neurons include rectifier linear unit (ReLU), hyperbolic tangent, and sigmoid functions. Computationally, the ReLU function exhibits a faster learning rate than sigmoid and hyperbolic tangent functions in deep neural networks (Su et al. 2017) since it does not saturate the output to a given value by increasing or decreasing the input features (Achieng 2019). This study will employ the ReLU function in all hidden layers except for the last hidden layer. Instead, a linear function was used to connect the last hidden layer to the output layer.

A backpropagation learning algorithm is extensively exploited for training the networks, involving a feedforward and a backward process (Erzin et al. 2010). In the feedforward process, the past observations are fed into the input layer and then propagated to the hidden layers to extract further information. The connection weights are determined to transfer the extracted information to the output layer to predict the outputs. The backward process updates the connection weights and biases based on the predicted outputs and actual values. The training cycle of networks is repeated many times to find the optimal set of weights that will yield the optimal output for any input (Caglar and Arman 2007).

In this study, deep learning models will be trained by four input geotechnical properties including water content, dry unit weight, plasticity index, and fine fraction to estimate the output that is the soil electrical resistivity values. The data was standardized by subtracting the mean from all observations and then scaling to unit variance to speed up the model training, which is essential when dealing with a large volume of data (Jayalakshmi and Santhakumaran 2011). Then the data were randomly split into two sets by a ratio of 80 to 20 before model training. In other words, 80 percent of the observations were used to train the deep learning models, and the remaining 20 percent of the observations were used to evaluate the developed model accuracies. The number of hidden layers for deep learning model shall be chosen appropriately to ensure the best accuracy of the model (Choldun et al. 2019). The maximum number of neurons in the hidden layers is determined by 2I+1, where I represents the number of input variables (Caudill 1988). Therefore, the optimum number of neurons for the hidden layers was selected based on a trial-and-error by altering the number of neurons from one to nine. Note that selection of many hidden layers and hidden layer's neurons may lead to overfitting (i.e., high variance) if the level of complexity of the problem is disregarded (Uzair and Jamil 2020). The optimal model was then selected based on the minimum root mean square of errors (RMSE) and mean absolute errors (MAE) for the testing dataset using 100 iterations. For model's hyperparameter tuning (to mitigate any potential overfitting and assess the model performance to new unseen data), cross-validation was used during model training (Hastie et al. 2009). An *n*-fold cross-validation method divides the training data into *n* equal parts (i.e., folds). The model is then trained based on *n-1* parts and then evaluated on the remaining part. The process is repeated *n* times until every part was used once for validation. Then the final model performance is calculated by averaging the results of each iteration. The hyperparameters of the model, such as epoch number and batch size, was chosen based on a grid search using 10-fold cross-validation with a learning rate of 0.001. Table 4.2 presents the ranges of the model hyperparameters that will be used in the grid search. The batch size was also examined in conjunction with the execution time of the training process (Abediniangerabi et al. 2021).

Table 4.2 Model hyperparameters' ranges in grid search

Hyperparameters	Values
Number of neurons in different layers	1 to 9
Number of epochs	10, 20, 30, 40, 50, 100, 150, 200, 300, 400, 500
Batch sizes	64, 128
Activation function	ReLU, Linear
Optimizer	Adam
Learning rate	0.001
Losses	RMSE, MAE

As a result, a deep learning model will be adopted to evaluate the applicability of DNNs in determining the associations between the geotechnical properties and electrical resistivity values in clayey soils. The performance of the trained deep learning model shall be compared to artificial neural networks, support vector machines, and multivariate linear regressions.

4.2. Results

4.2.1. Descriptive Statistics

This section provides descriptive analyses of the data obtained by laboratory experiments to identify the most influencing factors affecting electrical resistivities. Figures 4.3 to 4.8 illustrate the frequency histograms of the measured geotechnical properties for the soil samples. Accordingly, all geotechnical properties show a wide range of values (i.e., high variance), except for the specific gravity. The high variance in the geotechnical properties (i.e., water content, plasticity index, dry unit weight, fine fraction, and clay fraction) indicates that these variables can be useful in determining the variance of the electrical resistivity.

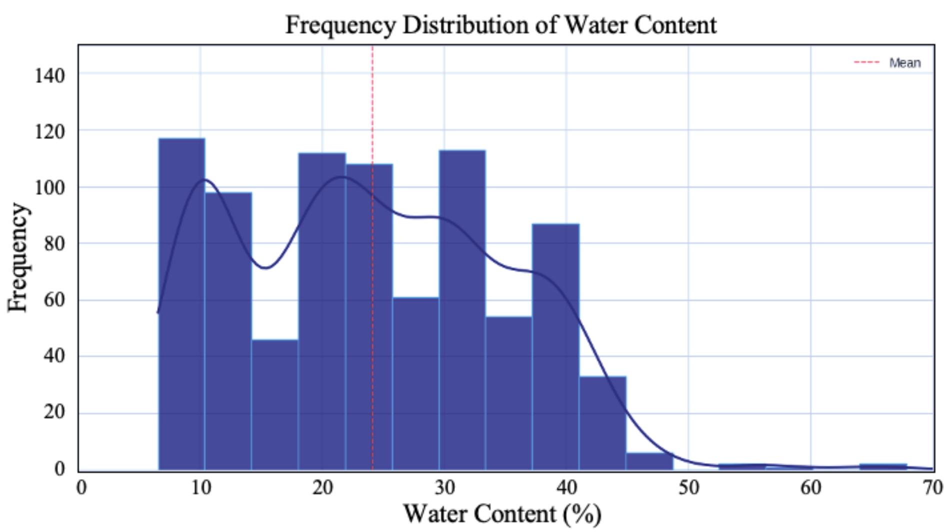

Figure 4.3 Water content frequency distribution

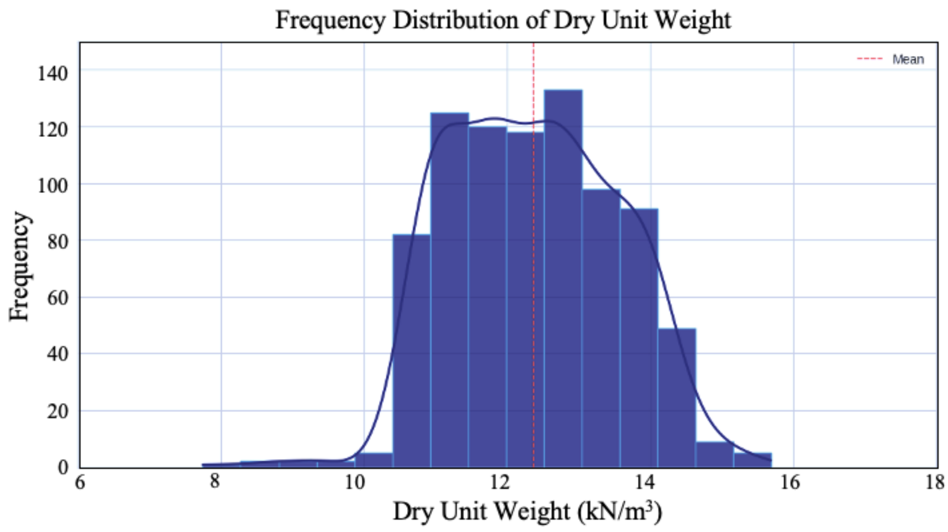

Figure 4.4 Dry unit weight frequency distribution

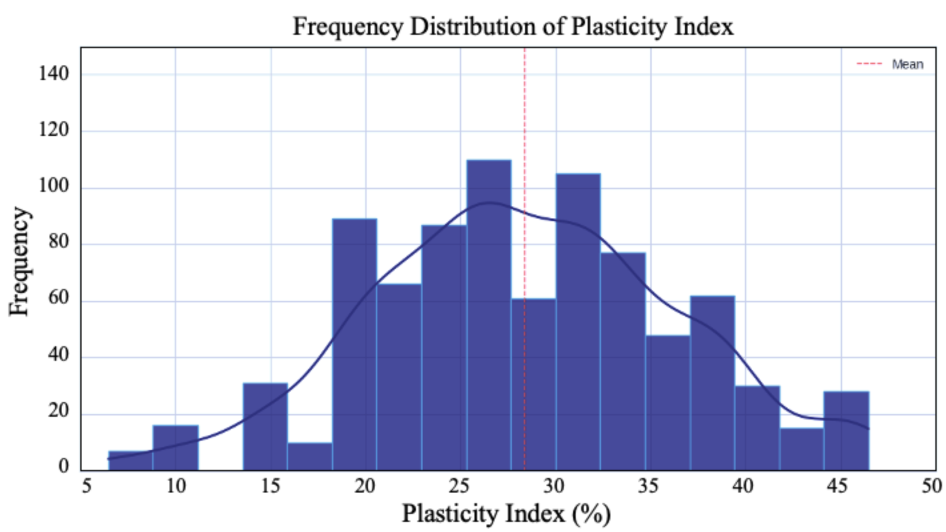

Figure 4.5 Plasticity index frequency distribution

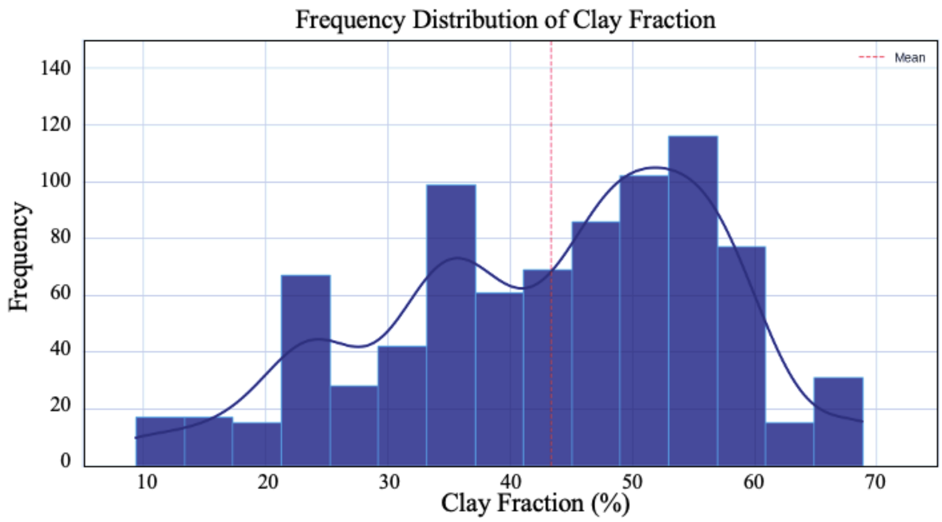

Figure 4.6 Clay fraction frequency distribution

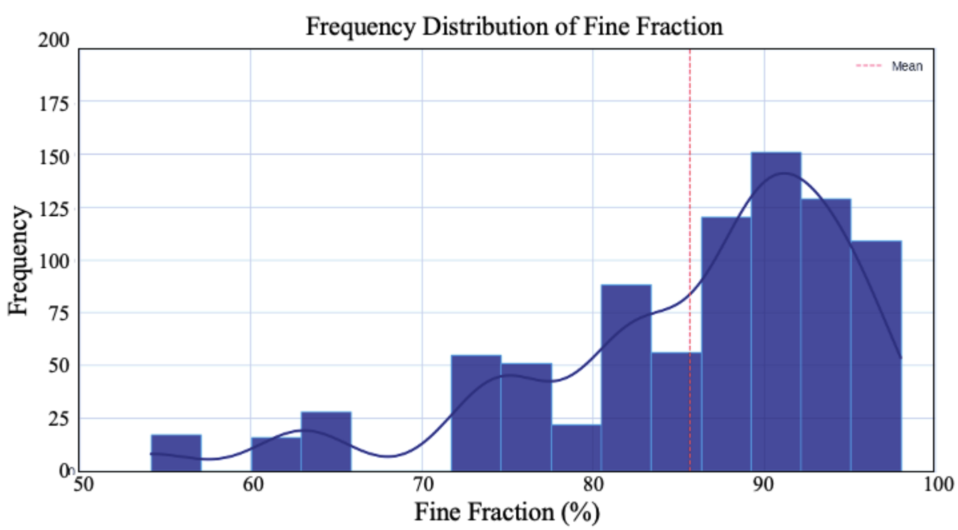

Figure 4.7 Fine fraction frequency distribution

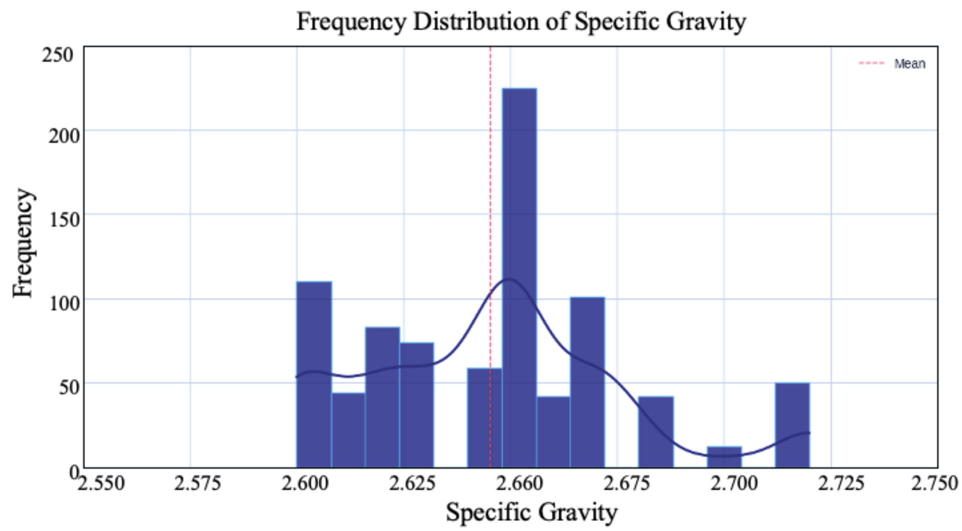

Figure 4.8 Specific gravity frequency distribution

Moreover, Spearman's correlation analysis was performed to describe the strength of the pairwise relationships between electrical resistivities and geotechnical properties. Spearman's correlation tests for a monotonic dependence between the ranked values of two variables, without assuming linearity of the relationship (Deebani and Kachouie 2022). Figure 4.9 presents Spearman's correlation coefficients for the electrical resistivity and geotechnical properties on a heatmap. Spearman's coefficients range between −1 and 1. A positive coefficient indicates monotonic changes in the same direction, whereas a negative coefficient shows monotonic changes in the opposite direction (Schober et al. 2018). According to Figure 4.9, electrical resistivity shows a strong negative correlation with the water content (r_s = -0.77). In other words, the electrical resistivity of soil significantly decreases with an increase in the water content. The literature also confirms that the water content inversely influences the electrical resistivity of clayey or sandy soils (Zamanian and Shahandashti 2022; Alsharari et al. 2020). Based on Figure 4.9, the electrical resistivity shows weak correlations with dry unit weight, plasticity index, fine fraction, and clay fraction. Note that Spearman's correlation solely measures the degree of a monotonic relationship between two variables. However, there might be strong non-monotonic relationships between the variables which cannot be captured by Spearman's correlation (Griessenberger et al. 2022).

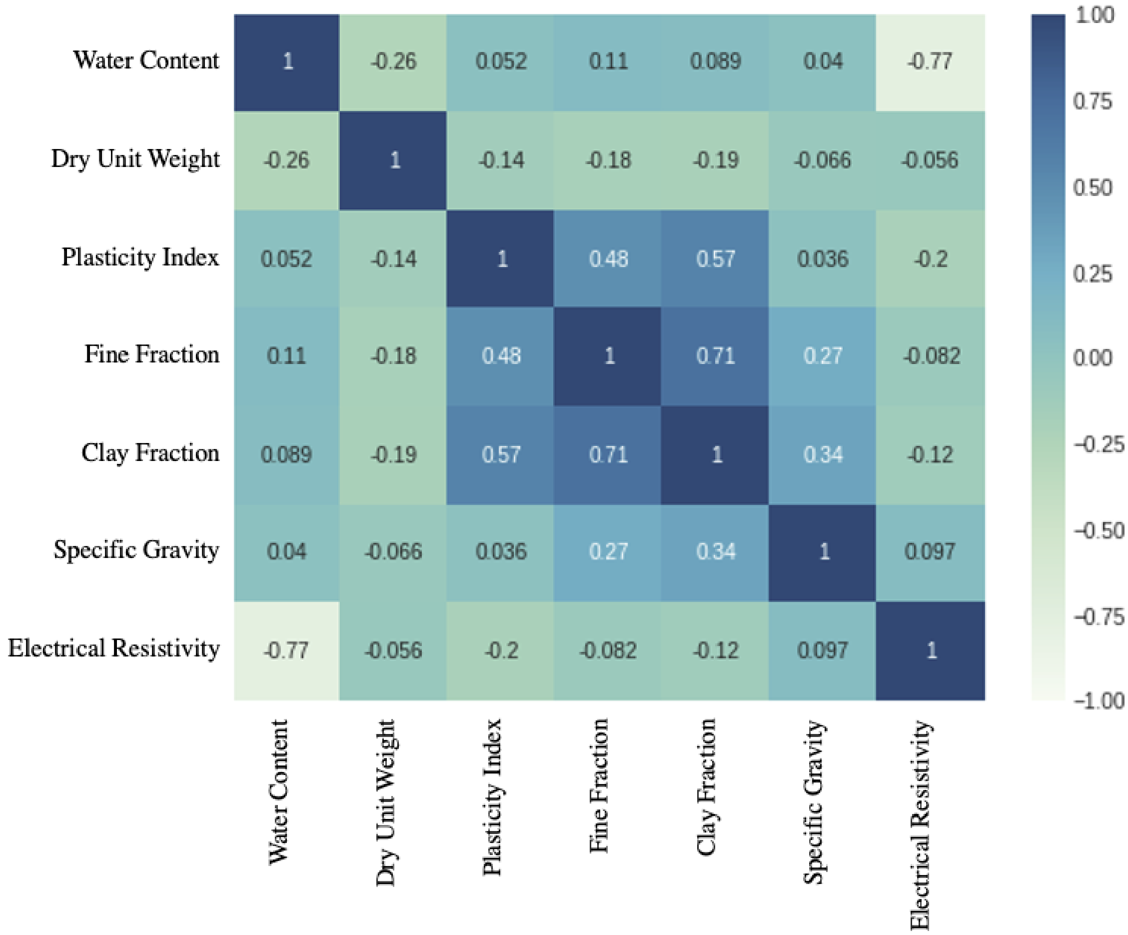

Figure 4.9 Spearman's correlation coefficient heatmap of the electrical resistivity and geotechnical properties

4.2.2. Deep Learning Results

A deep learning model consisting of three hidden layers was constructed, with each layer containing 8, 8, and 9 neurons, respectively. Four geotechnical properties such as water content, plasticity index, dry unit weight, and fine fraction were fed into the neurons of the input layer to estimate the soil electrical resistivities. Figures 4.10 and 4.11 illustrate the training and testing loss functions (mean squared and absolute errors) for the developed deep learning model across different epochs, ranging from 1 up to 500. The epoch upper limit was set to the highest possible value to ensure that the loss functions converge during the training process (Abediniangerabi et al. 2021). According to Figures 4.10 and 4.11, the deep learning loss functions converge to a constant value as the number of epochs increases. The MSE and MAE loss functions start to saturate around the same value and converges in about 100 epochs. The fluctuations observed on the training and testing curves do not affect the model's overall accuracy (Zhang et al. 2021).

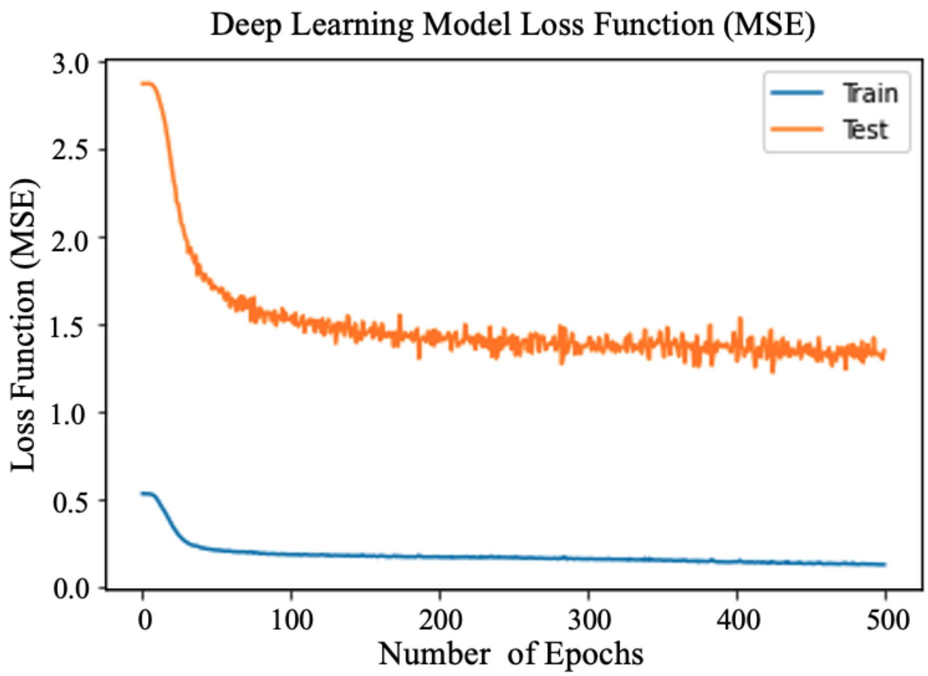

Figure 4.10 MSE loss function for the training and testing datasets

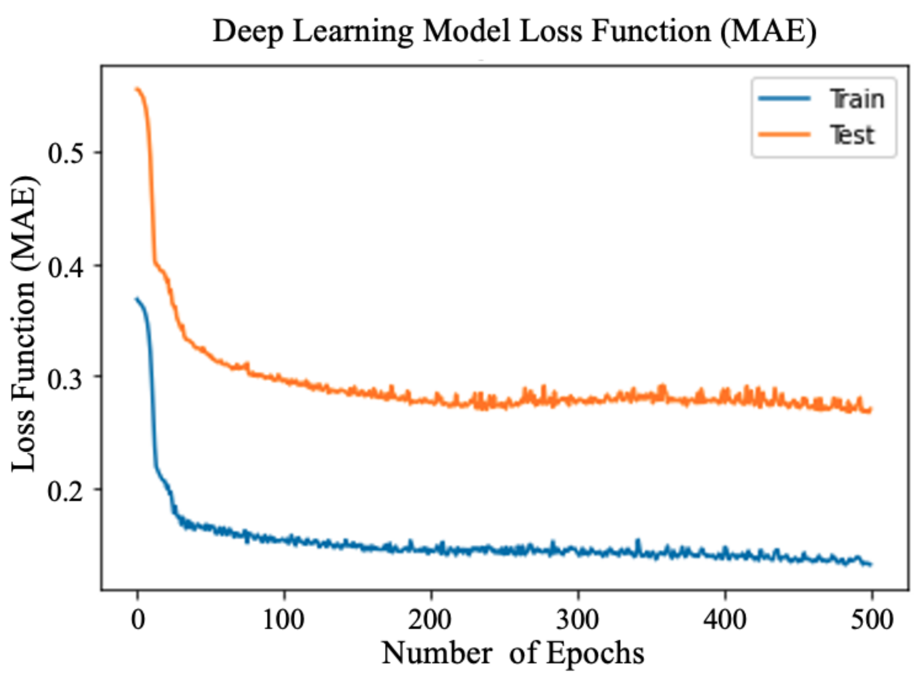

Figure 4.11 MAE loss function for the training and testing datasets

Validating black-box models such as deep learning requires an understanding of the underlying relationships between input and output variables, which can be achieved by extracting features' importance (Zhong et al. 2021). Figure 4.12 illustrates the relative importance of each geotechnical property in predicting the electrical resistivities. A geotechnical property that contributes to more substantial losses in the model is assigned a higher importance score. Conversely, a feature with a score close to zero indicates the minimal impact of that feature on the predictions. According to Figure 4.12, water content exhibits the highest level of influence on the variability in the electrical resistivities. This finding also aligns with the results of Spearman's correlation analysis. The results are consistent with the literature which identifies water content as the primary factor affecting electrical resistivities (Zamanian et al. 2023b; Robinson et al. 2008). Pore water facilitates the passage of electrical current through pore spaces by moving ions, which reduces Earth's resistance (Siddiqui and Osman 2012). Shahandashti et al. (2021) showed that about 66% of the variability of electrical resistivity can be explained by the water content. Moreover, Figure 4.12 indicates that dry unit weight is the second most influencing geotechnical property affecting the electrical resistivity variations following water content. Although this finding contradicts the result of the correlation analysis, which shows a weak correlation between the dry unit weight and electrical resistivity, the existing literature shows that the dry unit weight is useful in explaining the variability in the electrical resistivities (Shahandashti et al. 2021; Alsharari et al. 2020). Changes in dry unit weights result in changes in pore spaces and interparticle contacts. Therefore, especially at low water contents, continuous pathways for the flow of electrical current can be created at high dry unit weights, which result in lower electrical resistivities (Rashid et al. 2018). The plasticity index and fine fraction demonstrate significant but least important scores among the other geotechnical properties, implying that they have lower impacts on the electrical resistivity predictions. Lin et al. (2016) also found some correlations between the electrical resistivity of clayey soils and the plasticity index. Theoretically, fine-grained soil yields lower electrical resistivities than coarse-grained soils because they have higher specific surface areas, which promotes the transmission of electrical current (Morin 2006).

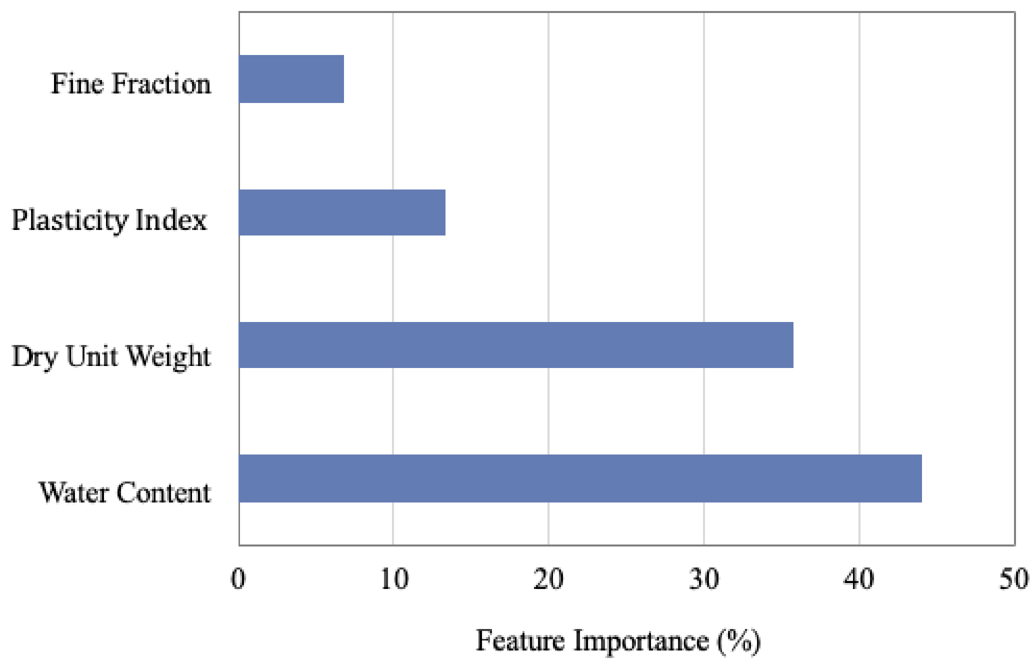

Figure 4.12 Relative importance of geotechnical properties in predicting electrical resistivity

4.2.3. Model Comparison of Deep Learning Model with ANNs, SVMs, and MLR

In this study, a deep learning model with an optimal number of hidden layers and hidden layers' neurons was adopted to assess the applicability of DNNs in investigating the non-linear and complex relationships between electrical resistivities and geotechnical properties. The performance of the trained deep learning model was then compared to artificial neural networks, support vector machines, and multivariate linear regressions – the existing methods in the literature. An ANN was trained to compare the performance of the shallow with deep network architectures in investigating the relationships between geotechnical properties and electrical resistivities. The ANN model consists of an input layer with four neurons (i.e., water content, plasticity index, dry unit weight, and fine fraction), a hidden layer with nine neurons, and an output layer with one neuron (i.e., electrical resistivity). The number of hidden layer's neurons was selected based on a trial-and-error by changing the number of neurons from one to nine and examining the model accuracy for the testing dataset through 100 iterations. An SVM with a radial basis function kernel was also trained to predict electrical resistivities based on the same geotechnical properties. The radial basis function kernel transforms the non-linear relationship between the input and output features into a linear relationship within a higher-dimensional space. The adopted deep learning model, ANN, and SVM were compared to the multiple linear regression developed by Shahandashti et al. (2021). A Box-Cox and a natural log transformation were used on the input and output variables to meet the linear regression requirements (i.e., linearity, homoskedasticity, and normality).

Figures 4.13 to 4.16 illustrate the measured and predicted electrical resistivities for the training and testing datasets by deep learning, artificial neural network, support vector machine, and multiple linear regression. The accuracy of the deep learning model (R-squared) is about 87% for the training and 70% for the testing datasets. Accordingly, it is concluded that the deep learning model yields more accurate predictions on both training and testing datasets compared to other methods. Moreover, the results imply that the deep learning model with three hidden layers is more robust than the other methods. In other words, due to the slight difference between the training and testing accuracies for deep learning, it is concluded that the model performance remains approximately the same for predicting out-of-sample data. On the other hand, the MLR shows the lowest performance for training and testing datasets.

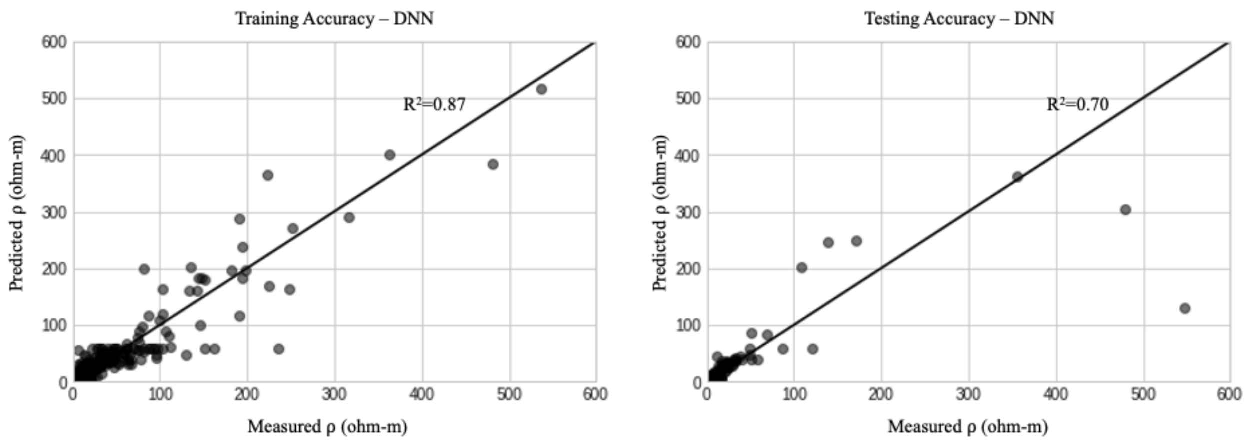

Figure 4.13 Training and testing accuracies for the developed deep learning to predict the electrical resistivities

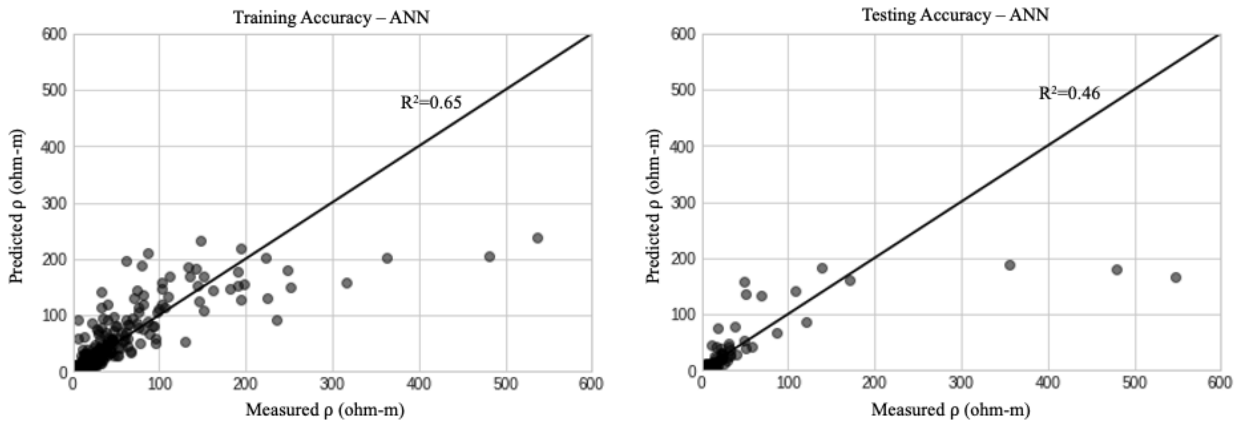

Figure 4.14 Training and testing accuracies for the developed ANN to predict the electrical resistivities

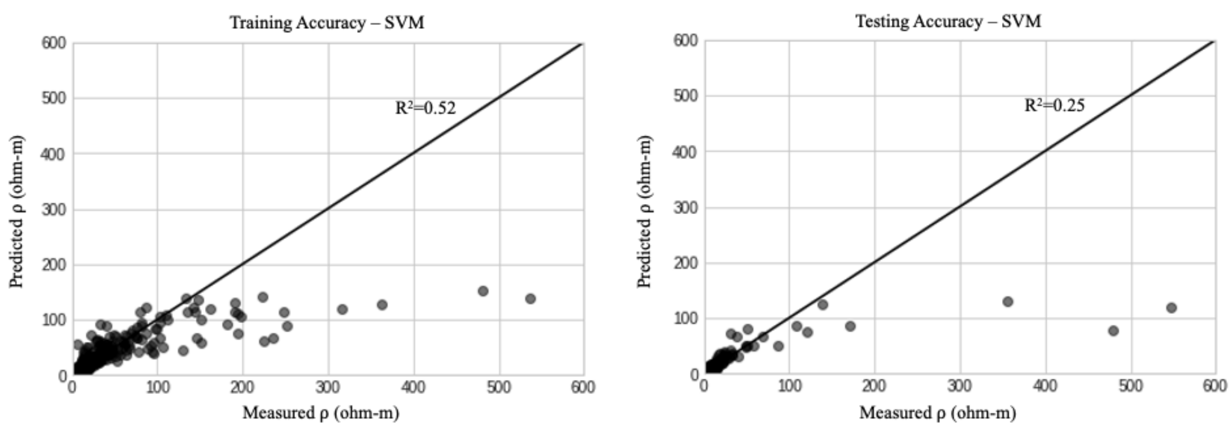

Figure 4.15 Training and testing accuracies for the developed SVM to predict the electrical resistivities

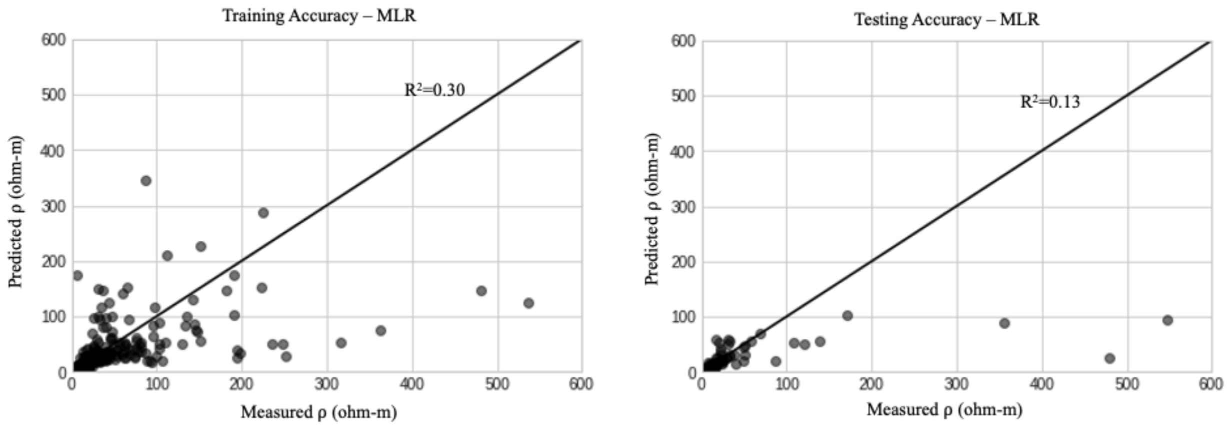

Figure 4.16 Training and testing accuracies for the developed MLR to predict the electrical resistivities

Figure 4.17 shows the testing accuracy of deep learning, ANN, SVM, and MLR for predicting electrical resistivity based on RMSE and MAE metrics. The testing accuracies show the outperformance of the deep learning model to the other models in predicting the electrical resistivities with a root mean square of errors (RMSE) of 68.9 and mean absolute error (MAE) of 17.8, followed by the ANN with an RMSE of 92.9 and MAE of 23.4. The outperformance of the deep learning model to ANN is due to the ability of deep network architectures to extract more meaningful information among the input and output features than shallow network architectures. Compared to all other methods, linear regression shows the most errors with an RMSE of 115.5 and an MAE of 25.7. The low performance of the multiple linear regression is because of its inability to handle the non-linear and complex relationship between electrical resistivities and geotechnical properties.

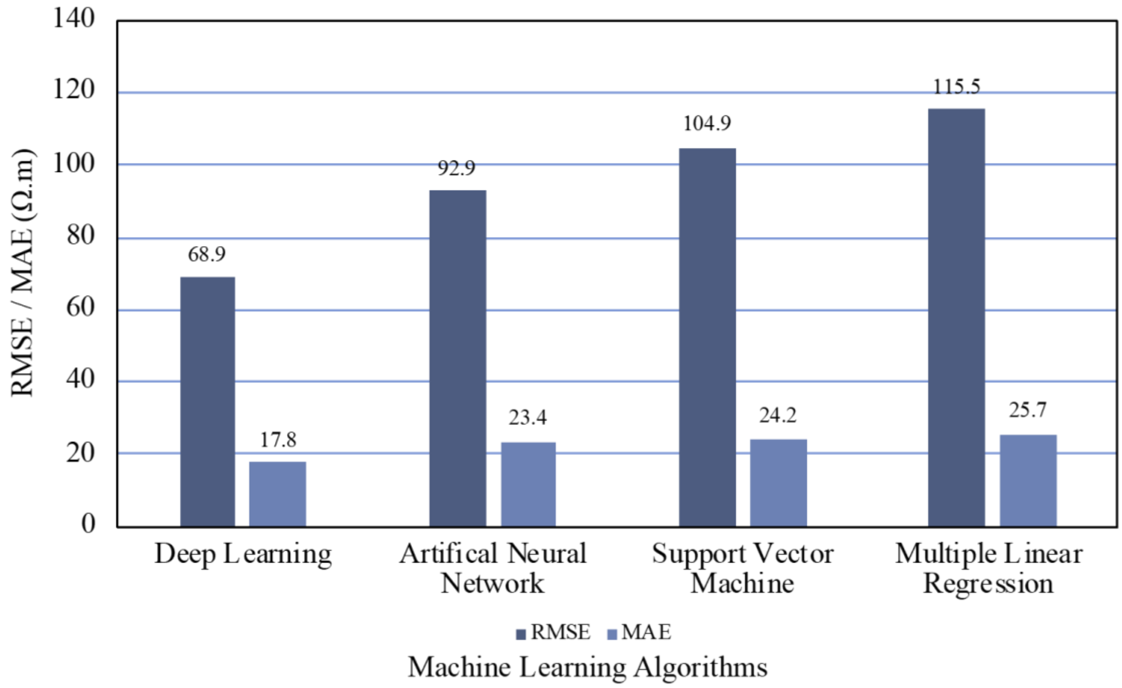

Figure 4.17 Accuracy metrics of the deep neural network, artificial neural network, support vector machine, and multiple linear regression for the testing dataset

CHAPTER 5 CONCLUSION AND FUTURE WORK

A successful design and construction of infrastructure systems such as highways and bridges highly depend on accurate estimation of geotechnical properties and understanding their spatial distributions. Insufficient and inaccurate subsurface information has a major contribution to cost overruns and delays in up to 50% of all infrastructure projects. Insufficient site investigation may also contribute to inadequate or conservative designs, leading to costly failures or increased project's costs. Hence, geophysical methods, such as electrical resistivity imaging, that can potentially transform the existing subsurface investigations are used to develop practical tools for subsurface characterization based on the data analytic approaches. This study aimed to (1) assess the presence of spatial association between electrical resistivity and geotechnical properties and propose the most appropriate spatial regression model to explain the variability of electrical resistivity values considering the spatial effects and (2) explore non-linearity and complexity of interactions between the electrical resistivity values and geotechnical properties using artificial intelligence techniques with deep structures such as deep learning model.

This research investigated the presence of spatial association between the electrical resistivity values and geotechnical properties such as gravimetric water content, dry unit weight, and plasticity index to validate the developed linear regressions in the literature. The analyses were performed based on the results of a full factorial design with 627 observations obtained from the laboratory physical property and electrical resistivity tests. Linear regression analysis was performed, and its critical assumptions were examined. Moran's I of the OLS regression residuals showed a highly significant value, indicating that the linear regression residuals are spatially autocorrelated. Since linear regression analysis cannot consider the spatial autocorrelations among the data in the modeling, the spatial regression analysis was employed. The results showed that the SEM (spatial error model) is the most appropriate model compared to standard regression and other spatial models (SAR and SDM) in explaining the spatial variability of geotechnical properties on the electrical resistivity values. These findings indicate that the inclusion of spatial autocorrelation of residuals in the regression model could improve the performance of the regression model and lead to more accurate estimates of the effects of geotechnical properties on electrical resistivity values. These findings help engineers to have a better understanding of the effects of geotechnical properties on the variability of electrical resistivity values to obtain more reliable evaluations of the subsurface characteristics using the electrical resistivity values. The proposed approach helps create and use spatial regression models for a given site to determine the spatial distribution of geotechnical properties at each point (not necessarily those sampled using conventional site investigation methods) and conduct reliability analysis accordingly.

Moreover, an analytical approach was proposed to explore the non-linear and complex relationships between the geotechnical properties (e.g., water content, dry unit weight, plasticity index, and fine fraction) and electrical resistivity values using deep learning. A deep learning model was developed based on an empirical dataset (842 observations), comprising three hidden layers with 8, 8, and 9 neurons in each hidden layer, to relate the associations between electrical resistivities and geotechnical properties. The pairwise dependence of variables was analyzed by Spearman’s correlation. Besides, the relative importance of the geotechnical properties in predicting the electrical resistivities was derived from the trained model. The performance of the deep learning model was then compared to the performance of the artificial neural network, support vector machine, and multiple linear regression. The results showed that the water content has a significant contribution to the predictions of the electrical resistivities in clayey soils. The findings of this study also confirm that the dry unit weight plays a crucial role in electrical resistivity variations which can be attributed to the pore spaces that provide pathways for the electrical current. Furthermore, the results illustrated that the electrical resistivity of clayey soils is more influenced by the percentage of fines and plasticity index than the clay fraction and liquid limit. This study found that the deep learning model provides more accurate estimates for electrical resistivity compared to all other methods, with an RMSE of 68.9 and an MAE of 17.8. This study also showed that the deep learning model yields a more robust and generalized model since there is a slight difference between the training and testing accuracies. The outperformance of the deep learning model to ANN indicates a high level of complexity among the geotechnical properties and electrical resistivities. The research's findings help better understand the variability of electrical resistivities due to changes in geotechnical properties and improve subsurface characterization using electrical resistivity imaging technology. The proposed methodology can also be used to validate findings from electrical resistivity surveys by leveraging geotechnical properties, particularly where intrusive investigation methods are prohibited. The research results can also be applied to other applications in which understanding electrical resistivity and its relationship with the geotechnical properties is essential, such as designing grounding systems (Ackerman et al. 2013).

Future Work

This research results shed light on the spatial impacts of geotechnical properties on the electrical resistivities in clayey soils and proposed an analytical framework for explaining complexity among the electrical resistivity data. The following recommendations could be incorporated into future research:

- Due to the complexity of interactions among geotechnical and geoelectrical properties, slight changes in the geotechnical properties can result in significant variations in electrical resistivity. Future experimental designs may consider smaller increments for the factor levels such as water content to enhance the accuracy of the analysis results.
- It would be beneficial to scrutinize the effects of other geotechnical properties such as clay fraction and plasticity index on the electrical resistivity by considering multiple factor levels for each in the experimental design. These factors can be adjusted by considering different combinations of commercially available soils.
- To improve the accuracy of the spatial analysis and generalization of the findings, it would be advantageous to integrate additional data from various locations across Texas and, thereby increasing the number of neighbors in the spatial weight matrix.
- The practical recommendations for developing deep learning models in this research are limited to multivariate prediction models based on experimental data. Nevertheless, continuous geotechnical data are not always available from the field sites. In future work, it is of interest to integrate the proposed approach with a technique that leverages publicly available data to determine unknown geotechnical properties that show minimal variations over time, such as fine fraction, to simplify the developed machine leaning

models. Consequently, to be practically implemented, pairwise relationships between electrical resistivity and geotechnical properties may be established.

- To enhance the model inference through a deep learning approach, it is encouraged to conduct uncertainty analysis for evaluating the model's uncertainties and incorporating them into probability-based analyses.

APPENDIX BOREHOLE LOGS

Beaumont District (October 2019)

LOGO

The University of Texas at Arlington
416 Yates Stress
76010

BORING NUMBER P1

CLIENT

PROJECT NAME

PROJECT NUMBER First Visit

PROJECT LOCATION Beaumont

DATE STARTED 10/13/19 **COMPLETED** 10/13/19

GROUND ELEVATION **HOLE SIZE** inches

DRILLING CONTRACTOR

GROUND WATER LEVELS:

DRILLING METHOD

AT TIME OF DRILLING ---

LOGGED BY **CHECKED BY**

AT END OF DRILLING ---

NOTES

AFTER DRILLING ---

DEPTH (ft)	GRAPHIC LOG	MATERIAL DESCRIPTION	SAMPLE TYPE NUMBER	RECOVERY % (RQD)	BLOW COUNTS (N VALUE)	POCKET PEN. (tsf)	DRY UNIT WT. (pcf)	MOISTURE CONTENT (%)	ATTERBERG LIMITS: LIQUID LIMIT	ATTERBERG LIMITS: PLASTIC LIMIT	ATTERBERG LIMITS: PLASTICITY INDEX	FINES CONTENT (%)
0		(SC) Gray to Brown; Sandy Clay	SS		8-11-3 (14)							
		(CL) Brown to Dark Brown; Clay; Moist										
5		(CH) Brown; Clay	SPT		2-2-2 (4)							
			ST									
		(CH) Brown; Clay; Moist										
10			SPT		1-2-2 (4)							

Bottom of borehole at 11.5 feet.

GEOTECH BH COLUMNS - GINT STD US LAB.GDT - 4/3/20 01:46 - C:\USERS\MXA0516\ONEDRIVE - UNIVERSITY OF TEXAS AT ARLINGTON\LAB DOCS\RESISTIVITY IMAGING\TEST RESULTS\SITE RESISTIVITY RESULT\BEAUMONT\P1\BORELOG_P1\BORELOG INF

LOGO

The University of Texas at Arlington
416 Yates Stress
76010

BORING NUMBER P4

CLIENT ______

PROJECT NAME ______

PROJECT NUMBER First Visit

PROJECT LOCATION Beaumont

DATE STARTED 10/14/19 **COMPLETED** 10/14/19

GROUND ELEVATION ______ **HOLE SIZE** inches

DRILLING CONTRACTOR ______

GROUND WATER LEVELS:

DRILLING METHOD ______

AT TIME OF DRILLING ---

LOGGED BY ______ **CHECKED BY** ______

AT END OF DRILLING ---

NOTES ______

AFTER DRILLING ---

DEPTH (ft)	GRAPHIC LOG	MATERIAL DESCRIPTION	SAMPLE TYPE NUMBER	RECOVERY % (RQD)	BLOW COUNTS (N VALUE)	POCKET PEN. (tsf)	DRY UNIT WT. (pcf)	MOISTURE CONTENT (%)	ATTERBERG LIMITS: LIQUID LIMIT	ATTERBERG LIMITS: PLASTIC LIMIT	ATTERBERG LIMITS: PLASTICITY INDEX	FINES CONTENT (%)
0		(CL) Light Brown, gray; Silty Clay; Moist;	ST									
		(CL-CH) Brown to Light Brown; Clay with sand;	ST									
5		(CH) Brown to Dark Brown; Clay;	SPT		1-0-1 (1)							
		(CH) Brown to Dark Brown; Clay; Moist	ST									
10			ST									
			SPT		2-1-3 (4)							

Bottom of borehole at 11.5 feet.

LOGO

The University of Texas at Arlington
416 Yates Stress
76010

BORING NUMBER P6

PAGE 1 OF 1

CLIENT	**PROJECT NAME**
PROJECT NUMBER First Visit	**PROJECT LOCATION** Beaumont
DATE STARTED 10/15/19 **COMPLETED** 10/15/19	**GROUND ELEVATION** **HOLE SIZE** inches
DRILLING CONTRACTOR	**GROUND WATER LEVELS:**
DRILLING METHOD	**AT TIME OF DRILLING** ---
LOGGED BY **CHECKED BY**	**AT END OF DRILLING** ---
NOTES	**AFTER DRILLING** ---

DEPTH (ft)	GRAPHIC LOG	MATERIAL DESCRIPTION	SAMPLE TYPE NUMBER	RECOVERY % (RQD)	BLOW COUNTS (N VALUE)	POCKET PEN. (tsf)	DRY UNIT WT. (pcf)	MOISTURE CONTENT (%)	ATTERBERG LIMITS: LIQUID LIMIT	ATTERBERG LIMITS: PLASTIC LIMIT	ATTERBERG LIMITS: PLASTICITY INDEX	FINES CONTENT (%)
0												
		(CL) Brown; Silty Clay;	ST									
		(CL) Brown; Clay	ST									
5		(CH) Brown; Clay	SPT		2-2-4 (6)							
			ST									
		(CH) Dark Brown; Clay										
10					1-1-2 (3)							

Bottom of borehole at 11.5 feet.

LOGO

The University of Texas at Arlington
416 Yates Stress
76010

BORING NUMBER P17

PAGE 1 OF 1

CLIENT

PROJECT NAME

PROJECT NUMBER First Visit

PROJECT LOCATION Beaumont

DATE STARTED 10/14/19 **COMPLETED** 10/14/19

GROUND ELEVATION **HOLE SIZE** inches

DRILLING CONTRACTOR

GROUND WATER LEVELS:

DRILLING METHOD

AT TIME OF DRILLING ---

LOGGED BY **CHECKED BY**

AT END OF DRILLING ---

NOTES

AFTER DRILLING ---

DEPTH (ft)	GRAPHIC LOG	MATERIAL DESCRIPTION	SAMPLE TYPE NUMBER	RECOVERY % (RQD)	BLOW COUNTS (N VALUE)	POCKET PEN. (tsf)	DRY UNIT WT. (pcf)	MOISTURE CONTENT (%)	ATTERBERG LIMITS: LIQUID LIMIT	ATTERBERG LIMITS: PLASTIC LIMIT	ATTERBERG LIMITS: PLASTICITY INDEX	FINES CONTENT (%)
0		(CL) Gray to Light gray; Slighly moist; Silty Sand with clay; sand seam	SS		11-9-6 (15)							
		(CL) Gray; Sandy silty clay;										
5		(CL-CH) Gray to brown; Silty Clay	SPT		1-2-4 (6)							
		(CL-CH) Gray to brown; silty clay	ST									
10			SPT		2-1-2 (3)							

Bottom of borehole at 11.5 feet.

Beaumont District (December 2019)

LOGO

The University of Texas at Arlington
416 Yates Stress
76010

BORING NUMBER BR-6A

CLIENT SWIS Lab
PROJECT NAME Md Asif Akhtar
PROJECT NUMBER
PROJECT LOCATION Beaumont
DATE STARTED 12/12/19 **COMPLETED** 12/13/19
GROUND ELEVATION **HOLE SIZE** inches
DRILLING CONTRACTOR
GROUND WATER LEVELS:
DRILLING METHOD Wash Boring
∇ **AT TIME OF DRILLING** 6.50 ft
LOGGED BY **CHECKED BY**
AT END OF DRILLING ---
NOTES Wet Rotary set @ 8 ft due to Ground Water Table found at 6.5 ft
AFTER DRILLING ---

DEPTH (ft)	MATERIAL DESCRIPTION	SAMPLE TYPE NUMBER	RECOVERY % (RQD)	BLOW COUNTS (N VALUE)	POCKET PEN. (tsf)	DRY UNIT WT. (pcf)	MOISTURE CONTENT (%)	ATTERBERG LIMITS: LIQUID LIMIT	PLASTIC LIMIT	PLASTICITY INDEX	FINES CONTENT (%)
0	(CL) Silty Clay; Dark Brown; Moist	ST	88								
5	(CH) Clay; Dark Brown to Light Brown; Moist	ST	89								
		SPT		1-1-1 (2)							
	∇ (CH) Very soft clay; Light brown to light grey; Moist	ST	89								
10	(CH) Very soft clay; Light brown to light grey; Moist	ST	79								
	(CL) Slightly Silty Clay; Light brown with some orange and gray; Moist	SPT		6-8-6 (14)							
15	(CL) Slightly Silty Clay; Light brown with some orange and gray; Moist	ST	58								
		SPT		4-5-9 (14)							
20	(SW-SC) Clayey Sand; Reddish-brown; Moist	ST	46								
		SPT		7-12-9 (21)							
25	(CL) Silty Clay; Light brown with some orange; Moist and Soft	ST	88								
		SPT		6-8-8 (16)							
30	(CL) Silty Clay; Light brown with some orange; Moist and Soft	ST	100								
		SPT		6-6-8 (14)							
35	(CL) Slightly Silty Clay; Light brown with some orange; Moist	ST	92								

(Continued Next Page)

LOGO
The University of Texas at Arlington
416 Yates Stress
76010

CLIENT SWIS Lab
PROJECT NUMBER
PROJECT NAME Md Asif Akhtar
PROJECT LOCATION Beaumont

DEPTH (ft)	MATERIAL DESCRIPTION	SAMPLE TYPE NUMBER	RECOVERY % (RQD)	BLOW COUNTS (N VALUE)	POCKET PEN. (tsf)	DRY UNIT WT. (pcf)	MOISTURE CONTENT (%)	LIQUID LIMIT	PLASTIC LIMIT	PLASTICITY INDEX	FINES CONTENT (%)
35–40	(CH) Clay; Gray; Moist	SPT		7-6-6 (12)							
		ST	96								
40–45	(CH) Clay; Gray-Blue Gray; Moist	SPT		5-6-6 (12)							
		ST	90								
45–60		SPT		5-5-6 (11)							
		ST	96								
		SPT		6-6-4 (10)							
		ST	88								
		SPT		4-5-6 (11)							
		ST	60								
60–65	(CH) Clay; Gray Moist	SPT		5-6-5 (11)							
		ST	81								
65–70	(CL) Clay into Clayey Sand; Gray; Moist	SPT		6-6-4 (10)							
		ST	73								
70–75	(CH) Clay; Gray; Moist	SPT		8-13-15/5"							
		ST									

(Continued Next Page)

LOGO

The University of Texas at Arlington
416 Yates Stress
76010

BORING NUMBER BR-6A

CLIENT SWIS Lab **PROJECT NAME** Md Asif Akhtar

PROJECT NUMBER **PROJECT LOCATION** Beaumont

DEPTH (ft)	GRAPHIC LOG	MATERIAL DESCRIPTION	SAMPLE TYPE NUMBER	RECOVERY % (RQD)	BLOW COUNTS (N VALUE)	POCKET PEN. (tsf)	DRY UNIT WT. (pcf)	MOISTURE CONTENT (%)	ATTERBERG LIMITS LIQUID LIMIT	PLASTIC LIMIT	PLASTICITY INDEX	FINES CONTENT (%)
75		(CH) Clay; Gray; Moist *(continued)*	SPT		8-8-6 (14)							
			ST	90								
80			SPT		6-6-6 (12)							
			ST	90								
85			SPT		6-35-35/0"							
		Very Little Recovert; Sample looks like just cutting	SS									
90			SPT		8-35-35/0"							
		Large Grain Sand with Rock; Gray into Whte	SS									
95			SPT		8-35-35/0"							
		Large Grain Sand; Gray: Wet	SS									
100			SPT		8-35-35/0"							
		(CH) Shale/ Clay; Blue Gray; Moist	SS									
105			SPT		8-16-11/1"							
		(CH) Shale to Slightly Silty Clay; Blue Gray; Moist	SS									
110			SPT		8-17-27/1"							
		Sandy Clay to Silty Clay; Blue gray; Very Moist	SS									
115												

(Continued Next Page)

LOGO

The University of Texas at Arlington
416 Yates Stress
76010

BORING NUMBER BR-6A

CLIENT SWIS Lab

PROJECT NAME Md Asif Akhtar

PROJECT NUMBER

PROJECT LOCATION Beaumont

DEPTH (ft)	GRAPHIC LOG	MATERIAL DESCRIPTION	SAMPLE TYPE NUMBER	RECOVERY % (RQD)	BLOW COUNTS (N VALUE)	POCKET PEN. (tsf)	DRY UNIT WT. (pcf)	MOISTURE CONTENT (%)	ATTERBERG LIMITS: LIQUID LIMIT	ATTERBERG LIMITS: PLASTIC LIMIT	ATTERBERG LIMITS: PLASTICITY INDEX	FINES CONTENT (%)
115			SPT		8-35-35/0"							
		Sandy/ Silty Clay; Gray; Moist	SS									
120		Bottom of borehole at 120.0 feet.	SPT		8-35-35/0"							

BORING NUMBER BR-10A

PAGE 1 OF 3

LOGO

The University of Texas at Arlington
416 Yates Stress
76010

CLIENT

PROJECT NUMBER

DATE STARTED 12/12/19 **COMPLETED** 12/13/19

DRILLING CONTRACTOR

DRILLING METHOD Wash Boring

LOGGED BY **CHECKED BY**

NOTES

PROJECT NAME Beaumont Site Investigation with Electrical Resisitivity

PROJECT LOCATION Beaumont (SH 96 and SH69 Intersection)

GROUND ELEVATION **HOLE SIZE** inches

GROUND WATER LEVELS:

AT TIME OF DRILLING ---

AT END OF DRILLING ---

AFTER DRILLING ---

DEPTH (ft)	GRAPHIC LOG	MATERIAL DESCRIPTION	SAMPLE TYPE NUMBER	RECOVERY % (RQD)	BLOW COUNTS (N VALUE)	POCKET PEN. (tsf)	DRY UNIT WT. (pcf)	MOISTURE CONTENT (%)	ATTERBERG LIMITS: LIQUID LIMIT	ATTERBERG LIMITS: PLASTIC LIMIT	ATTERBERG LIMITS: PLASTICITY INDEX	FINES CONTENT (%)
0		Dark Brown; Sandy Clay; Organics				1.0						
		Dark Brown; Clay				1.0						
						1.0						
5					0-0-1 (1)	0						
						0						
						.5						
10					0-0-1 (1)							
15					4-8-8 (16)	1.0						
		Gray to Brown; Sandy Clay										
20					5-7-7 (14)	2.0						
		Gray, Brown, Tan; Sandy Clay with White seams			3-5-5 (10)							
25												
30					5-5-5 (10)	2.0						
35												

(Continued Next Page)

LOGO

The University of Texas at Arlington
416 Yates Stress
76010

BORING NUMBER BR-10A

CLIENT

PROJECT NUMBER

PROJECT NAME Beaumont Site Investigation with Electrical Resisitivity

PROJECT LOCATION Beaumont (SH 96 and SH69 Intersection)

DEPTH (ft)	GRAPHIC LOG	MATERIAL DESCRIPTION	SAMPLE TYPE NUMBER	RECOVERY % (RQD)	BLOW COUNTS (N VALUE)	POCKET PEN. (tsf)	DRY UNIT WT. (pcf)	MOISTURE CONTENT (%)	ATTERBERG LIMITS: LIQUID LIMIT	ATTERBERG LIMITS: PLASTIC LIMIT	ATTERBERG LIMITS: PLASTICITY INDEX	FINES CONTENT (%)
35					3-5-7 (12)	1.75						
40					3-4-4 (8)	1.25						
		Gray Clay										
45					5-5-5 (10)	1.5						
50					3-4-4 (8)	1.25						
55					3-5-4 (9)	1.25						
		Gray; Clay Sand										
60					5-4-6 (10)	1.0						
65					5-6-7 (13)	1.5						
		Gray; Sandy Clay with Organics										
70					4-5-5 (10)							
		Brown-gray; Clay Sand; Organics										
75												

(Continued Next Page)

LOGO The University of Texas at Arlington
416 Yates Stress
76010

BORING NUMBER BR-10A

CLIENT ____

PROJECT NUMBER ____

PROJECT NAME Beaumont Site Investigation with Electrical Resisitivity

PROJECT LOCATION Beaumont (SH 96 and SH69 Intersection)

DEPTH (ft)	GRAPHIC LOG	MATERIAL DESCRIPTION	SAMPLE TYPE NUMBER	RECOVERY % (RQD)	BLOW COUNTS (N VALUE)	POCKET PEN. (tsf)	DRY UNIT WT. (pcf)	MOISTURE CONTENT (%)	ATTERBERG LIMITS: LIQUID LIMIT	ATTERBERG LIMITS: PLASTIC LIMIT	ATTERBERG LIMITS: PLASTICITY INDEX	FINES CONTENT (%)
75					3-12-30 (42)	.5						
80		Gray; Sand Clay with wood in Bedded Organics			4-3-4 (7)							
85		Tan Gray sand with wood organics in bed			12-19-36/5"							
90					5-6-23 (29)							
95					12-50-50/0"							
100					12-50-50/0"							

Bottom of borehole at 100.4 feet.

GEOTECH BH COLUMNS - GINT STD US LAB.GDT - 12/18/19 12:18 - C:\USERS\PUBLIC\DOCUMENTS\BENTLEY\GINT\PROJECTS\GINT STD US LAB.GPJ

Corpus Christi District (February 2020)

LOGO

The University of Texas at Arlington
416 Yates Stress
76010

BORING NUMBER BR 201

PAGE 1 OF 2

CLIENT		PROJECT NAME	The University of Texas at Arlington
PROJECT NUMBER		PROJECT LOCATION	Corpus Christi
DATE STARTED	2/25/20 COMPLETED 2/25/20	GROUND ELEVATION	0 ft HOLE SIZE inches
DRILLING CONTRACTOR		GROUND WATER LEVELS:	
DRILLING METHOD	Wash Boring	∇ AT TIME OF DRILLING	15.00 ft / Elev -15.00 ft
LOGGED BY	CHECKED BY	AT END OF DRILLING	---
NOTES		AFTER DRILLING	---

DEPTH (ft)	GRAPHIC LOG	MATERIAL DESCRIPTION	SAMPLE TYPE NUMBER	RECOVERY % (RQD)	BLOW COUNTS (N VALUE)	POCKET PEN. (tsf)	DRY UNIT WT. (pcf)	MOISTURE CONTENT (%)	ATTERBERG LIMITS: LIQUID LIMIT	PLASTIC LIMIT	PLASTICITY INDEX	FINES CONTENT (%)
0		LEAN CLAY WITH SAND, (CL) ;Dark Brown;	SS		4-6-5 (11)							
		SILTY SAND, (SM) ;Brown; moist;	SS		4-9-11 (20)							
5		LEAN CLAY WITH SAND, (CL) ;Brown; slightly moist; soft;	SPT		8-7-6 (13)							
10			SPT		1-5-5 (10)							
		SILTY SAND, (SM) ;Very Pale brown; soft; wet;	SS		2-2-3 (5)							
15		∇	SPT		2-4-8 (12)							
20			SPT		4-13-14 (27)							
		SILTY SAND, (SM) ;Very Pale Brown; Wet;										
25			SPT		12-33-50/2"							
		WELL GRADED SAND WITH SILT, (SW-SM) ;Very Pale brown to light gray; soft;										
30			SPT		12-33-50/3"							
		WELL GRADED SAND, (SW) ;Light Grayish;										
35		CLAYEY SAND, (SC) ;Light Gray; Stiff;	ST			4.5+						

(Continued Next Page)

GEOTECH BH COLUMNS - GINT STD US LAB.GDT - 3/5/20 12:27 - C:\USERS\MXA0516\ONEDRIVE - UNIVERSITY OF TEXAS AT ARLINGTON\LAB DOCS\RESISTIVITY IMAGING\TEST RESULTS\SITE RESULTS\CORPUS CHRISTI\BR 201\BORELOG\CC_BR201.GPJ

LOGO

The University of Texas at Arlington
416 Yates Stress
76010

BORING NUMBER BR 201

CLIENT ______

PROJECT NUMBER ______

PROJECT NAME The University of Texas at Arlington

PROJECT LOCATION Corpus Christi

DEPTH (ft)	GRAPHIC LOG	MATERIAL DESCRIPTION	SAMPLE TYPE NUMBER	RECOVERY % (RQD)	BLOW COUNTS (N VALUE)	POCKET PEN. (tsf)	DRY UNIT WT. (pcf)	MOISTURE CONTENT (%)	ATTERBERG LIMITS: LIQUID LIMIT	ATTERBERG LIMITS: PLASTIC LIMIT	ATTERBERG LIMITS: PLASTICITY INDEX	FINES CONTENT (%)
35			SPT		12-50-50/0"							
			ST			4.5+						
40			SPT		12-34-50/0"							
		LEAN CLAY WITH SAND, (CL) ;Slight Gray; very Stiff with orangeish Stain;	ST			4.5+						
45			SPT		8-33-34/2"							
		LEAN CLAY WITH SAND, (CL) ;Light Gray, Pale Brown; Stiff;	ST			2.5						
50			SPT		12-50-50/0"							
		WELL GRADED SAND, (SW) ;Pale Brown; Wet;	SPT		12-50-50/0"							
55												
		LEAN CLAY, (CL) ;Brown, yellowish strain; very stiff;	ST			4.5+						
60			SPT		8-15-15/4"							
			ST			4.5+						
65			SPT		8-17-20/5"							
		LEAN CLAY WITH SAND, (CL) ;Light Gray;	ST			4.5+						
70			SPT		8-22-28/3"							
75												

Bottom of borehole at 75.0 feet.

BORING NUMBER BR 202

LOGO

The University of Texas at Arlington
416 Yates Stress
76010

CLIENT ______
PROJECT NUMBER ______
DATE STARTED 2/24/20 COMPLETED 2/24/20
DRILLING CONTRACTOR ______
DRILLING METHOD Wash Boring
LOGGED BY ______ CHECKED BY ______
NOTES ______

PROJECT NAME The University of Texas at Arlington
PROJECT LOCATION Corpus Christi
GROUND ELEVATION 0 ft HOLE SIZE inches
GROUND WATER LEVELS:
∇ AT TIME OF DRILLING 16.00 ft / Elev -16.00 ft
AT END OF DRILLING —
AFTER DRILLING —

DEPTH (ft)	GRAPHIC LOG	MATERIAL DESCRIPTION	SAMPLE TYPE NUMBER	RECOVERY % (RQD)	BLOW COUNTS (N VALUE)	POCKET PEN. (tsf)	DRY UNIT WT. (pcf)	MOISTURE CONTENT (%)	ATTERBERG LIMITS: LIQUID LIMIT	ATTERBERG LIMITS: PLASTIC LIMIT	ATTERBERG LIMITS: PLASTICITY INDEX	FINES CONTENT (%)
0		LEAN CLAY WITH SAND, (CL) ; Brown Sandy;	SS		4-5-8 (13)							
		LEAN CLAY WITH SAND, (CL) ; Brown; Slightly Moist;	SS		9-10-6 (16)							
5		LEAN CLAY, (CL) ; Light Tan, Reddish; Slightly Moist; Stiff;	SPT		1-3-5 (8)							
			SS		3-4-4 (8)							
		WELL GRADED SAND WITH CLAY, (SW-SC) ; Light Tan; Loose; Slightly Moist;	ST			0.5						
10		WELL GRADED SAND, (SW) ; Light Tan; Loose; Wet;	SPT		6-8-12 (20)							
			SS		7-8-8 (16)							
15		∇	SPT		4-8-9 (17)							
			SS		2-4-7 (11)							
20			SPT		8-11-7/2"							
			SS		2-3-6 (9)							
25		WELL GRADED SAND WITH GRAVEL, (SW) ; Light Tan; Wet;	SPT		12-35-50/3"							
			SS		5-12-25 (37)							
30		WELL GRADED SAND WITH SILT, (SW-SM) ; Light Gray with Small Seam of Sandy Clay; Stiff;	SPT		12-50-50/0"							
			SS		16-24-28 (52)							
35												

(Continued Next Page)

GEOTECH BH COLUMNS - GINT STD US LAB.GDT - 3/5/20 12:29 - C:\USERS\MXA0516\ONEDRIVE - UNIVERSITY OF TEXAS AT ARLINGTON\LAB DOCS\RESISTIVITY IMAGING\TEST RESULTS\SITE RESULT\CORPUS CHRISTI\BR 201\BORELOG\CC_BR201.GPJ

LOGO

The University of Texas at Arlington
416 Yates Stress
76010

BORING NUMBER BR 202

PAGE 2 OF 2

CLIENT ______

PROJECT NUMBER ______

PROJECT NAME The University of Texas at Arlington

PROJECT LOCATION Corpus Christi

DEPTH (ft)	GRAPHIC LOG	MATERIAL DESCRIPTION	SAMPLE TYPE NUMBER	RECOVERY % (RQD)	BLOW COUNTS (N VALUE)	POCKET PEN. (tsf)	DRY UNIT WT. (pcf)	MOISTURE CONTENT (%)	ATTERBERG LIMITS LIQUID LIMIT	ATTERBERG LIMITS PLASTIC LIMIT	ATTERBERG LIMITS PLASTICITY INDEX	FINES CONTENT (%)
35			SPT		12-50-50/0"							
		WELL GRADED SAND, (SW) ; Pale Brown, Lioght Grayish; Loose; Wet;	SS		5-12-17 (29)							
40			SPT		8-28-21/4"							
		WELL GRADED SAND WITH SILT, (SW-SM) ; Pale Brown; Dense Sand;	SS		4-9-15 (24)							
			ST									
45		LEAN CLAY WITH SAND, (CL) ; Light Grayish; Pale Brown; Sandy Clay; Stiff;	SPT		12-50-50/0"							
50			SPT		12-50-50/0"							
		WELL GRADED SAND, (SW) ; Pale Brown, Grayish; Soft Sand;	SS		23-29-27 (56)							
55			SPT		8-20-13/3"							
		WELL GRADED SAND WITH CLAY, (SW-SC) ; Pale Brown; Very Stiff; Slightly Moist;	SS		8-12-17 (29)							
		Seam of Clay										
			ST									
60		LEAN CLAY, (CL) ; Pale Brown, Orange;	SPT		8-11-20/6"							
			ST									
65			SPT		8-25-27/2"							
			ST									
70		Bottom of borehole at 70.0 feet.	SPT		9-27-27/2"							

GEOTECH BH COLUMNS - GINT STD US LAB.GDT - 3/5/20 12:29 - C:\USERS\MXA0516\ONEDRIVE - UNIVERSITY OF TEXAS AT ARLINGTON\LAB DOCS\RESISTIVITY IMAGING\TEST RESULTS\SITE RESULTS\CORPUS CHRISTI\BR 201\BORELOGCC_BR201.GPJ

LOGO

The University of Texas at Arlington
416 Yates Stress
76010

BORING NUMBER RW 214

CLIENT	PROJECT NAME: The University of Texas at Arlington
PROJECT NUMBER	PROJECT LOCATION: Corpus Christi
DATE STARTED: 2/25/20 COMPLETED: 2/25/20	GROUND ELEVATION: 0 ft HOLE SIZE: inches
DRILLING CONTRACTOR	GROUND WATER LEVELS:
DRILLING METHOD: Wash Boring	▽ AT TIME OF DRILLING: 13.00 ft / Elev -13.00 ft
LOGGED BY CHECKED BY	AT END OF DRILLING: ---
NOTES	AFTER DRILLING: ---

DEPTH (ft)	GRAPHIC LOG	MATERIAL DESCRIPTION	SAMPLE TYPE NUMBER	RECOVERY % (RQD)	BLOW COUNTS (N VALUE)	POCKET PEN. (tsf)	DRY UNIT WT. (pcf)	MOISTURE CONTENT (%)	ATTERBERG LIMITS: LIQUID LIMIT	PLASTIC LIMIT	PLASTICITY INDEX	FINES CONTENT (%)
0		LEAN CLAY WITH SAND, (CL) ; Dark Brown sandy Clay;	SS		3-3-3 (6)							
		CLAYEY SAND, (SC) ; Sandy Clay with brown sand;	SS		4-5-8 (13)							
5			SPT		5-4-4 (8)							
		CLAYEY SAND, (SC) ; Brown Sand with some clayey Sand;	SS		4-4-6 (10)							
10			SPT		6-6-7 (13)							
		WELL GRADED SAND, (SW) ; Tan; Sand; Moist; ▽	SS		4-6-8 (14)							
15			SPT		6-6-6 (12)							
		WELL GRADED SAND, (SW) ; Tan; Sand followed by Tan Coarse sand with some gravel at 17.5';	SS		2-3-5 (8)							
20			SPT		8-6-5 (11)							
		WELL GRADED SAND WITH SILT, (SW) ; Coarse sand with some gravel; Wet; Dense;	SS		3-4-4 (8)							
25			SPT		8-8-8/5"							
		LEAN CLAY WITH SAND, (CL) ; Tan; Sandy Clay;	SS		5-7-6 (13)							
30		LEAN CLAY WITH SAND, (CL) ; Tan; Sany Clay followed by Tan Sand;	ST									
			SPT		8-9-9 (18)							
		WELL GRADED SAND WITH SILT, (SW) ; Tan; Sand;										
35												

(Continued Next Page)

LOGO

The University of Texas at Arlington
416 Yates Stress
76010

BORING NUMBER RW 214

CLIENT ______

PROJECT NUMBER ______

PROJECT NAME The University of Texas at Arlington

PROJECT LOCATION Corpus Christi

DEPTH (ft)	GRAPHIC LOG	MATERIAL DESCRIPTION	SAMPLE TYPE NUMBER	RECOVERY % (RQD)	BLOW COUNTS (N VALUE)	POCKET PEN. (tsf)	DRY UNIT WT. (pcf)	MOISTURE CONTENT (%)	ATTERBERG LIMITS: LIQUID LIMIT	ATTERBERG LIMITS: PLASTIC LIMIT	ATTERBERG LIMITS: PLASTICITY INDEX	FINES CONTENT (%)
35			SPT		12-26-50 (76)							
		WELL GRADED SAND WITH SILT, (SW) ; Tan; sand; Wet; Dense;	SS		6-13-18 (31)							
40												
			SPT		8-19-17 (36)							
		LEAN CLAY WITH SAND, (CL) ; Tan; Silty Sandy Clay with sand seam;	SS		9-12-13 (25)							

Bottom of borehole at 43.0 feet.

LOGO

The University of Texas at Arlington
416 Yates Stress
76010

BORING NUMBER RW 215

CLIENT ______
PROJECT NUMBER ______
DATE STARTED 2/25/20 COMPLETED 2/25/20
DRILLING CONTRACTOR ______
DRILLING METHOD Wash Boring
LOGGED BY ______ CHECKED BY ______
NOTES ______

PROJECT NAME The University of Texas at Arlington
PROJECT LOCATION Corpus Christi
GROUND ELEVATION 0 ft HOLE SIZE inches
GROUND WATER LEVELS:
AT TIME OF DRILLING 13.00 ft / Elev -13.00 ft
AT END OF DRILLING ---
AFTER DRILLING ---

DEPTH (ft)	MATERIAL DESCRIPTION	SAMPLE TYPE NUMBER	RECOVERY % (RQD)	BLOW COUNTS (N VALUE)	POCKET PEN. (tsf)	DRY UNIT WT. (pcf)	MOISTURE CONTENT (%)	ATTERBERG LIMITS: LIQUID LIMIT	PLASTIC LIMIT	PLASTICITY INDEX	FINES CONTENT (%)
0	LEAN CLAY WITH SAND, (CL) ; Dark Brown; Sandy Clay;	SS		2-4-4 (8)							
	SILT WITH SAND, (ML) ; Dark Brown; Sandy Clay followed by Brown Sand;	SS		5-8-9 (17)							
5	LEAN CLAY WITH SAND, (CL) ; Brown; Sandy Clay;	SPT		7-6-5 (11)							
		SS		3-3-4 (7)							
10		ST			3.5						
	WELL GRADED SAND, (SW) ; Tan; Sand; Wet; soft;	SPT		9-6-7 (13)							
15		SS		6-7-6 (13)							
	WELL GRADED SAND, (SW) ; Coarse Sand; Wet; Dense;	SPT		12-8-10 (18)							
20		SS		2-3-4 (7)							
		SPT		12-11-10 (21)							
		SS		4-5-6 (11)							
25		SPT		12-50-50/0"							
		SS		7-5-16 (21)							
30		SPT		12-26-14/5"							
		SS		3-3-4 (7)							
35											

GEOTECH BH COLUMNS - GINT STD US LAB.GDT - 3/5/20 12:22 - C:\USERS\MXA0516\ONEDRIVE - UNIVERSITY OF TEXAS AT ARLINGTON\LAB DOCS\RESISTIVITY IMAGING\TEST RESULTS\SITE RESULTS\CORPUS CHRISTI\BR 201\BORELOG\CC_BR201.GPJ

(Continued Next Page)

LOGO

The University of Texas at Arlington
416 Yates Stress
76010

BORING NUMBER RW 215

CLIENT

PROJECT NUMBER

PROJECT NAME The University of Texas at Arlington

PROJECT LOCATION Corpus Christi

DEPTH (ft)	GRAPHIC LOG	MATERIAL DESCRIPTION	SAMPLE TYPE NUMBER	RECOVERY % (RQD)	BLOW COUNTS (N VALUE)	POCKET PEN. (tsf)	DRY UNIT WT. (pcf)	MOISTURE CONTENT (%)	ATTERBERG LIMITS LIQUID LIMIT	ATTERBERG LIMITS PLASTIC LIMIT	ATTERBERG LIMITS PLASTICITY INDEX	FINES CONTENT (%)
35		LEAN CLAY, (CL-ML) ; Tan; Clay Seam;	SPT		12-24-16/4"							
		LEAN CLAY WITH SAND, (CL) ; Slight Recovery; Moist;										
		; Seam of Sand;										
40			SPT		12-46-45 (91)							
		LEAN CLAY WITH SAND, (CL) ; Sand Followed by tan clay;	SS		22-20-25 (45)							

Bottom of borehole at 43.5 feet.

Fort Worth District (July 2019)

BORING NUMBER BH-1
PAGE 1 OF 1

Logo uta

CLIENT TxDOT - Fort Worth
PROJECT NAME Fort Worth Slope Stabilization
PROJECT NUMBER 1
PROJECT LOCATION I30 and Fielder Road (North)
DATE STARTED 6/20/19 COMPLETED 6/20/19
GROUND ELEVATION HOLE SIZE
DRILLING CONTRACTOR
GROUND WATER LEVELS:
DRILLING METHOD Hollow Stem Auger
AT TIME OF DRILLING ---
LOGGED BY UTA CHECKED BY UTA
AT END OF DRILLING ---
NOTES
AFTER DRILLING ---

DEPTH (ft)	GRAPHIC LOG	MATERIAL DESCRIPTION	SAMPLE TYPE NUMBER	BLOW COUNTS (N VALUE)	MOISTURE CONTENT (%)
0		Light gray Clay	SH		
5			TCP	18-18 (36)	
		Light gray Clay	AU		
		Brown Clay	TCP	50 (5")-50(4")	
10		Light gray Limestone			
		Limestone	AU		
15			TCP	50 (4")-50(3")	

Bottom of borehole at 15.0 feet.

Logo uta

BORING NUMBER BH-2

PAGE 1 OF 1

CLIENT TxDOT - Fort Worth
PROJECT NAME Fort Worth Slope Stabilization
PROJECT NUMBER 1
PROJECT LOCATION I30 and Fielder Road (North)
DATE STARTED 6/20/19 COMPLETED 6/20/19
GROUND ELEVATION HOLE SIZE
DRILLING CONTRACTOR
GROUND WATER LEVELS:
DRILLING METHOD Hollow Stem Auger
AT TIME OF DRILLING ---
LOGGED BY UTA CHECKED BY UTA
AT END OF DRILLING ---
NOTES
AFTER DRILLING ---

DEPTH (ft)	GRAPHIC LOG	MATERIAL DESCRIPTION	SAMPLE TYPE NUMBER	BLOW COUNTS (N VALUE)	MOISTURE CONTENT (%)
0		Brown Clay	ST		
5			TCP	21-25 (46)	
		Brown Clay			
			AU		
		Gray Clay			
10			TCP	40-50 (3")	
		Brown Limestone			
		Light gray Limestone	AU		
15			TCP	50 (2")-50(2")	

Bottom of borehole at 15.0 feet.

GEOTECH BH COLUMNS - GINT STD US GDT - 6/20/19 21:18 - C:\USERS\PXB3031\ONEDRIVE - UNIVERSITY OF TEXAS AT ARLINGTON\FORTWORTH INSTALLATION\DRILLING\BORELOG\I30 AND FIELDER ROAD - NORTH\I30 AND FIELDER ROAD (NORTH).GPJ

Logo uta

BORING NUMBER BH-1

CLIENT TxDOT - Fort Worth
PROJECT NAME Fort Worth Slope Stabilization
PROJECT NUMBER 2
PROJECT LOCATION I30 and Fielder Road (South)
DATE STARTED 6/20/19 **COMPLETED** 6/20/19
GROUND ELEVATION **HOLE SIZE**
DRILLING CONTRACTOR
GROUND WATER LEVELS:
DRILLING METHOD Hollow Stem Auger
AT TIME OF DRILLING ---
LOGGED BY UTA **CHECKED BY** UTA
AT END OF DRILLING ---
NOTES
AFTER DRILLING ---

DEPTH (ft)	GRAPHIC LOG	MATERIAL DESCRIPTION	SAMPLE TYPE NUMBER	BLOW COUNTS (N VALUE)	MOISTURE CONTENT (%)
0–6		Brown Clay	SH; AU TCP	3-5 (8)	
6–7		Reddish brown Clay			
7–11		Light red Clay	AU; ST TCP	12-18 (30)	
11–13		Reddish brown Clay			
13–14		Yellowish brown Clay	AU		
14–15		Grayish white Limestone	ST; TCP	50 (2")-50 (2")	

Bottom of borehole at 15.0 feet.

BORING NUMBER BH-2
PAGE 1 OF 1

Logo uta

CLIENT TxDOT - Fort Worth	PROJECT NAME Fort Worth Slope Stabilization
PROJECT NUMBER 2	PROJECT LOCATION I30 and Fielder Road (South)
DATE STARTED 6/20/19 COMPLETED 6/20/19	GROUND ELEVATION HOLE SIZE
DRILLING CONTRACTOR	GROUND WATER LEVELS:
DRILLING METHOD Hollow Stem Auger	AT TIME OF DRILLING ---
LOGGED BY UTA CHECKED BY UTA	AT END OF DRILLING ---
NOTES	AFTER DRILLING ---

DEPTH (ft)	GRAPHIC LOG	MATERIAL DESCRIPTION	SAMPLE TYPE NUMBER	BLOW COUNTS (N VALUE)	MOISTURE CONTENT (%)
0		Dark brown Clay	ST		
5		Brown Clay	TCP	4-5 (9)	
		Brownish red Clay	SH		
10		Brown Clay	TCP	10-14 (24)	
		Light gray Clay	AU		
15		Light gray Limestone	TCP	50 (2")-50 (2")	

Bottom of borehole at 15.0 feet.

GEOTECH BH COLUMNS - GINT STD US GDT - 6/21/19 18:49 - C:\USERS\PXB3017\ONEDRIVE - UNIVERSITY OF TEXAS AT ARLINGTON\FORTWORTH INSTALLATION\DRILLING\BORELOGS\I820 AND SUN VALLEY DRIVE\I820 AND SUN VALLEY DRIVE.GPJ

Logo uta

BORING NUMBER BH-1

PAGE 1 OF 1

CLIENT TxDOT - Fort Worth
PROJECT NAME Fort Worth Slope Stabilization
PROJECT NUMBER 3
PROJECT LOCATION I820 and Sun Valley Drive
DATE STARTED 6/21/19 COMPLETED 6/21/19
GROUND ELEVATION HOLE SIZE
DRILLING CONTRACTOR
GROUND WATER LEVELS:
DRILLING METHOD Hollow Stem Auger
AT TIME OF DRILLING ---
LOGGED BY UTA CHECKED BY UTA
AT END OF DRILLING ---
NOTES
AFTER DRILLING ---

DEPTH (ft)	GRAPHIC LOG	MATERIAL DESCRIPTION	SAMPLE TYPE NUMBER	BLOW COUNTS (N VALUE)	MOISTURE CONTENT (%)
0		Dark gray Clay	AU		
			SH		
5			TCP	7-8 (15)	
		Brown Clay	AU		
		Dark brownish gray Clay	SH		
10			TCP	10-14 (24)	
		Brown Clay	AU		
15			SH		
			TCP	50 (5.5")-50(5.5")	
		Grayish brown Clay with traces of limestone	AU		
20			TCP	50 (5.75")-50(5.5")	
		Whiteish gray Very stiff clay	AU		
25			TCP	50 (0")-50(0")	

Bottom of borehole at 25.0 feet.

Logo uta

BORING NUMBER BH-2

PAGE 1 OF 1

CLIENT TxDOT - Fort Worth
PROJECT NAME Fort Worth Slope Stabilization
PROJECT NUMBER 3
PROJECT LOCATION I820 and Sun Valley Drive
DATE STARTED 6/21/19 COMPLETED 6/21/19
GROUND ELEVATION HOLE SIZE
DRILLING CONTRACTOR
GROUND WATER LEVELS:
DRILLING METHOD Hollow Stem Auger
AT TIME OF DRILLING ---
LOGGED BY UTA CHECKED BY UTA
AT END OF DRILLING ---
NOTES
AFTER DRILLING ---

DEPTH (ft)	GRAPHIC LOG	MATERIAL DESCRIPTION	SAMPLE TYPE NUMBER	BLOW COUNTS (N VALUE)	MOISTURE CONTENT (%)
0		Brown Clay	AU		
5			SH TCP	4-3 (7)	
			SH		
10			TCP	5-11 (16)	
			AU		
15		Light brown Clay	SH TCP	46-50 (4")	
		Brown Very stiff clay	AU		
20			TCP	50 (4")-50 (3")	
25			TCP	50 (1")-50 (0")	

Bottom of borehole at 25.0 feet.

GEOTECH BH COLUMNS - GINT STD US.GDT - 6/21/19 18:40 - C:\USERS\PXB3310\ONEDRIVE - UNIVERSITY OF TEXAS AT ARLINGTON\FORTWORTH INSTALLATION\DRILLING\BORELOGS\3. I820 AND SUN VALLEY DRIVE\I820 AND SUN VALLEY DRIVE.GPJ

Logo uta

BORING NUMBER BH-1

PAGE 1 OF 1

CLIENT TxDOT - Fort Worth	**PROJECT NAME** Fort Worth Slope Stabilization
PROJECT NUMBER 4	**PROJECT LOCATION** I20 and Park Springs Blvd.
DATE STARTED 6/21/19 **COMPLETED** 6/21/19	**GROUND ELEVATION** **HOLE SIZE**
DRILLING CONTRACTOR	**GROUND WATER LEVELS:**
DRILLING METHOD Hollow Stem Auger	**AT TIME OF DRILLING** ---
LOGGED BY UTA **CHECKED BY** UTA	**AT END OF DRILLING** ---
NOTES	**AFTER DRILLING** ---

DEPTH (ft)	GRAPHIC LOG	MATERIAL DESCRIPTION	SAMPLE TYPE NUMBER	BLOW COUNTS (N VALUE)	MOISTURE CONTENT (%)
0		Brown Fill clayey sand	AU		
		Reddish brown Clayey sand	AU		
5		Whiteish gray Silty sand	TCP	14-9 (23)	
		Dark brown Silty clay	AU		
10		Gray Clay with traces of silt	SH TCP	24-35 (59)	
		Brown Clay	AU		
15		Reddish brown Clay with traces of water and silt	SH TCP	17-50 (3")	
20		Dark reddish brown Sandstone	AU TCP	50 (0")-50 (0")	

Bottom of borehole at 20.0 feet.

GEOTECH BH COLUMNS - GINT STD US GDT - 6/21/19 15:26 - C:\USERS\PXB3107\ONEDRIVE - UNIVERSITY OF TEXAS AT ARLINGTON\FORTWORTH INSTALLATION\DRILLING\BORELOG\4. I20 AND PARK SPRINGS BLVD\I20 AND PARK SPRINGS BLVD.GPJ

Logo uta

BORING NUMBER BH-2

PAGE 1 OF 1

CLIENT TxDOT - Fort Worth

PROJECT NAME Fort Worth Slope Stabilization

PROJECT NUMBER 4

PROJECT LOCATION I20 and Park Springs Blvd.

DATE STARTED 6/21/19 **COMPLETED** 6/21/19

GROUND ELEVATION ______ **HOLE SIZE** ______

DRILLING CONTRACTOR ______

GROUND WATER LEVELS:

DRILLING METHOD Hollow Stem Auger

AT TIME OF DRILLING ---

LOGGED BY UTA **CHECKED BY** UTA

AT END OF DRILLING ---

NOTES ______

AFTER DRILLING ---

DEPTH (ft)	GRAPHIC LOG	MATERIAL DESCRIPTION	SAMPLE TYPE NUMBER	BLOW COUNTS (N VALUE)	MOISTURE CONTENT (%)
0		Reddish brown Sandy clay	AU TCP	25-27 (52)	
5		Reddish brown Silty clay	AU		
		Reddish brown Clay			
		Gray Shally clay	SH TCP	29-35 (64)	
10		Light gray Silty sand			
15		Brown Clay with traces of sandstone	AU SH TCP	50 (0.5")- 50 (0.5")	
20		Dark brown Sandstone	AU TCP	50 (0.75")- 50 (0.5")	

Bottom of borehole at 20.0 feet.

LOGO UTA

BORING NUMBER BH-1

CLIENT TxDOT - Fort Worth

PROJECT NAME Fort Worth Slope Stabilization

PROJECT NUMBER 5

PROJECT LOCATION I820 and Rosedale St

DATE STARTED 10/1/19 **COMPLETED** 10/1/19

GROUND ELEVATION **HOLE SIZE** inches

DRILLING CONTRACTOR

GROUND WATER LEVELS:

DRILLING METHOD Hollow Stem Auger

AT TIME OF DRILLING ---

LOGGED BY UTA **CHECKED BY** UTA

AT END OF DRILLING ---

NOTES

AFTER DRILLING ---

DEPTH (ft)	GRAPHIC LOG	MATERIAL DESCRIPTION	SAMPLE TYPE NUMBER	BLOW COUNTS (N VALUE)	MOISTURE CONTENT (%)
0–5		Gray Silty clay	ST TCP	6-6 (12)	
5–8		Brown Clay with traces of small stones	AU		
8–10		Brown Clay	ST TCP	9-8 (17)	
10–20		Light brown Clay	AU		
			ST TCP	3-4 (7)	
			AU		
			ST TCP	8-9 (17)	
20–30		Dark brown Clay	AU		
			ST TCP	7-10 (17)	
			AU		
			ST TCP	7-11 (18)	

Bottom of borehole at 30.0 feet.

LOGO UTA

BORING NUMBER BH-2

PAGE 1 OF 1

CLIENT TxDOT - Fort Worth
PROJECT NAME Fort Worth Slope Stabilization
PROJECT NUMBER 5
PROJECT LOCATION I820 and Rosedale St
DATE STARTED 10/1/19 **COMPLETED** 10/1/19
GROUND ELEVATION **HOLE SIZE** inches
DRILLING CONTRACTOR
GROUND WATER LEVELS:
DRILLING METHOD Hollow Stem Auger
AT TIME OF DRILLING ---
LOGGED BY UTA **CHECKED BY** UTA
AT END OF DRILLING ---
NOTES
AFTER DRILLING ---

DEPTH (ft)	GRAPHIC LOG	MATERIAL DESCRIPTION	SAMPLE TYPE NUMBER	BLOW COUNTS (N VALUE)	MOISTURE CONTENT (%)
0–5		Gray Silty clay	ST TCP	2-2 (4)	
5–10		Brown Clay	AU		
			ST TCP	5-7 (12)	
10–15		Brown Clay	AU		
			ST		
			TCP	4-5 (9)	
15–20		Light brown Clay	AU		
			ST TCP	6-8 (14)	
20–30		Dark brown Clay	AU		
			ST TCP	7-9 (16)	
			AU		
			ST TCP	7-10 (17)	

Bottom of borehole at 30.0 feet.

GEOTECH BH COLUMNS - GINT STD US LAB.GDT - 12/5/19 15:36 - C:\USERS\PXB3319\ONEDRIVE - UNIVERSITY OF TEXAS AT ARLINGTON\2. FORTWORTH INSTALLATION\DRILLING\BORELOGS\I820 AND ROSEDALE ST\I820 AND ROSEDALE ST.GPJ

Fort Worth District (October 2020)

LOGO University of Texas at Arlington

BORING NUMBER BH-1
PAGE 1 OF 1

CLIENT TxDOT-Forth Worth	**PROJECT NAME** Forth Worth Slope Stabilization
PROJECT NUMBER 1	**PROJECT LOCATION** US 67 & W Henderson St (South)
DATE STARTED 10/7/20 **COMPLETED** 10/7/20	**GROUND ELEVATION** **HOLE SIZE** inches
DRILLING CONTRACTOR	**GROUND WATER LEVELS:**
DRILLING METHOD Auger Drilling	**AT TIME OF DRILLING** ---
LOGGED BY UTA **CHECKED BY** UTA	**AT END OF DRILLING** ---
NOTES	**AFTER DRILLING** ---

DEPTH (ft)	GRAPHIC LOG	MATERIAL DESCRIPTION	SAMPLE TYPE NUMBER	BLOW COUNTS (N VALUE)	MOISTURE CONTENT (%)
0.0		Brown clay	ST		
		Dark grey clay weathered rock			
2.5					10.4 %
			AU		
		Light gray clay with traces of limestone	TCP	50(6")-50(3")	
5.0					
7.5			AU		10.4 %
			AU		
10.0					11.7 %
			TCP	41-40 (81)	

Bottom of borehole at 12.0 feet.

GEOTECH BH COLUMNS - GINT STD US LAB.GDT - 10/12/20 12:42 - C:\USERS\PUBLIC\DOCUMENTS\BENTLEY\GINT\PROJECTS\US 67 & W HENDERSON ST (SOUTH).GPJ

BORING NUMBER BH-2

LOGO University of Texas at Arlington

CLIENT TxDOT-Forth Worth
PROJECT NAME Forth Worth Slope Stabilization
PROJECT NUMBER 1
PROJECT LOCATION US 67 & W Henderson St (South)
DATE STARTED 10/7/20 COMPLETED 10/7/20
GROUND ELEVATION HOLE SIZE inches
DRILLING CONTRACTOR
GROUND WATER LEVELS:
DRILLING METHOD Auger Drilling
AT TIME OF DRILLING ---
LOGGED BY UTA CHECKED BY UTA
AT END OF DRILLING ---
NOTES
AFTER DRILLING ---

DEPTH (ft)	GRAPHIC LOG	MATERIAL DESCRIPTION	SAMPLE TYPE NUMBER	BLOW COUNTS (N VALUE)	MOISTURE CONTENT (%)
0.0		Dark borwn clay	ST		
2.5					
		Light gray clay with traces of limestone	AU		5.9 %
5.0			TCP	50(1")-50(1")	
					10.2 %
7.5		Grey weathered rock	AU		
10.0			TCP	50(0.5")-50(0.5")	10.5 %
12.5					
15.0			AU		

Bottom of borehole at 15.0 feet.

LOGO University of Texas at Arlington

BORING NUMBER BH-3

CLIENT TxDOT-Forth Worth

PROJECT NAME Forth Worth Slope Stabilization

PROJECT NUMBER 1

PROJECT LOCATION US 67 & W Henderson St (South)

DATE STARTED 10/8/20 **COMPLETED** 10/8/20

GROUND ELEVATION **HOLE SIZE** inches

DRILLING CONTRACTOR

GROUND WATER LEVELS:

DRILLING METHOD Auger Drilling

AT TIME OF DRILLING ---

LOGGED BY UTA **CHECKED BY** UTA

AT END OF DRILLING ---

NOTES

AFTER DRILLING ---

DEPTH (ft)	MATERIAL DESCRIPTION	SAMPLE TYPE NUMBER	BLOW COUNTS (N VALUE)	MOISTURE CONTENT (%)
0	Dark brown stiff clay	ST		
	Grey weathered rock	TCP	48-50(3")	6.9 %
		AU		
	Light gray weathered limestone			
5				6.8 %
		TCP	50(3")-50(1")	
10		TCP	50(5")-25	
	Yellow brown stiff clay			
				10.8 %
15		AU		18.6 %
		TCP	50(4.25")-50(4.25")	
		AU		18.4 %
	Grey brown stiff clay	ST		
20		ST		
25		TCP	50(0.5")-50(0)	18.4 %

Bottom of borehole at 25.0 feet.

LOGO University of Texas at Arlington

BORING NUMBER BH-4

PAGE 1 OF 1

CLIENT TxDOT-Forth Worth

PROJECT NUMBER 1

DATE STARTED 10/8/20 COMPLETED 10/8/20

DRILLING CONTRACTOR

DRILLING METHOD Auger Drilling

LOGGED BY UTA CHECKED BY UTA

NOTES

PROJECT NAME Forth Worth Slope Stabilization

PROJECT LOCATION US 67 & W Henderson St (South)

GROUND ELEVATION HOLE SIZE inches

GROUND WATER LEVELS:

AT TIME OF DRILLING ---

AT END OF DRILLING ---

AFTER DRILLING ---

DEPTH (ft)	GRAPHIC LOG	MATERIAL DESCRIPTION	SAMPLE TYPE NUMBER	BLOW COUNTS (N VALUE)	MOISTURE CONTENT (%)
0.0		Dark brown stiff clay with gravel			
			ST		
2.5			ST		
			ST		
5.0					17.6 %
			AU TCP	30-26 (56)	
7.5		Yellow brown clay with crushed limesotne			15.5 %
			AU		21.8 %
			ST		
10.0			TCP	50(3")-39	
			TCP	50(6")-50(6")	

Bottom of borehole at 12.0 feet.

GEOTECH BH COLUMNS - GINT STD US LAB.GDT - 10/12/20 12:42 - C:\USERS\PUBLIC\DOCUMENTS\BENTLEY\GINT\PROJECTS\US 67 & W HENDERSON ST (SOUTH).GPJ

BORING NUMBER BH-1

PAGE 1 OF 1

LOGO University of Texas at Arlington

CLIENT: University of Texas at Arlington	PROJECT NAME: TxDOT-Fort Worth
PROJECT NUMBER: 1	PROJECT LOCATION: US 67 and W Henderson St (North)
DATE STARTED: 10/7/20 COMPLETED: 10/7/20	GROUND ELEVATION: HOLE SIZE: inches
DRILLING CONTRACTOR:	GROUND WATER LEVELS:
DRILLING METHOD: Auger Drilling	AT TIME OF DRILLING: ---
LOGGED BY: UTA CHECKED BY: UTA	AT END OF DRILLING: ---
NOTES:	AFTER DRILLING: ---

DEPTH (ft)	MATERIAL DESCRIPTION	SAMPLE TYPE NUMBER	BLOW COUNTS (N VALUE)	MOISTURE CONTENT (%)
0.0	Brown clay			
		ST		
2.5	Light brown clay			
		ST		
5.0		ST TCP	50(1")-50(1")	
				21.5 %
		ST		
7.5				
		ST		
10.0		ST		
	Weathered limestone	TCP	50(1")-50(0)	
	Grey clay			
12.5		AU		19.9 %
	Brown clay	AU		21.8 %
15.0		TCP	50(0)-50(0)	

Bottom of borehole at 15.0 feet.

LOGO University of Texas at Arlington

BORING NUMBER BH-2

PAGE 1 OF 1

CLIENT University of Texas at Arlington
PROJECT NAME TxDOT-Fort Worth
PROJECT NUMBER 1
PROJECT LOCATION US 67 and W Henderson St (North)
DATE STARTED 10/8/20 **COMPLETED** 10/8/20
GROUND ELEVATION **HOLE SIZE** inches
DRILLING CONTRACTOR
GROUND WATER LEVELS:
DRILLING METHOD Auger Drilling
AT TIME OF DRILLING ---
LOGGED BY UTA **CHECKED BY** UTA
AT END OF DRILLING ---
NOTES
AFTER DRILLING ---

DEPTH (ft)	MATERIAL DESCRIPTION	SAMPLE TYPE NUMBER	BLOW COUNTS (N VALUE)	MOISTURE CONTENT (%)
0	Dark brown stiff clay with rock	ST		
	Light brown clay with traces of limestone			
		AU		
	Grey clay			
		AU		9.9 %
5		TCP	50(1.5")-50(0)	
	Yellow brown clay			
				14.8 %
		AU		
10		ST	14-11 (25)	
15				19.3 %
		AU	15-10 (25)	
		ST		
	Borwn clay			
20				22.7 %
		AU	21-35 (56)	
		TCP	50(0.25")-50(0.125")	

Bottom of borehole at 22.0 feet.

GEOTECH BH COLUMNS - GINT STD US LAB.GDT - 10/12/20 12:09 - C:\USERS\PUBLIC\DOCUMENTS\BENTLEY\GINT\PROJECTS\US 67 & W HENDERSON ST (NORTH).GPJ

LOGO University of Texas at Arlington

BORING NUMBER BH-1

PAGE 1 OF 1

CLIENT TxDOT-Fort Worth
PROJECT NAME Fort Worth Slope Stabilization
PROJECT NUMBER 1
PROJECT LOCATION I35W and W Cotter Ave
DATE STARTED 10/9/20 COMPLETED 10/9/20
GROUND ELEVATION HOLE SIZE inches
DRILLING CONTRACTOR
GROUND WATER LEVELS:
DRILLING METHOD Auger Drilling
AT TIME OF DRILLING 20.00 ft
LOGGED BY UTA CHECKED BY UTA
AT END OF DRILLING ---
NOTES
AFTER DRILLING ---

DEPTH (ft)	MATERIAL DESCRIPTION	SAMPLE TYPE NUMBER	BLOW COUNTS (N VALUE)	MOISTURE CONTENT (%)
0	Brown clay	ST		
		ST		
5		ST		
		ST		
10		AU		17.9 %
		TCP	6-3 (9)	
15		AU		16.4 %
		ST	9-8 (17)	
		AU		18.1 %
20		ST	5-10 (15)	22.1 %
				21.7 %
	Sandy clay	AU		
25	Gray clay	ST	15-18 (33)	
		AU		
				24.2 %
30		TCP	13-12 (25)	

Bottom of borehole at 30.0 feet.

GEOTECH BH COLUMNS - GINT STD US LAB.GDT - 10/12/20 11:42 - C:\USERS\PUBLIC\DOCUMENTS\BENTLEY\GINT\PROJECTS\I35W AND W COTTER AVENUE.GPJ

BORING NUMBER BH-2

PAGE 1 OF 1

LOGO University of Texas at Arlington

CLIENT TxDOT-Fort Worth	**PROJECT NAME** Fort Worth Slope Stabilization
PROJECT NUMBER 1	**PROJECT LOCATION** I35W and W Cotter Ave
DATE STARTED 10/9/20 **COMPLETED** 10/9/20	**GROUND ELEVATION** **HOLE SIZE** inches
DRILLING CONTRACTOR	**GROUND WATER LEVELS:**
DRILLING METHOD Auger Drilling	∇ **AT TIME OF DRILLING** 22.00 ft
LOGGED BY UTA **CHECKED BY** UTA	**AT END OF DRILLING** ---
NOTES	**AFTER DRILLING** ---

DEPTH (ft)	MATERIAL DESCRIPTION
0	Brown Clay
5	Dark Brown Clay
15	Grey Brown Clayey Sand
20	∇ Yellow Flowing Sand
25	
30	Limestone

SAMPLE TYPE NUMBER	BLOW COUNTS (N VALUE)	MOISTURE CONTENT (%)
ST		
ST		
TCP	7-19 (26)	
ST		16.8 %
AU		
ST	17-21 (38)	
		16.6 %
AU		
ST	10-9 (19)	15.5 %
AU		
TCP ST	13-9 (22)	
		23.8 %
TCP	10-8 (18)	
AU		31.9 %
TCP	45-50(4.5")	

Bottom of borehole at 30.0 feet.

El Paso District

LOGO

The University of Texas at Arlington
416 Yates Stress
76010

BORING NUMBER B-4

PAGE 1 OF 2

CLIENT El-Paso

PROJECT NAME El-Paso Soil Sample Collection

PROJECT NUMBER 1

PROJECT LOCATION

DATE STARTED **COMPLETED**

GROUND ELEVATION **HOLE SIZE** inches

DRILLING CONTRACTOR

GROUND WATER LEVELS:

DRILLING METHOD Hollow Stem Auger 2"

AT TIME OF DRILLING ---

LOGGED BY **CHECKED BY**

AT END OF DRILLING ---

NOTES

AFTER DRILLING ---

DEPTH (ft)	GRAPHIC LOG	MATERIAL DESCRIPTION	SAMPLE TYPE NUMBER	RECOVERY % (RQD)	BLOW COUNTS (N VALUE)	POCKET PEN. (tsf)	DRY UNIT WT. (pcf)	MOISTURE CONTENT (%)	ATTERBERG LIMITS: LIQUID LIMIT	ATTERBERG LIMITS: PLASTIC LIMIT	ATTERBERG LIMITS: PLASTICITY INDEX	FINES CONTENT (%)
0			SPT		6-5-4 (9)							
			SPT		2-3-2 (5)							
5			SPT		5-4-6 (10)							
			SPT		3-2-3 (5)							
10			SPT		8-18-22 (40)							
			SPT		8-6-8 (14)							
15			SPT		7-7-8 (15)							
			SPT		4-5-5 (10)							
20		SILTY SAND, (SM) Silty Sand (SM); Brown	SPT		8-10-13 (23)							
			SPT		5-7-10 (17)							
		CLAYEY SAND, (SC) Clayey Sand; Brown;										
25			SPT		8-20-16 (36)							
		SILTY SAND, (SM) Silty Sand (SM); Brown;	SPT		9-13-15 (28)							
		CLAYEY SAND, (SC) Clayey Sand (SC); Brown;										
30			SPT		8-18-35 (53)							
			SPT		13-12-9 (21)							
35												

(Continued Next Page)

LOGO

The University of Texas at Arlington
416 Yates Stress
76010

BORING NUMBER B-4

CLIENT El-Paso

PROJECT NAME El-Paso Soil Sample Collection

PROJECT NUMBER 1

PROJECT LOCATION

DEPTH (ft)	GRAPHIC LOG	MATERIAL DESCRIPTION	SAMPLE TYPE NUMBER	RECOVERY % (RQD)	BLOW COUNTS (N VALUE)	POCKET PEN. (tsf)	DRY UNIT WT. (pcf)	MOISTURE CONTENT (%)	ATTERBERG LIMITS: LIQUID LIMIT	ATTERBERG LIMITS: PLASTIC LIMIT	ATTERBERG LIMITS: PLASTICITY INDEX	FINES CONTENT (%)
35		SILTY SAND, (SM) Silty Sand (SM); Brown;	SPT		8-21-34 (55)							
		LEAN CLAY, (CL) Lean Clay with Sand; Brown;	SPT		12-14-11 (25)							
		CLAYEY SAND, (SC) Clayey Sand (SC); Brown;										
40			SPT		8-35-35 (70)							
			SPT		22-26-20 (46)							
45												
			SPT		8-29-35 (64)							
			SPT		12-23-20 (43)							
50												
		POORLY GRADED SAND, (SP) Poorly Graded Sand with Silt; (SP-SM), Grayish Brown;	SPT		8-25-35 (60)							

Bottom of borehole at 50.0 feet.

GEOTECH BH COLUMNS - GINT STD US LAB.GDT - 3/15/21 13:47 - C:\USERS\MXA0516\ONEDRIVE - UNIVERSITY OF TEXAS AT ARLINGTON\LAB DOCS\RESISTIVITY IMAGING\TEST RESULTS\SITE INVESTIGATION\EL PASO\BOREHOLE -2\BOREHOLE 2.GPJ

REFERENCES

Abediniangerabi, B., Makhmalbaf, A., & Shahandashti, M. (2021). Deep learning for estimating energy savings of early-stage facade design decisions. Energy and AI, 5, 100077.

Abidin, M. H. Z., Ahmad, F., Wijeyesekera, D. C., Saad, R., & Baharuddin, M. F. T. (2013). Soil resistivity measurements to predict water content and density in loose and dense soil. In Applied Mechanics and Materials (Vol. 353, pp. 911-917). Trans Tech Publications Ltd.

Abu-Hassanein, Z. S., Benson, C. H., & Blotz, L. R. (1996). Electrical resistivity of compacted clays. Journal of geotechnical engineering, 122(5), 397-406.

Achieng, K. O. (2019). Modelling of soil moisture retention curve using machine learning techniques: Artificial and deep neural networks vs support vector regression models. Computers & Geosciences, 133, 104320.

Ackerman, A., Sen, P. K., & Oertli, C. (2013). Designing safe and reliable grounding in AC substations with poor soil resistivity: An interpretation of IEEE Std. 80. IEEE Transactions on Industry Applications, 49(4), 1883-1889.

Adhikari, I., Baral, A., Zahed, E., Abediniangerabi, B., & Shahandashti, M. (2021). *Early stage multi-criteria decision support system for recommending slope repair methods*. Civil Engineering and Environmental Systems, 1-18.

Akingboye, A. S., & Ogunyele, A. C. (2019). Insight into seismic refraction and electrical resistivity tomography techniques in subsurface investigations. Rudarsko-geološko-naftni zbornik (The Mining-Geological-Petroleum Engineering Bulletin), 34(1).

Akinlabi, I., & Adeyemi, G. (2014). Determination of empirical relations between geoelectrical data and geotechnical parameters in foundation studies for a proposed earth dam. Pac. J. Sci. Technol, 15(2), 279-287.

Alsharari, B., Olenko, A., & Abuel-Naga, H. (2020). Modeling of electrical resistivity of soil based on geotechnical properties. Expert Systems with Applications, 141, 112966.

Anderson, N. L., Croxton, N., Hoover, R., & Sirles, P. (2008). *Geophysical methods commonly employed for geotechnical site characterization*. Transportation Research Circular, (E-C130).

Anselin, L. (2005). Spatial regression analysis in R: a workbook. Urbana, 51, 61801.

Anselin, Luc. & Sergio J. Rey. (2014). Modern Spatial Econometrics in Practice, a Guide to Geoda, Geodaspace and Pysal. Chicago, IL: GeoDa Press.

Antony, J. (2014). Design of experiments for engineers and scientists. Elsevier. 63-85.

ASTM D4318-17e1 (2017). Standard Test Methods for Liquid Limit, Plastic Limit, and Plasticity Index of Soils. ASTM International, West Conshohocken, PA.

ASTM D854-14 (2014). Standard Test Methods for Specific Gravity of Soil Solids by Water Pycnometer. ASTM International, West Conshohocken, PA.

ASTM G187-05 (2005). Standard Test Method for Measurement of Soil Resistivity Using the Two-Electrode Soil Box Method. ASTM International, West Conshohocken, PA.

ASTM G57-20 (2020). Standard Test Method for Measurement of Soil Resistivity Using the Wenner Four-Electrode Method. ASTM International, West Conshohocken, PA.

Baral, A., & Shahandashti, M. (2022a). Risk-averse rehabilitation decision framework for roadside slopes vulnerable to rainfall-induced geohazards. *Journal of Infrastructure Preservation and Resilience*, *3*(1), 12.

Baral, A., & Shahandashti, S. M. (2022b). Identifying critical combination of roadside slopes susceptible to rainfall-induced failures. *Natural Hazards*, *113*(2), 1177-1198.

Baral, A., Darghiasi, P., & Shahandashti, M. (2023). Risk-Averse Maintenance Decision Framework for Roadside Slopes along Highway Corridors. In *International Conference on Transportation and Development 2023* (pp. 383-392).

Baral, A., Poumand, P., Adhikari, I., Abediniangerabi, B., & Shahandashti, M. (2021). GIS-based data integration approach for rainfall-induced slope failure susceptibility mapping in clayey soils. Natural Hazards Review, 22(3), 04021026.

Baral, A., Sadegh Nasr, M., Darghiasi, P., Abediniangerabi, B., & Shahandashti, M. (2022). Detection and Classification of Vegetation for Roadside Vegetation Inspection and Rehabilitation Using Deep Learning Techniques. In International Conference on Transportation and Development 2022 (pp. 143-152).

Baynes, F.J. (2010). Sources of geotechnical risk. Quarterly Journal of Engineering Geology and Hydrogeology, 43, 321–331.

Bengio, Y., & LeCun, Y. (2007). Scaling learning algorithms towards AI. Large-scale kernel machines, 34(5), 1-41.

Bernard, J., Leite, O., Vermeersch, F., Instruments, I. R. I. S., & Orleans, F. (2006). Multi-electrode resistivity imaging for environmental and mining applications. IRIS Instruments, Orleans.

Besson, A., Cousin, I., Bourennane, H., Nicoullaud, B., Pasquier, C., Richard, G., ... & King, D. (2010). The spatial and temporal organization of soil water at the field scale as described by electrical resistivity measurements. European Journal of Soil Science, 61(1), 120-132.

Bian, H., Liu, S., Cai, G., & Tian, L. (2015). Artificial neural network model for predicting soil electrical resistivity. Journal of Intelligent & Fuzzy Systems, 29(5), 1751-1759.

Boeckmann, A. Z., & Loehr, J. E. (2016). *Influence of Geotechnical Investigation and Subsurface Conditions on Claims, Change Orders, and Overruns* (No. Project 20-05, Topic 46-04).

Briggs, A. H., Weinstein, M. C., Fenwick, E. A., Karnon, J., Sculpher, M. J., & Paltiel, A. D. (2012). Model parameter estimation and uncertainty analysis: a report of the ISPOR-SMDM Modeling Good Research Practices Task Force Working Group–6. Medical decision making, 32(5), 722-732.

Bryson, L. S. (2005). Evaluation of geotechnical parameters using electrical resistivity measurements. In Earthquake Engineering and Soil Dynamics (pp. 1-12).

Caglar, N., & Arman, H. (2007). The applicability of neural networks in the determination of soil profiles. Bulletin of Engineering Geology and the Environment, 66(3), 295-301.

Calderón, G. F. A. (2009). Spatial regression analysis vs. kriging methods for spatial estimation. International Advances in Economic Research, 15(1), 44-58.

Caudill, M. (1988). Neural networks primer, Part III. AI Expert, 3(6), 53-59.

Chen, Y. (2012). On the four types of weight functions for spatial contiguity matrix. Letters in Spatial and Resource Sciences, 5(2), 65-72.

Chi, G., & Zhu, J. (2008). Spatial regression models for demographic analysis. Population Research and Policy Review, 27(1), 17-42.

Choldun, I., Santoso, J., & Surendro, K. (2019, September). Determining the number of hidden layers in neural network by using principal component analysis. In Proceedings of SAI Intelligent Systems Conference (pp. 490-500). Springer, Cham.

Cosenza, P., Marmet, E., Rejiba, F., Cui, Y. J., Tabbagh, A., & Charlery, Y. (2006). Correlations between geotechnical and electrical data: A case study at Garchy in France. Journal of Applied Geophysics, 60(3-4), 165-178.

Cressie, N. (2015). Statistics for spatial data. John Wiley & Sons.

Crisp, M. P., Jaksa, M. B., & Kuo, Y. L. (2018, November). Influence of site investigation borehole pattern and area on pile foundation performance. In Proceedings of the 12th ANZ Young Geotechnical Professionals Conference, Hobart.

Darghiasi, P., Baral, A., & Shahandashti, M. (2023a). Developing a Cost-Effective Mobile-Based System for Collecting On-Demand Road Condition Images for Snowplow Operations Management. In International Conference on Transportation and Development 2023 (pp. 127-137).

Darghiasi, P., Baral, A., Abediniangerabi, B., & Shahandashti, M. (2022). A Multi-Purpose All-in-One Mobile Data Collection System for Snowplow Operation Management. In International Conference on Transportation and Development 2022 (pp. 39-50).

Darghiasi, P., Baral, A., Abediniangerabi, B., Makhmalbaf, A. & Shahandashti, M. (2023b). Multilevel optimization of UHP-FRC sandwich panels for building façade systems. Handbook of Artificial Intelligence in performance-driven design.

Darghiasi, P., Baral, A., Mattingly, S., & Shahandashti, M. (2023c). Estimation of Road Surface Temperature Using NOAA Gridded Forecast Weather Data for Snowplow Operations Management. Journal of Cold Regions Engineering. https://doi.org/10.1061/JCRGEI/CRENG-691.

Darghiasi, P., Zamanian, M., & Shahandashti, M. (2024). Enhancing Winter Maintenance Decision Making through Deep Learning-Based Road Surface Temperature Estimation. In Construction Research Congress 2024 (*Forthcoming*).

Davim, J. P. (Ed.). (2012). Mechatronics and Manufacturing Engineering: Research and Development. Elsevier. 159-226.

Deebani, W., & Kachouie, N. N. (2022). Monte Carlo ensemble correlation coefficient for association detection. Communications in Statistics-Simulation and Computation, 51(12), 7095-7109.

Edet, A. (2009). *Environmental Monitoring*. Encyclopedia of Life Support Systesms. Inyang, H. I., and Daniels, J. L. (Eds.). Oxford, United Kingdom: Eolss Publishers Co. Ltd.

Ekwue, E. & Bartholomew, J. (2010). Electrical conductivity of some soils in Trinidad as affected by density, water, and peat content. Biosystems Engineering, 108(2), 95–103.

Elhorst, J. P. (2010). Applied spatial econometrics: raising the bar. Spatial economic analysis, 5(1), 9-28.

Erzin, Y., Rao, B. H., Patel, A., Gumaste, S. D., & Singh, D. N. (2010). Artificial neural network models for predicting electrical resistivity of soils from their thermal resistivity. International Journal of Thermal Sciences, 49(1), 118-130.

Fallah-Safari, M., Hafizi, M. K., & Ghalandarzadeh, A. (2010). Correlation between electrical resistivity data and geotechnical data on a clay soil. In 19th International Geophysical Congress and Exhibition of Turkey, ID (Vol. 162).

Fenning, P. J., & Donnelly, L. J. (2004). *Geophysical techniques for forensic investigation*. Geological Society, London, Special Publications, 232(1), 11-20.

Fernández-Avilés Calderón, G. (2009). Spatial regression analysis vs. kriging methods for spatial estimation. International Advances in Economic Research, 15, 44-58.

FHWA (2018). *Advanced Geotechnical Exploration Methods*. Federal Highway Association. Retreived from: https://www.fhwa.dot.gov/innovation/everydaycounts/edc_5/geotech_methods.cfm (Aug. 18, 2019).

Friedman, S. P. (2005). Soil properties influencing apparent electrical conductivity: a review. Computers and electronics in agriculture, 46(1-3), 45-70.

Getis, A. (2009). *Spatial weights matrices.* Geographical Analysis, 41(4), 404-410.

Getis, A. (2009). Spatial weights matrices. Geographical Analysis, 41(4), 404-410.

Giao, P., Chung, S., Kim, D. & Tanaka, H. (2003). Electric imaging and laboratory resistivity testing for geotechnical investigation of Pusan clay deposits. Journal of Applied Geophysics, 52(4), 157–175.

Godfrey, C. L., McKee, G. S., Oakes, H. (1973). General Soil Map of Texas. Published by Texas Agricultural Experiment Station, Texas A&M University in cooperation with Soil

Conservation Service, U.S. Department of Agriculture. Available from: https://texashistory.unt.edu/ark:/67531/metapth298904/m1/1/

Griessenberger, F., Trutschnig, W., & Junker, R. R. (2022). qad: An R-package to detect asymmetric and directed dependence in bivariate samples. Methods in Ecology and Evolution, 13(10), 2138-2149.

Hastie, T., Tibshirani, R., Friedman, J. H., & Friedman, J. H. (2009). *The elements of statistical learning: data mining, inference, and prediction* (Vol. 2, pp. 1-758). New York: springer.

Hession, S. L., & Moore, N. (2011). A spatial regression analysis of the influence of topography on monthly rainfall in East Africa. International journal of climatology, 31(10), 1440-1456.

Jalal, H., Trikalinos, T. A., & Alarid-Escudero, F. (2021). BayCANN: streamlining Bayesian calibration with artificial neural network metamodeling. Frontiers in Physiology, 12, 662314.

Jayalakshmi, T., and Santhakumaran, A. (2011). Statistical normalization and back propagation for classification. International Journal of Computer Theory and Engineering, 3(1), 1793-8201.

Jusoh, H., & Osman, S. B. S. (2017). The correlation between resistivity and soil properties as an alternative to soil investigation. Indian Journal of Science and Technology, 10, 6.

Kearey, P., Brooks, M., & Hill, I. (2013). *An introduction to geophysical exploration*. John Wiley & Sons.

Keller, G. V., & Frischknecht, F. C. (1966). Electrical methods in geophysical prospecting.

Kibria, G., & Hossain, M. S. (2012). Investigation of geotechnical parameters affecting electrical resistivity of compacted clays. Journal of Geotechnical and Geoenvironmental Engineering, 138(12), 1520-1529.

Kim, Y. S., Oh, M. H., & Park, J. (2009). Analysis of resistivity data obtained from cone penetrometer in contaminated soil layers. Environmental geology, 58(6), 1309-1317.

Klein, K. A., & Santamarina, J. C. (2003). Electrical conductivity in soils: Underlying phenomena. Journal of Environmental & Engineering Geophysics, 8(4), 263-273.

Lapenna, V., Lorenzo, P., Perrone, A., Piscitelli, S., Rizzo, E., & Sdao, F. (2005). 2D electrical resistivity imaging of some complex landslides in Lucanian Apennine chain, southern Italy. Geophysics, 70(3), B11-B18.

LeCun, Y., Bengio, Y. & Hinton, G. (2015). Deep learning. Nature 521, 436–444.

LeSage, J. P. (2014). What regional scientists need to know about spatial econometrics. Available at SSRN 2420725.

LeSage, J. P., & Dominguez, M. (2012). *The importance of modeling spatial spillovers in public choice analysis.* Public Choice, 150(3-4), 525-545.

Lin, J., Cai, G., Liu, S., Puppala, A. J., & Zou, H. (2017). Correlations between electrical resistivity and geotechnical parameters for Jiangsu marine clay using Spearman's coefficient test. International Journal of Civil Engineering, 15(3), 419-429.

Long, M., Donohue, S., L'Heureux, J. S., Solberg, I. L., Rønning, J. S., Limacher, R., ... & Lecomte, I. (2012). Relationship between electrical resistivity and basic geotechnical parameters for marine clays. Canadian Geotechnical Journal, 49(10), 1158-1168.

Maroñas, J., Ramos, D., & Paredes, R. (2021). On calibration of mixup training for deep neural networks. In Structural, Syntactic, and Statistical Pattern Recognition: Joint IAPR International Workshops, S+ SSPR 2020, Padua, Italy, January 21–22, 2021, Proceedings (pp. 67-76). Springer International Publishing.

Michot, D., Benderitter, Y., Dorigny, A., Nicoullaud, B., King, D., & Tabbagh, A. (2003). Spatial and temporal monitoring of soil water content with an irrigated corn crop cover using surface electrical resistivity tomography. Water Resources Research, 39(5).

Morin, R. H. (2006). Negative correlation between porosity and hydraulic conductivity in sand-and-gravel aquifers at Cape Cod, Massachusetts, USA. Journal of Hydrology, 316(1-4), 43-52.

Neter, J., Kutner, M. H., Nachtsheim, C. J., & Wasserman, W. (1996). Applied linear statistical models.

Olive, W. W., Chleborad, A. F., Frahme, C. W., Schlocker, J., Schneider, R. R., & Schuster, R. L. (1989). Swelling clays map of the conterminous United States (No. 1940).

Osman, S. S., Baharom, S., & Siddiqui, F. I. (2014). Correlation of electrical resistivity with some soil parameters for the development of possible prediction of slope stability and bearing capacity of soil using electrical parameters. Pertanika J Sci Technol, 22(1), 139-152.

Paleontological Research Institution. Available at https://earthathome.org/hoe/sc/climate/, Accessed on May 18, 2023.

Peng, Y., Albuquerque, P. H. M., Kimura, H., & Saavedra, C. A. P. B. (2021). Feature selection and deep neural networks for stock price direction forecasting using technical analysis indicators. Machine Learning with Applications, 5, 100060.

Rashid, Q. A., Abuel-Naga, H. M., Leong, E. C., Lu, Y., & Al Abadi, H. (2018). Experimental-artificial intelligence approach for characterizing electrical resistivity of partially saturated clay liners. Applied Clay Science, 156, 1-10.

Rezaei, S., Shooshpasha, I., & Rezaei, H. (2018). Empirical Correlation between Geotechnical and Geophysical Parameters in a Landslide Zone (Case Study: Naigeschal Landslide). Earth Sciences Research Journal, 22(3), 195-204.

Rhoades, J. D., Manteghi, N. A., Shouse, P. J., & Alves, W. J. (1989). Soil electrical conductivity and soil salinity: New formulations and calibrations. Soil Science Society of America Journal, 53(2), 433-439.

Rinaldi, V.A. & Cuestas, G.A. (2002). Ohmic conductivity of a compacted silty clay. Journal of Geotechnical and Geoenvironmental Engineering, 128(10), 824–835.

Rivers, B. S. (2016). *Measurement While Drilling (MWD)* [PowerPoint Slides]. FHWA – Resource Center.

Robinson, D. A., Campbell, C. S., Hopmans, J. W., Hornbuckle, B. K., Jones, S. B., Knight, R., ... & Wendroth, O. (2008). Soil water measurement for ecological and hydrological watershed-scale observatories: A review. Vadose Zone Journal, 7(1), 358-389.

Rogers, J. D. (2009). *Fundamentals of Cone Penetrometer Test (CPT) Soundings*. Missouri University of Science and Technology: USA.

Rosenblad, B. L., & Boeckmann, A. Z. (2020). Advancements in Use of Geophysical Methods for Transportation Projects (No. Project 20-05, Topic 50-01).

Samouëlian, A., Cousin, I., Tabbagh, A., Bruand, A., & Richard, G. (2005). Electrical resistivity survey in soil science: a review. Soil and Tillage research, 83(2), 173-193.

Samui, P. (2013). Applicability of data mining techniques for predicting electrical resistivity of soils based on thermal resistivity. International Journal of Geomechanics, 13(5), 692-697.

Samui, P. (2014). Utilization of Gaussian process regression for determination of soil electrical resistivity. Geotechnical and Geological Engineering, 32, 191-195.

Schabenberger, O., & Gotway, C. A. (2017). Statistical methods for spatial data analysis. CRC press.

Schober, P., Boer, C., & Schwarte, L. A. (2018). Correlation coefficients: appropriate use and interpretation. Anesthesia & analgesia, 126(5), 1763-1768.

Seber, G. A., & Lee, A. J. (2012). Linear regression analysis (Vol. 329). John Wiley & Sons.

Shah, P. H., & Singh, D. N. (2005). Generalized Archie's law for estimation of soil electrical conductivity. Journal of ASTM International, 2(5), JAI13087.

Shahandashti M., Hossain, S., & Zamanian, M. (2023). *Implementation of Electrical Resistivity Imaging Manual*. Texas Department of Transportation.

Shahandashti, M., Hossain, S., Baral, A., Adhikari, I., Pourmand, P., & Abediniangerabi, B. (2022a). *Slope repair and maintenance management system* (No. FHWA/TX-20/5-6957-01-1). Texas Department of Transportation.

Shahandashti, M., Hossain, S., Khankarli, G., Zahedzahedani, S. E., Abediniangerabi, B., & Nabaei, M. (2019). *Synthesis on rapid repair methods for embankment slope failure* (No. FHWA/TX-18/0-6957-1). University of Texas at Arlington.

Shahandashti, M., Hossain, S., Zamanian, M., & Akhtar, M. A. (2021). *Advanced Geophysical Tools for Geotechnical Analysis* (No. FHWA/TX-20/0-7008-1).

Shahandashti, M., Mattingly, S., Darghiasi, P., Baral, A., & Abediniangerabi, B. (2022b). *Snowplow Operations Management System* (No. FHWA/TX-22/5-6996-01-1). Texas Department of Transportation. Research and Technology Implementation Office.

Siddiqui, F. I., & Osman, S. B. A. S. (2012). Integrating geo-electrical and geotechnical data for soil characterization. International Journal of Applied Physics and Mathematics, 2(2), 104-106.

Sirles, P. C. (2006). Use of geophysics for transportation projects (Vol. 357). Transportation Research Board.

Spatial Climate Analysis Service (2000). Average Annual Precipitation Data, Oregon State University.

Stakhovych, S., & Bijmolt, T. H. (2009). Specification of spatial models: A simulation study on weights matrices. Papers in Regional Science, 88(2), 389-408.

Su, B., & Ang, B. W. (2017). Multiplicative structural decomposition analysis of aggregate embodied energy and emission intensities. Energy Economics, 65, 137-147.

Sudha, K., Israil, M., Mittal, S., & Rai, J. (2009). Soil characterization using electrical resistivity tomography and geotechnical investigations. Journal of Applied Geophysics, 67(1), 74-79.

Tiwari, B., & Marui, H. (2005). A new method for the correlation of residual shear strength of the soil with mineralogical composition. Journal of Geotechnical and Geoenvironmental Engineering, 131(9), 1139-1150.

Uzair, M., & Jamil, N. (2020, November). Effects of hidden layers on the efficiency of neural networks. In 2020 IEEE 23rd international multitopic conference (INMIC) (pp. 1-6). IEEE.

Voss, P. R., Long, D. D., Hammer, R. B., & Friedman, S. (2006). County child poverty rates in the US: a spatial regression approach. Population Research and Policy Review, 25, 369-391.

Walker, R., Moran, E., & Anselin, L. (2000). Deforestation and cattle ranching in the Brazilian Amazon: external capital and household processes. World development, 28(4), 683-699.

Wang, H., Wang, J. H., & Liu, G. H. (2007). *Spatial regression analysis on the variation of soil salinity in the Yellow River Delta-art.* no. 67531U. In 15th International Conference on Geoinformatics, Nanjing, PR China (pp. U7531-U7531).

Weary, D. J. (2015). The Cost of Karst Subsidence and Sinkhole Collapse in The United States Compared With Other Natural Hazards. 14TH SINKHOLE CONFERENCE.

Wightman, W., Jalinoos, F., Sirles, P., & Hanna, K. (2004). *Application of geophysical methods to highway related problems* (No. FHWA-IF-04-021).

Williams, J. H., & Johnson, C. D. (2004). *Acoustic and optical borehole-wall imaging for fractured-rock aquifer studies*. Journal of Applied Geophysics, 55(1-2), 151-159. DOI: 10.1016/j.jappgeo.2003.06.009.

Yan-guang, C. H. E. N. (2009). Reconstructing the mathematical process of spatial autocorrelation based on Moran’s statistics. Geographical Research, 28(6), 1449-1463.

Yang, J.S. (2002). Three Dimensional Complex Resistivity Analysis for Clay Characterization in Hydrogeologic Study. Ph.D. thesis, University of California, Berkeley.

Yang, Y., & Fik, T. (2014). Spatial effects in regional tourism growth. Annals of Tourism Research, 46, 144-162.

Zamanian, M., & Shahandashti, M. (2022). Investigation of Relationship between Geotechnical Parameters and Electrical Resistivity of Sandy Soils. In Construction Research Congress 2022 (pp. 686-695).

Zamanian, M., & Shahandashti, M. (2023). Investigating Spatial Association Between Electrical Resistivity Values and Geotechnical Properties of Clayey Soils: An Empirical Study.

Zamanian, M., & Yazdandoost, M. (2021). Influence of chemical fertilizers and bioinoculants on growth and yield of sunflower (Helianthus annuus L.). Journal of Central European Agriculture, 22(2), 317-328.

Zamanian, M., & Yazdandoost, M. (2022). The Effects of Biological and Chemical Fertilizer Sources on the Production and Quality of Sunflower. Indonesian Journal of Agricultural Science, 23 (1), 15-24.

Zamanian, M., Asfaw, N., Chavda, P., & Shahandashti, M. (2023). Classifying Soil Sulfate Concentration Using Electrical Resistivity Imaging and Random Forest Algorithm. In Airfield and Highway Pavements 2023 (pp. 204-213).

Zamanian, M., Asfaw, N., Chavda, P., & Shahandashti, M. (2023c). Deep Learning for Exploring the Relationship Between Geotechnical Properties and Electrical Resistivities.

Zamanian, M., Darghiasi, P., Shahandashti, M. (2024). Empirical Study of the Correlation Between Geoelectrical and Soil-Index Properties of Clayey Soils. In Construction Research Congress 2024 (*Forthcoming*).

Zamanian, M., Thorat, Y. A., Asfaw, N., Chavda, P., & Shahandashti, M. (2023b). Electrical Resistivity Imaging for Identifying Critical Sulfate Concentration Zones Along Highways. Transportation Research Record, 03611981231167162.

Zhang, W., Li, H., Li, Y., Liu, H., Chen, Y., & Ding, X. (2021). Application of deep learning algorithms in geotechnical engineering: a short critical review. Artificial Intelligence Review, 1-41.

Zhang, Y., Xie, Y., Zhang, Y., Qiu, J., & Wu, S. (2021). The adoption of deep neural network (DNN) to the prediction of soil liquefaction based on shear wave velocity. Bulletin of Engineering Geology and the Environment, 80(6), 5053-5060.

Zhong, S., Zhang, K., Bagheri, M., Burken, J.G., Gu, A., Li, B., Ma, X., Marrone, B.L., Ren, Z.J., Schrier, J. and Shi, W (2021). Machine learning: new ideas and tools in environmental science and engineering. Environmental Science & Technology, Vol. 55, No. 19, pp. 12741-12754.